Phase boundary propagation in heterogeneous media

Thesis by

Bogdan Craciun

In Partial Fulfillment of the Requirements

for the Degree of

Doctor of Philosophy

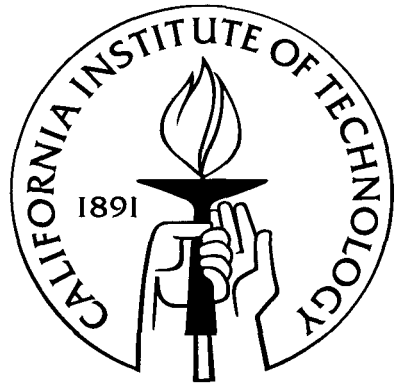

California Institute of Technology

Pasadena, California

2002

(Submitted October 29, 2001)

Acknowledgements

I am greatly indebted to my advisor, Professor Kaushik Bhattacharya, for his invaluable guidance, encouragement and patience during my time at Caltech. This thesis would not have been possible without his support and I am thankful for the opportunity to have learned with him.

I would like to thank Dr. Donald Cohen, Dr. Lawrence C. Evans, Dr. Stefan Muller, Dr. Robert Kohn, Dr. Thomas Y. Hou, Dr. Leonid Kunyansky, Dr. John Pelesko and Dr. Niles Pierce for useful discussions. A very stimulating and supportive academic environment has been provided by the entire department of Applied and Computational Mathematics.

I am also grateful for the support of the U. S. National Science Foundation and the Air-Force Office of Scientific Research through a MURI grant.

Finally, I thank my family, colleagues and friends for their support through my graduate career. With their kindness and friendship, my life at Caltech has been an enjoyable one.

Abstract

There has been much recent progress in the study of free boundary problems motivated by phase transformations in materials science. Much of this literature considers fronts propagating in homogeneous media. However, usual materials are heterogeneous due to the presence of defects, grains and precipitates. This thesis addresses the propagation of phase boundaries in heterogeneous media.

A particular motivation is a material undergoing martensitic phase transformation. Given a martensitic material with many non-transforming inclusions, there are well established microscopic laws that give the complex evolution of a particular twin or phase boundary as it encounters the many inclusions. The issue of interest is the overall evolution of this interface and the effect of defects and impurities on this evolution. In particular, if the defects are small, it is desirable to find the effective macroscopic law that governs the overall motion, without having to follow all the microscopic details but implicitly taking them into account. Using a theory of phase transformations based on linear elasticity, we show that the normal velocity of the martensitic phase or twin boundary may be written as a sum of several terms: first a homogeneous (but non-local) term that one would obtain for the propagation of the boundary in a homogeneous medium, second a heterogeneous term describing the effects of the inclusions but completely independent of the phase or twin boundary and third an interfacial energy term proportional to the mean curvature of the boundary.

As a guide to understanding this problem, we begin with two simplified settings which are also of independent interest. First, we consider the homogenization for the case when the normal velocity depends only on position (the heterogeneous term only). This is equivalent to the homogenization of a Hamilton-Jacobi equation. We establish several variational principles which give useful formulas to characterize the effective Hamiltonian. We illustrate the usefulness of these results through examples and we also provide a qualitative study of the effective normal velocity.

Second, we address the case when the interfacial energy is not negligible, so we keep the heterogeneous and curvature terms. This leads to a problem of homogenization of a degenerate parabolic initial value problem. We prove a homogenization theorem and obtain a characterization for the effective normal velocity, which however proves not to be too useful a tool for actual calculations. We therefore study some interesting examples and limiting cases and provide explicit formula in these situations. We also provide some numerical examples.

We finally address the problem in full generality in the setting of anti-plane shear. We explicitly evaluate the term induced by the presence of the inclusions and we propose a numerical method that allows us to trace the evolution of the phase boundary. We use this numerical method to evaluate the effect of the inclusions and show that their effect is quite localized. We use it to explain some experimental observations in NiTi.

Contents

Chapter 1

Introduction

Free boundary problems occur naturally in many areas of engineering: phase boundary propagation in materials science, multiphase flows, seismic waves, photolitography, etching and image processing. We study a series of problems motivated by solid to solid phase transitions; we note, however, that these results and ideas have implications for the other areas mentioned above.

Materials undergoing solid to solid phase transitions spontaneously form microstructure (like fine twins in martensitic transformation). An issue of great current interest is the evolution of this microstructure and the effect of defects and impurities on this evolution. To be specific, consider a martensitic material with many non-transforming inclusions and a phase (twin) boundary propagating in this material. There are well established microscopic laws that give the evolution of this boundary but its motion is very complex as it encounters the many inclusions. We are interested in finding the effective macroscopic law that governs the overall motion, without having to follow all the microscopic details but implicitly taking them into account.

Consider a body $\Omega \subset \mathbb{R}^3$ and let it contain N inclusions $A_i \subset \Omega$, $i = 1, \dots N$, as in Figure 1.1. Assume that A_i are disjoint, and Ω, A_i open. Now suppose that this body with inclusions has a phase boundary Γ which separates it into the $+$ and the $-$ phases. Thus,

$$\Omega = \Omega^+ \cup \Omega^- \cup_{i=1}^N A_i \cup \Gamma \cup_{i=1}^N \partial A_i.$$

Suppose the transformation strain or stress-free or eigenstrain of the $+$, $-$ phase is E_+, E_- respectively while that of the ith inclusion is E_i. Above, E_+, E_-, E_i are given symmetric 3×3 matrices. Suppose further that all the inclusions and both the phases have the same elastic modulus $\mathbb{C}$. Then the energy density is

$$W = \frac{1}{2}(\nabla u - E_T) \cdot \mathbb{C}(\nabla u - E_T) \tag{1.1}$$

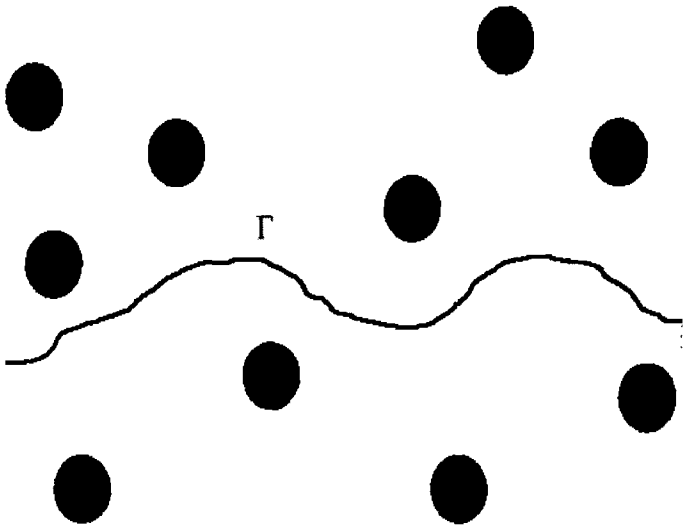

Figure 1.1: A twin boundary in a medium with precipitates

and the stress tensor T is given by

$$T = \mathbb{C}(\nabla u - E_T)\,, \tag{1.2}$$

where u denotes the displacement field,

$$E_T = \chi_+ E_+ + \chi_- E_- + \sum_{i=1}^{N} \chi_i E_i = \begin{cases} E_+ & \text{in } \Omega_+, \\ E_- & \text{in } \Omega_-, \\ E_i & \text{in } A_i \end{cases}$$

and χ_+ is the characteristic function of Ω_+, etc. If the phase boundary Γ is stationary, we can find the displacement u and stress t by solving the equilibrium equation (balance of linear momentum assuming no external body force)

$$\nabla \cdot T = 0, \tag{1.3}$$

subject to appropriate boundary conditions.

Note that we can solve this problem by superposition. Let u^0 solve the problem

$$\nabla \cdot T^0 = 0,$$
$$T^0 = \mathbb{C}\left(\nabla u^0 - \chi_+ E_+ - \chi_- E_-\right),$$

subject to the given boundary conditions, and let u^i solve the problem

$$\nabla \cdot T^i = 0,$$
$$T^i = \mathbb{C}\left(\nabla u^i - \chi_i E_i\right),$$

subject to homogeneous Dirichlet boundary conditions. Set $u = \sum_{i=0}^{N} u^i$ and notice that it solves (1.3).

Now suppose that the phase boundary Γ evolves quasistatically, i.e., its normal velocity is small compared to any of the sound speeds in the medium. We can then find the displacement u and stress T by solving (1.3) at each time t. It remains to describe the law that governs the evolution of Γ. To this end, Abeyaratne and Knowles [2] and Gurtin [15] have shown that the dissipation rate associated with the motion of the twin boundary is

$$\Delta(t) = \int_{\Gamma} f v_n dl, \tag{1.4}$$

where v_n is the normal velocity of the interface and f is given quasistatically by

$$f = [[W]] - n \cdot [[(\nabla u)^T T]] n - c\kappa = [[W]] - \langle T \rangle \cdot [[\nabla u]] - c\kappa. \tag{1.5}$$

Here c is the (positive constant) interfacial energy, κ isthe mean curvature of the interface, n is its normal and $[[q]]$ and $\langle q \rangle$ denote respectively the jump and the average in a quantity q across the phase boundary. Therefore, f is the thermodynamic force conjugate to the normal velocity and may be interpreted as the thermodynamic driving force that drives the phase boundary. It is natural therefore to assume that the normal velocity depends on the driving force and a simple model is obtained by making the following constitutive assumption:

$$v_n = f.$$

We note that this model automatically satisfies the requirement that the dissipation be non-negative.

Plugging (1.1) and (1.2) into (1.5), we find that

$$\begin{aligned} f &= \frac{1}{2}[[(\nabla u - E_T) \cdot \mathbb{C}(\nabla u - E_T)]] - \langle \mathbb{C}(\nabla u - E_T) \rangle \cdot [[\nabla u]] - c\kappa \\ &= \frac{1}{2}[[(\nabla u) \cdot \mathbb{C}(\nabla u)]] + \frac{1}{2}[[E_T \cdot \mathbb{C} E_T]] - [[(\nabla u) \cdot \mathbb{C} E_T]] \\ &\quad - \langle \mathbb{C}(\nabla u) \rangle \cdot [[\nabla u]] + \langle \mathbb{C} E_T \rangle \cdot [[\nabla u]] - c\kappa. \end{aligned}$$

Since $[[ab]] = \langle a \rangle [[b]] + [[a]] \langle b \rangle$, and since $\mathbb{C}$ is constant and symmetric, we conclude that

$$\begin{aligned} \tfrac{1}{2}[[(\nabla u) \cdot \mathbb{C}(\nabla u)]] &= \langle \mathbb{C}(\nabla u) \rangle \cdot [[\nabla u]], \\ [[(\nabla u) \cdot \mathbb{C} E_T]] &= \langle \mathbb{C} E_T \rangle \cdot [[\nabla u]] + [[\mathbb{C} E_T]] \cdot \langle \nabla u \rangle. \end{aligned}$$

Therefore, the model gives

$$v_n = f = \frac{1}{2}[[E_T \cdot \mathbb{C}E_T]] - [[\mathbb{C}E_T]] \cdot \langle \nabla u \rangle - c\kappa. \tag{1.6}$$

Substituting the solution of (1.3) into this expression, we find that the normal velocity of the phase boundary may be written as

$$v_n = \frac{1}{2}\left(E_+ \cdot \mathbb{C}E_+ - E_- \cdot \mathbb{C}E_-\right) - \mathbb{C}(E_+ - E_-) \cdot \left(\sum_{i=1}^{N} \nabla u^i\right) - \mathbb{C}(E_+ - E_-) \cdot \langle \nabla u^0 \rangle - c\kappa. \tag{1.7}$$

Above, we have used the fact that ∇u^i is continuous across Γ for $i = 1, \ldots, N$.

Thus, the normal velocity is written as a sum of four terms. The first term is constant, the second depends only on the inclusions and is independent of Γ (including its normal), the third depends only on Γ and is independent of the inclusions and the fourth is proportional to the mean curvature. In short,

$$v_n = f(x) + v_n^{\Gamma} - c\kappa.$$

If f oscillates on a length scale that is small compared to the size of Ω, then the evolution of Γ is extremely complicated. We are interested in understanding if one can define an overall or average interface which captures the correct overall evolution without explicitly tracking all the details, and if so, in determining the laws that govern the overall interface.

As a guide to understanding this problem, we study certain simplified examples that are also of independent interest.

Chapter 2 deals with the case $v_n = f(\frac{x}{\varepsilon}, n)$, with f continuous and periodic in the first variable with period $[0,1]^N$ (where N is the spatial dimension of the problem and ε is the typical lengthscale of the inclusions). We write the problem using the level set formulation: assume that the interface Γ can be described as the zero level set of some function $h(x)$. We find that its propagation may be written as a Hamilton Jacobi initial value problem and we seek to homogenize it.

If f assumes strictly positive values (or strictly negative values), the results of Lions, Papanicolaou and Varadhan [20] establish the well posedness of this homogenization issue. However, their result is hardly a useful tool for calculating the effective normal velocity $\bar{v}_n$. An alternate approach is to follow E [12] and use Γ-convergence in the Lax representation formula of the solution of the initial Hamilton-Jacobi equation. Using both these approaches, we establish several variational principles which give formulas that allow us to effectively calculate $\bar{v}_n$. We illustrate the usefulness of these results through examples. A noticeable detail is that, in spite of the Lipschitz continuity of f required for the proof of the theorems, the obtained formulae seem to be extendable to all functions for which they make sense. We also discuss the situation when f takes both positive and negative values.

Chapter 2 also addresses the qualitative study of the effective normal velocity $\bar{v}_n$, like the mono-

tonicity of $\bar{v}_n$ with respect to f and its continuity with respect to variations of f in $C(\mathbb{R}^N)$. The issue of bounds is also touched on and in the end of the third section of Chapter 2, some inequalities are derived that are sharper than the ones provided in [20] and show some parallelism to the ones for linear conductivity (effective normal velocity is caught between some sort of harmonic and arithmetic means).

We then move to the case when the interfacial energy c in (1.7) is no longer negligible and arrive at the normal velocity law $v_n = f(\frac{x}{\varepsilon}) + c\varepsilon\kappa$, with f a continuous and periodic function with period $[0,1]^N$ (where N is the spatial dimension of the problem) and c a positive real constant. Representing again the interface as the zero level set of a function h, we conclude that we need to homogenize a degenerate parabolic initial value problem. In Chapter 3 we prove a homogenization theorem that is equivalent to the one proved in [20] for the Hamilton-Jacobi problem. Unfortunately, the obtained characterization for the effective normal velocity is not too useful a computational tool. Moreover, the nature of this problem is such that there are no known representation formulae for its solution, which would allow use of the Γ convergence theory. We, however, study some interesting limiting cases and examples.

Of particular importance is the result for the case when c is very large. We show rigorously in Chapter 3 that, in the limit $c \to \infty$,

$$\lim_{c\to\infty} \bar{v}_n(p) = \limsup_{D\to\infty} \frac{D}{\int_0^D \frac{ds}{<f>_\perp(s)}},$$

where $< f >_\perp$ is the average of f on a $(N-1)$-dimensional period of f that is orthogonal to p. This limit for $\bar{v}_n$ is not at all surprising. When c is very large, curvature is highly penalized so any propagating interface is forced to be almost straight. As the speed of any straight line is obtained by averaging the normal velocity along the interface, this reduces the problem to the one-dimensional case, where the effective velocity is given by the harmonic mean of the velocities.

Finally, in Chapter 4 we study the effect of precipitates, including the key elastic term that depends on the interface. Rather than focusing on the difficult issue of homogenization, we try to expose the effect of the precipitates through simulation of certain examples. We specialize the problem to the case of an anti-plane shear deformation and obtain an estimate of the effect of the inclusions. We present a numerical method that allows us to simulate the propagation of the phase boundary. The results of certain simulations ahow, in particular, that the precipitate inclusions indeed have only a short range effect on the motion of the twin boundary.

Chapter 2

Homogenization of the geometric motion of an interface

2.1 Introduction

The present chapter deals with the propagation of fronts driven by a normal velocity that depends on the position only. Consider a phase boundary propagating with the normal velocity

$$v_n = f(x) = \sigma - \tilde{\sigma}(x)$$

inside some heterogeneous body occupying some region $\Omega \subset \mathbb{R}^N$, where σ is the constant applied load and $\tilde{\sigma} : \Omega \to \mathbb{R}$ is a spatially rapidly oscillating function which expresses the resistance of the medium to changing phase. If the length scale of the oscillations in $\tilde{\sigma}$ are small compared to typical length scales in Ω, then the detailed evolution of the front is rather complicated. Therefore, this study seeks to find an effective law that governs the overall evolution of the front. It is assumed henceforth that $\Omega = \mathbb{R}^N$ and that $\tilde{\sigma}$ is periodic.

Similar problems arise in the calculation of first arrivals in seismic travel times (with a velocity that varies depending on the type of rock) and the development process in photolitography, where the resistive strength of the material is differentially altered through optical processes and the material is then exposed to an etching beam that removes the weaker material.

An efficient tool for studying such problems is the level set formulation. If we assume that there exists a smooth function $h : \mathbb{R}^N \times [0, \infty) \to \mathbb{R}$ such that our front coincides with its zero level set at *all* times, a simple calculation yields that

$$n = \frac{\nabla h}{|\nabla h|}, \quad v_n = -\frac{h_t}{|\nabla h|},$$

where n denotes the normal to the front and h_t is the derivative of h with respect to the time t. It

follows that h satisfies the following Hamilton-Jacobi initial value problem:

$$\begin{cases} h_t + H(x, \nabla h) = 0 & \text{in} \quad \mathbb{R}^N \times [0, \infty) \\ h(x, 0) = h_0(x) & \text{in} \quad \mathbb{R}^N \end{cases},$$

with the Hamiltonian

$$H(x, p) = f(x)|p|$$

and the initial data $h_0 \in BUC(\mathbb{R}^N)$ (where BUC denotes the space of bounded and uniformly continuous functions) chosen such that its zero level set coincides with the initial position of the front. If $\mathcal{S}_0$ denotes the set of all points in the initial front, a common choice for h_0 is

$$h_0(x) = \min(d(x, \mathcal{S}_0), 1),$$

where $d(x, \mathcal{S}_0)$ is the distance from x to $\mathcal{S}_0$.

One problem that might occur when using this formulation is that the zero level set of the function h may develop a nonempty interior. However, this is ruled out in the case when the normal velocity depends on the position only, by a result of Barles, Soner and Souganidis (Theorem 4.1 in [4]).

Now, if the medium in which the front is propagating has a periodic structure, with unit cell $[0, \varepsilon]^N$, the corresponding Hamilton-Jacobi initial value problem is

$$\begin{cases} h_t^\varepsilon + f(\frac{x}{\varepsilon})|\nabla h^\varepsilon| = 0 & \text{in} \quad \mathbb{R}^N \times [0, \infty) \\ h^\varepsilon(x, 0) = h_0(x) & \text{in} \quad \mathbb{R}^N \end{cases}, \tag{2.1}$$

with f continuous and periodic with period $Y_N = [0, 1]^N$. Our aim is to study the homogenization of this phenomenon, i.e., to capture its limit behavior when the structure of the medium becomes infinitely fine ($\varepsilon \to 0$).

We say that a homogenized front exists and its level set formulation is given by the Hamilton-Jacobi initial value problem

$$\begin{cases} h_t + \bar{H}(\nabla h) = 0 & \text{in} \quad \mathbb{R}^N \times [0, \infty) \\ h(x, 0) = h_0(x) & \text{in} \quad \mathbb{R}^N \end{cases} \tag{2.2}$$

if the viscosity solution h^ε of problem (2.1) converges uniformly on $\mathbb{R}^N \times [0, T)$ (for all $T < \infty$) to the viscosity solution of problem (2.2). We call $\bar{H}$ the effective or homogenized Hamiltonian. Further, since $H(x, p) = f(x)|p|$, we write

$$\bar{H}(p) = \bar{v}_n(p)|p|$$

and call $\bar{v}_n$ the effective normal velocity.

The issue of the existence of the effective Hamiltonian $\bar{H}$ has been addressed in previous studies by Lions, Papanicolaou and Varadhan [20] and by Evans [13]. While their results establish the well posedness of the homogenization problem and prove certain properties of the effective Hamiltonian, they do not provide means for calculating it. The present chapter addresses this issue and its main results (Theorems 2, 4, and 6) give variational characterizations for $\bar{H}$, the effectiveness of which is illustrated in a series of examples.

In Section 2.2 we demonstrate that the homogenization of Equation (2.1) makes sense only when f assumes strictly positive values and we try to give an interpretation of this fact. In particular, we show how, for cases when f is not strictly positive, the front may assume an oscillatory shape with constant amplitude and frequency of order ε^{-1} as ε decreases. This is made possible by the fact that the present model allows the front to develop infinite curvature. Section 2.3 contains a brief review of existening results and Section 2.4 contains our main theorems, which give formulas for the effective normal velocity. Starting with these formulas, we derive some qualitative properties and, in Section 2.5, bounds on the effective normal velocity. We also make comparisons with some other results in the theory of homogenization. Finally, Section 2.6 lists a few examples which demonstrate the usefulness of our results. We show that the homogenization of isotropic media may give birth to anisotropic ones.

Even though the homogenization theory is valid only when f is strictly positive, we show through examples (specifically Example 3 in Section 2.2) that one can define an overall phase boundary when the regions where f is negative are isolated within the region where f is positive. We also show that the formulas we derive in Section 2.4 give the normal velocity of this overall phase boundary.

2.2 Defining the effective normal velocity

We start by addressing the issue of well posedness of the homogenization problem. Motivated by the fact that all the results in the previous literature assume coercivity of the Hamiltonian H (which in our case is equivalent to the strict positivity of f), we try to investigate, by examples, the evolution of fronts in a medium where f changes sign.

Denote by $\mathcal{F}^+$ (respectively $\mathcal{F}^-$) as the set of all x for which $f(x) > 0$ (respectively $f(x) < 0$). We may then have one of the following three interesting situations:

Example 1. We start by looking at the case when both $\mathcal{F}^+$ and $\mathcal{F}^-$ percolate. In such a situation, existence of a moving homogenized front fails either due to the creation of very dense oscillations or due to trapping.

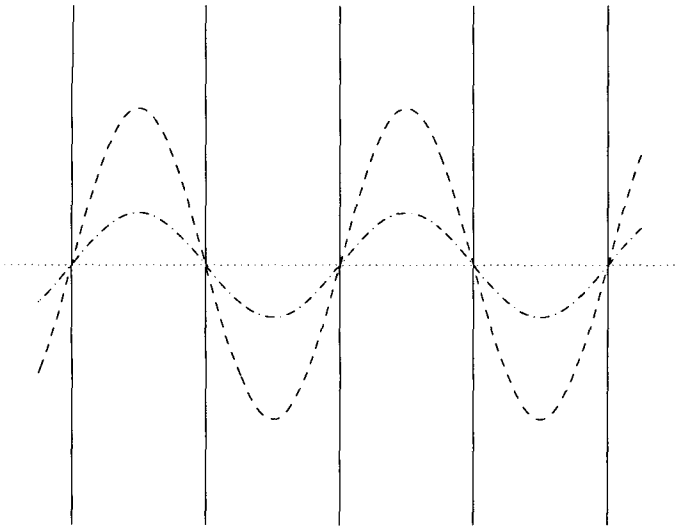

Figure 2.1: Propagation of a front with normal velocity law given by Equation (2.3)

As a representative example, consider the normal velocity law

$$f(x) = a\cos(\frac{\pi x_1}{2}), \quad \forall x \in \mathbb{R}^2, \tag{2.3}$$

where $a > 0$, and an initial shape parallel to the $x_2 = 0$ axis, say

$$h_0(x) = \min(x_2, 1).$$

The evolution of such a front is depicted in Figure 2.1. The lines where v_n vanishes are shown as continuous lines and the evolving front is pictured at three different instants of time (dotted line for the initial position followed, chronologically wise, by the dash-dot line and then the dashed line).

The front is pinned at all the points $x = (x_1, x_2)$ satisfying $x_1 \in \varepsilon(\mathbb{Z} \setminus 2\mathbb{Z})$ on the $x_2 = 0$ axis. By a simple symmetry argument, the normal in the points x with $x_1 \in 2\varepsilon\mathbb{Z}$ will always be e_2, which allows us to conclude that the points of the front with their first coordinate $x_1 \in 4\varepsilon\mathbb{Z}$ will move in the e_2 direction, while the ones with $x_1 \in \varepsilon(2\mathbb{Z} \setminus 4\mathbb{Z})$ will move in the $-e_2$ direction, all with the same constant velocity a. It is now easy to see that, as ε decreases, the front will assume an oscillatory shape with constant amplitude and frequency of order ε^{-1}. Obviously, it cannot converge uniformly to any homogenized shape.

Now, for the same normal velocity law, use the initial shape given by

$$h_0(x) = \min(x_1, 1).$$

The front is trapped inside the region $\{x \in \mathbb{R}^3 / |x_1| < \varepsilon\}$, so the homogenized front does not move.

This trapping phenomenon is totally analogous to the one-dimensional one observed by Bhattacharya in [6].

Example 2. We now look at the case when neither $\mathcal{F}^+$ nor $\mathcal{F}^-$ percolate. An example of a normal velocity law that falls within this case is

$$f(x) = a\cos(\frac{\pi x_1}{2})\cos(\frac{\pi x_2}{2}), \quad \forall x \in \mathbb{R}^2.$$

In such a situation, we are able to argue that the homogenized front is still. Indeed, since $\mathcal{F}^+$ does not percolate, any of its connected subsets must be bounded. Moreover, by periodicity of f, all the diameters of the connected subsets of $\mathcal{F}^+$ must have a common upper bound. By repeating this argument for $\mathcal{F}^-$, we obtain a positive real d_0 larger than the diameter of any connected subset in $\mathbb{R}^N$ on which f does not change sign. Any initial front $\mathcal{S}$ will then be confined to the region $\{x \in \mathbb{R}^N / d(x, \mathcal{S}) < \varepsilon d_0\}$. As ε decreases to 0, this region shrinks to $\mathcal{S}$ and traps the homogenized front. This is again the analogue of the one-dimensional trapping observed by Bhattacharya in [6].

Example 3. Finally, let us consider the case when $\mathcal{F}^+$ percolates while $\mathcal{F}^-$ is non-void and does not. An illustrative example for this case is

$$f(x) = \begin{cases} |x - (\frac{1}{2}, \frac{1}{2})|, & \text{if} \quad x \in B_{\frac{1}{4}}(\frac{1}{2}, \frac{1}{2}) \\ \frac{1}{4}, & \text{if} \quad x \in Y_2 \setminus B_{\frac{1}{4}}(\frac{1}{2}, \frac{1}{2}) \end{cases}, \tag{2.4}$$

extended by periodicity to all $\mathbb{R}^3$. Presume we start with the initial front given by $\{x_2 = 0\}$:

$$h_0(x) = \min(x_2, 1).$$

By an argument similar to the one in the first case, all points with $x_1 \in \varepsilon\mathbb{Z}$ will move in the e_3 direction with constant velocity $\frac{1}{4}$. These points will eventually pull all the front with them, as it will avoid passing through the points of vanishing f by taking a roundabout way. However, traces of the front, in the form of closed surfaces surrounding the points where f vanishes, will be left behind. As ε decreases to 0, the number of such trace-surfaces increases proportionally with ε^{-1}, impeding the existence of the homogenized front.

As for the leading part of the front, we may use a symmetry argument similar to the one in the previous examples and show that the normal in all points with $x_1 \in \mathbb{Z}$ has to be e_2, hence their normal velocity remains constant and equal to $\frac{1}{4}$ at all times.

The evolution of such a front is depicted in Figure 2.2. The points where v_n vanishes are represented by 'x'-s, while the evolving front is pictured at three different moments (dotted line for the initial position followed, chronologically wise, by the dash-dot line and then the dashed line). Note how, in the third snapshot, the front is no longer connected but consists of its leading part and

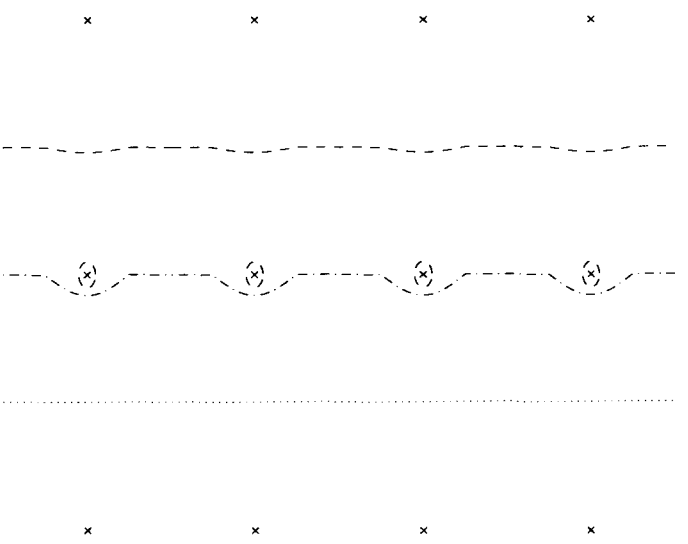

Figure 2.2: Propagation of a front with normal velocity law given by Equation (2.4)

traces around each of the points with $v_n = 0$ that were left behind.

One may neglect the trace-surfaces left behind and define the homogenized front by the remaining part. It is then reasonable to attempt an estimation of its effective velocity and Proposition 1 only states that this is not possible with the help of the level set formulation. One intuitive way of doing all this is to imitate Soravia's Definition 4.2 in [25] and consider the limit, as ε decreases to 0, of the evolutions with speed $\max(f, 0) + \varepsilon$. It is possible to use Lions' Theorem 1.12 in [19] and replace the negative parts of f with 0. The addition of the small positive constant ε deletes the trace-surfaces left behind without considerably altering the velocity of the leading front, as will be seen in Theorem 7.

Proposition 1 *Assume that f and h_0 belong to $W^{1,\infty}(\mathbb{R}^N)$. To have a homogenized level set function in motion, we need f to assume only strictly positive values or only strictly negative values.*

Proof: We prove this result by contradiction: assume that the function f is neither strictly positive nor strictly negative. By continuity and periodicity of f, in any unit cell we can find a point where it vanishes.

Since the homogenized front does move, there exists some compact set D in $\mathbb{R}^N$, with non-void interior, in which the function h changes sign. Without loss of generality, we may assume that $h_0(x) > 0$, $h(x,t) < 0$ for all x in D and for some strictly positive t (note that we may need to change f to $-f$ and h_0 to $-h_0$ for this to be true). By the uniform convergence of h^ε to h, there has to exist a positive ε_D such that, for any ε smaller than ε_D, $h^\varepsilon(x,t) < 0$ in D.

On the other hand, since the interior of D is not void, there exists some positive $\bar{\varepsilon}_D$ and some x_D in D such that $x_D + \varepsilon Y_n \subset D, \forall \varepsilon \leq \bar{\varepsilon}_D$.

Now fix ε to be the minimum of ε_D and $\bar{\varepsilon}_D$. By our assumption on f, we get a point $x \in D$ in which f_ε vanishes, where f_ε is defined by

$$f_\varepsilon(x) = f(\frac{x}{\varepsilon}).$$

Due to the uniform continuity of h^ε, there exists a positive real m such that

$$h^\varepsilon(x,0) > m, \quad h^\varepsilon(x,t) < -m, \quad \forall x \in D. \tag{2.5}$$

Using the existence results developed by Lions in Chapter 9 of [19], we see that the viscosity solution of problem (2.1) belongs to $W^{1,\infty}(\mathbb{R}^N \times (0,t])$. Hence its spatial gradient is bounded:

$$|\nabla h^\varepsilon| \leq M \quad \text{a.e. in} \quad D \times (0,t], \tag{2.6}$$

for some positive real M. Finally, using the continuity of f and the fact that it vanishes in x, we obtain a ball $B_\rho(x)$ contained in D for which

$$f(y) < \frac{2m}{tM}, \forall y \in B_\rho(x). \tag{2.7}$$

Now, inequalities (2.5) give us that

$$\int_0^t h_t(z,\theta)d\theta < -2m, \forall z \in B_\rho(x),$$

which implies

$$\int_0^t f(z)|\nabla h^\varepsilon|d\theta > 2m, \forall z \in B_\rho(x).$$

Using (2.6) and (2.7), we reach

$$\int_0^t \frac{2m}{tM} M d\theta > 2m, \forall z \in B_\rho(x),$$

an obvious contradiction, since

$$\int_0^t \frac{2m}{tM} M d\theta = 2m.$$

■

Having this result, we may assume without loss of generality that f is strictly positive everywhere (if f is strictly negative everywhere, change f to $-f$).

2.3 Homogenization

We seek the homogenized Hamiltonian $\bar{H}$. Let us begin with a formal asymptotic expansion (see [5] for a systematic presentation of such ansatz)

$$h^\varepsilon(x,t) = h^0(x,t) + \varepsilon h^1(\frac{x}{\varepsilon},t) + o(\varepsilon).$$

Plugging this into (2.1) and collecting terms of order 0, we find

$$h^0_t + f(y)|\nabla h^0 + \nabla_y h^1| = 0,$$

where $y = \frac{x}{\varepsilon}$. This is a partial differential equation for the corrector h^1 and its solvability condition provides a constraint between the partial derivatives of the average h^0:

$$h^0_t + \bar{H}(\nabla h^0) = 0,$$

with the effective Hamiltonian $\bar{H}$ (uniquely) determined by the condition that a periodic solution v of

$$H(y, p + \nabla_y v) = \bar{H}(p) \tag{2.8}$$

exists.

This result has also been obtained rigorously by Lions, Papanicolaou and Varadhan in [20]:

Theorem 1 *Let $H \in C(\mathbb{R}^N \times \mathbb{R}^N)$ be periodic in x and satisfy*

$$H(x,p) \to \infty \quad as \quad |p| \to \infty \quad uniformly\ for \quad x \in \mathbb{R}^N.$$

For each $p \in \mathbb{R}^N$, there exists a unique $\lambda \in \mathbb{R}$ - that we denote by $\bar{H}(p)$ - such that there exists $v \in C(\mathbb{R}^N)$, periodic, viscosity solution of

$$H(y, p + D_y v) = \lambda \quad in\ \mathbb{R}^N.$$

And $\bar{H}$ is continuous in p.

For any $u_0 \in BUC(\mathbb{R}^N)$ (the space of bounded and uniformly continuous functions on $\mathbb{R}^N$), the solution u^ε of the Hamilton-Jacobi equation

$$\begin{cases} \frac{\partial u^\varepsilon}{\partial t} + H(\frac{x}{\varepsilon}, Du^\varepsilon) = 0 & in \quad \mathbb{R}^N \times [0,\infty) \\ u^\varepsilon(x,0) = u_0(x) & in \quad \mathbb{R}^N \end{cases}$$

converges uniformly on $\mathbb{R}^N \times [0,T]$ $(\forall\, T < \infty)$ *to the viscosity solution of*

$$\begin{cases} \frac{\partial u}{\partial t} + \bar{H}(Du) = 0 & in \quad \mathbb{R}^N \times [0,\infty) \\ u(x,0) = u_0(x) & in \quad \mathbb{R}^N \end{cases},$$

in $BUC(\mathbb{R}^N \times [0,T])$.

Moreover, they state that $\bar{H}$ is a continuous convex function and that $\bar{H}(p)$ goes uniformly to infinity as $|p| \to \infty$. They also derive some elementary bounds:

$$\inf_x f(x)|p| \le \bar{H}(p) \le \sup_x f(x)|p|. \tag{2.9}$$

A useful characterization of $\bar{H}$ can be obtained by looking at its dual. Define the Lagrangian associated to H by its Legendre dual

$$L(x,q) = \sup_{p \in \mathbb{R}^N} (q \cdot p - H(x,p)) = \begin{cases} 0, & \text{if} \quad |q| \le f(y) \\ \infty, & \text{if} \quad |q| > f(y) \end{cases}. \tag{2.10}$$

In [12], E uses Γ-convergence techniques for the Lax representation formula

$$h^\varepsilon(x,t) = \inf_y \Big(h_0(y) + \inf_\xi \Big(\int_0^t L(\frac{\xi}{\varepsilon}, \dot{\xi}) d\tau | \xi(0) = y, \xi(t) = x, \xi \in W^{1,\infty}(0,t) \Big) \Big)$$

and proves that the solution of problem (2.1) converges uniformly to

$$\inf_y \{ h_0(y) + t\bar{L}\Big(\frac{x-y}{t}\Big) \},$$

where

$$\bar{L}(\lambda) = \liminf_{D \to \infty} \frac{1}{D} \inf_{\phi \in H_0^1(0,D)} \int_0^D L(\lambda t + \phi(t), \lambda + \dot{\phi}(t)) dt, \tag{2.11}$$

and that $\bar{L}$ is the dual of $\bar{H}$.

2.4 Characterization of the effective normal velocity

We now use the results listed in the section above to obtain suitable characterization of the homogenized Hamiltonian in the problem motivated by phase boundary propagation where

$$H(x,p) = f(x)|p|.$$

We set

$$\bar{H}(p) = \bar{v}_n(p)|p|$$

and call $\bar{v}_n$ the effective normal velocity.

Lemma 1 *If f is Lipschitz continuous, Y-periodic and $f > 0$, the effective Hamiltonian is given by*

$$\bar{H}(p) = \sup_{\lambda}\Big(\cos(\lambda, p)\limsup_{D\to\infty}\frac{D}{\inf_{\gamma\in\mathcal{D}_D^{0,\lambda}} T(\gamma)}\Big)|p|, \tag{2.12}$$

where $\mathcal{D}_D^{x,\lambda}$ is the set of all H^1 paths connecting x with $x+\frac{\lambda}{|\lambda|}D$ and $T(\gamma) = \int_\gamma \frac{dl}{f}$ (dl is the arclength). Moreover, $\bar{v}_n$ is an even function and depends only on the direction $\frac{p}{|p|}$.

Proof: If v is a viscosity solution corresponding to p in (2.8), then for any $\lambda > 0$ notice that λv is a solution corresponding to λp and $\bar{H}(\lambda p) = \lambda \bar{H}(p)$:

$$H(y, \lambda p + \lambda\nabla_y v) = f(y)|\lambda p + \lambda\nabla_y v| = \lambda f(y)|p + \nabla_y v| = \lambda H(y, p + \nabla_y v) = \lambda\bar{H}(p).$$

It follows that $\bar{v}_n$ is a function of direction only:

$$\bar{v}_n(p) = \bar{v}_n(\frac{p}{|p|}).$$

Moreover, Proposition 2 in [20] ensures that $\bar{v}_n$ is even.

Using this property of $\bar{H}$, we get a first formula for its Legendre dual:

$$\begin{aligned}\bar{L}(\lambda) &= \sup_p(\lambda\cdot p - \bar{H}(p)) = \sup_p |p|(|\lambda|\cos(\lambda, p) - \bar{v}_n(p)) = \\ &= \begin{cases} 0, & \text{if } |\lambda| \le F(\lambda) \\ \infty, & \text{if } |\lambda| > F(\lambda)\end{cases},\end{aligned} \tag{2.13}$$

where F is defined by

$$F(\lambda) = \inf_p\{\frac{\bar{v}_n(p)}{\cos(\lambda, p)} : \cos(\lambda, p) > 0\}.$$

Further, since $\bar{H}$ is continuous and convex, it coincides with the dual of its dual, so

$$\bar{H}(p) = \sup_\lambda(\lambda\cdot p - \bar{L}(\lambda)) = \sup_{|\lambda|\le F(\lambda)} |\lambda|\cos(\lambda, p)|p|,$$

from which we infer

$$\bar{v}_n(p) = \sup_\lambda(F(\lambda)\cos(\lambda, p)). \tag{2.14}$$

An alternative formula for $\bar{L}$ may be obtained from E's relation (2.11). Using (2.10),

$$\bar{L}(\lambda) = \begin{cases} 0, & \text{if } \exists\, D_n\to\infty, \exists\, \phi_n \in H_0^1(0, D_n) \ni: |\lambda + \dot{\phi}_n| \le f(\lambda t + \phi_n) \\ \infty, & \text{otherwise}\end{cases}. \tag{2.15}$$

Now consider some λ with $|\lambda| > F(\lambda)$. By (2.13), $\bar{L}(\lambda) = \infty$, so (2.15) implies that, for any D large enough and for any ϕ in $H_0^1(0, D)$,

$$\exists\ (a, b) \subset (0, D) \ni: |\lambda + \dot{\phi}(t)| > f(\lambda t + \phi(t)) \quad \text{a.e. in} \quad (a, b). \tag{2.16}$$

Having D and an arbitrary ϕ fixed, we pose the following initial value problem:

$$\begin{cases} \frac{dt}{ds} = \frac{f(\lambda t + \phi(t))}{|\lambda + \dot{\phi}(t)|} \\ t(0) = 0 \end{cases}$$

on the largest interval on which $|\lambda + \dot{\phi}(t)|$ stays strictly positive and $t \leq D$. Since f is periodic and continuous and ϕ is in $H_0^1(0, D)$, the derivative of t is bounded from below by a strictly positive number. This ensures that t will eventually get to assume the value D. Set S to be the corresponding value of s.

We now show that $S > D$. Assume by contradiction that $S \leq D$. Then we can define a function in $H_0^1(0, D)$ by

$$\psi(s) = \begin{cases} \phi(t(s)) + \lambda(t(s) - s), & \text{if} \quad s \leq S \\ \lambda(\min_x f(x) - 1)s, & \text{if} \quad S < s \leq D \end{cases},$$

which satisfies

$$|\lambda + \frac{d\psi}{ds}| \leq f(\lambda s + \psi(t(s))) \quad \text{a.e. in} \quad [0, D]. \tag{2.17}$$

Since (2.16) and (2.17) contradict each other, it must be that $S > D$, which yields

$$D < \int_0^S ds = \int_0^D \frac{ds}{dt} dt = \int_0^D \frac{|\lambda + \dot{\phi}(t)|}{f(\lambda t + \phi(t))} dt.$$

What we have proved up to now is the following: for any λ with $|\lambda| > F(\lambda)$, any sufficiently large D and any ϕ in $H_0^1(0, D)$, we have

$$|\lambda| > |\lambda| D \Big(\int_0^D \frac{|\lambda + \dot{\phi}(t)|}{f(\lambda t + \phi(t))} dt \Big)^{-1}. \tag{2.18}$$

Equivalently,

$$F(\lambda) \geq \limsup_{D \to \infty} \sup_{\phi \in H_0^1(0,D)} |\lambda| D \Big(\int_0^D \frac{|\lambda + \dot{\phi}(t)|}{f(\lambda t + \phi(t))} dt \Big)^{-1}. \tag{2.19}$$

We now aim at the converse inequality. Attempting the same trail, consider some λ with $|\lambda| < F(\lambda)$. By (2.13), $\bar{L}(\lambda) = 0$, so (2.15) implies that there exists a sequence $D_n \to \infty$ and $\phi_n \in H_0^1(0, D_n)$ such that $|\lambda + \dot{\phi}_n(t)| \leq f(\lambda t + \phi_n(t))$, a.e. in $[0, D_n]$. This yields

$$\int_0^{D_n} \frac{|\lambda + \dot{\phi}_n(t)|}{f(\lambda t + \phi_n(t))} dt \leq D_n,$$

hence

$$\sup_{\phi\in H_0^1(0,D_n)} |\lambda| D_n \Big(\int_0^{D_n} \frac{|\lambda+\dot{\phi}_n(t)|}{f(\lambda t+\phi_n(t))}dt\Big)^{-1} \geq |\lambda|.$$

Thus

$$|\lambda| \leq \limsup_{D\to\infty} \sup_{\phi\in H_0^1(0,D)} |\lambda| D \Big(\int_0^{D} \frac{|\lambda+\dot{\phi}(t)|}{f(\lambda t+\phi(t))}dt\Big)^{-1}, \forall \lambda \quad \text{with} \quad |\lambda| < F(\lambda),$$

which gives the converse inequality of (2.19). We conclude that

$$\begin{aligned} F(\lambda) &= \limsup_{D\to\infty} \sup_{\phi\in H_0^1(0,D)} |\lambda| D \Big(\int_0^{D} \frac{|\lambda+\dot{\phi}(t)|}{f(\lambda t+\phi(t))}dt\Big)^{-1} = \\ &= \limsup_{D\to\infty} \Big(\frac{1}{D} \inf_{\gamma\in\mathcal{D}_D^{0,\lambda}} \int_\gamma \frac{dl}{f}\Big)^{-1} \end{aligned} \tag{2.20}$$

and using (2.14) we reach (2.12). ■

This formula for $\bar{v}_n$ has an interesting interpretation. According to (2.20), $F(\lambda)$ is the fastest average velocity with which we can travel a long distance in the λ direction. Equation (2.12) then picks the direction λ such that the projected velocity in the direction p is the fastest. Therefore, $\bar{v}_n$ is the fastest projected average velocity in the direction p. In particular, a front need not directly develop in the direction p. If a quicker neighboring direction exists, the front will rather choose to develop portions with the corresponding normal at microscopical level and perform a translate-and-advance motion, thus obtaining a faster propagation.

Lemma 2 *The function*

$$G(x,y) = \inf_{\phi\in H_0^1(0,1)} \int_0^1 \frac{|y-x+\dot{\phi}(t)|}{f(x+t(y-x)+\phi(t))}dt$$

satisfies the Lipschitz continuity condition

$$|G(x_1,y_1) - G(x_2,y_2)| \leq \frac{|x_1-x_2|+|y_1-y_2|}{\inf_x f(x)}.$$

Proof: Given $\phi_1 \in H_0^1(0,1)$, define $\phi_2 \in H_0^1(0,1)$ by

$$x_2 + t(y_2-x_2) + \phi_2(t) = \begin{cases} x_2 + 3t(x_1-x_2) & \text{if} \quad t\in[0,\frac{1}{3}] \\ x_1 + (3t-1)(y_1-x_1) + \phi_1(3t-1) & \text{if} \quad t\in[\frac{1}{3},\frac{2}{3}] \\ y_1 + (3t-2)(y_2-y_1) & \text{if} \quad t\in[\frac{2}{3},1] \end{cases}.$$

We have that

$$G(x_2,y_2) \leq \int_0^1 \frac{|y_2-x_2+\dot{\phi}_2(t)|}{f(x_2+t(y_2-x_2)+\phi_2(t))}dt =$$

$$
\begin{aligned}
= & \int_0^{\frac{1}{3}} \frac{3|x_1 - x_2|}{f(x_2 + 3t(x_1 - x_2))} dt + \\
& + \int_{\frac{1}{3}}^{\frac{2}{3}} \frac{3|y_1 - x_1 + \dot{\phi}_1(3t-1)|}{f(x_1 + (3t-1)(y_1 - x_1) + \phi_1(3t-1))} dt + \\
& + \int_{\frac{2}{3}}^{1} \frac{3|y_2 - y_1|}{f(y_1 + (3t-2)(y_2 - y_1))} dt \leq \\
\leq & \frac{|x_1 - x_2|}{\min_x f} + \int_0^1 \frac{|y_1 - x_1 + \dot{\phi}_1(t)|}{f(x_1 + t(y_1 - x_1) + \phi_1(t))} dt + \frac{|y_1 - y_2|}{\min_x f}.
\end{aligned}
$$

Since this inequality is satisfied for any $\phi_1 \in H_0^1(0,1)$, we have verified that

$$
G(x_2, y_2) - G(x_1, y_1) \leq \frac{|x_1 - x_2|}{\min_x f} + \frac{|y_1 - y_2|}{\min_x f}.
$$

By symmetry of x, y, we reach the conclusion of the lemma. ■

Lemma 3 *(i) In formula (2.12), the starting point of the curves in the family $\mathcal{D}_D^{0,\lambda}$ is arbitrary:*

$$
F(\lambda) = \limsup_{D\to\infty} \frac{D}{\inf_{\gamma\in\mathcal{D}_D^{0,\lambda}} T(\gamma)} = \limsup_{D\to\infty} \frac{D}{\inf_{\gamma\in\mathcal{D}_D^{\lambda}} T(\gamma)},
$$

where $\mathcal{D}_D^{\lambda}$ is the set of all H^1 paths connecting x with $x + \frac{\lambda}{|\lambda|}D$ for some $x \in \mathbb{R}^N$.

(ii) The lim sup *occurring in formula (2.12) is actually a limit.*

Proof: (i) By considering the $[0,1]$ parametrizations of the paths in $\mathcal{D}_D^{0,\lambda}$, we get

$$
\inf_{\gamma\in\mathcal{D}_D^{0,\lambda}} T(\gamma) = \inf_{\phi\in H_0^1(0,1)} \int_0^1 \frac{|\frac{\lambda}{|\lambda|}D + \dot{\phi}(t)|}{f(\frac{\lambda}{|\lambda|}D + \phi(t))} dt = G(0, \frac{\lambda}{|\lambda|}D).
$$

Then Lemma 2 yields

$$
\frac{1}{D} \inf_{\gamma\in\mathcal{D}_D^{0,\lambda}} T(\gamma) \leq \frac{1}{D} \inf_{\gamma\in\mathcal{D}_D^{x,\lambda}} T(\gamma) + \frac{2|x|}{D \min_y f(y)}, \quad \forall D > 0, \forall x \in \mathbb{R}^N. \tag{2.21}
$$

By the definition of lim sup, there exists a sequence $D_n \to \infty$ such that

$$
\limsup_{D\to\infty} \frac{D}{\inf_{\gamma\in\mathcal{D}_D^{0,\lambda}} T(\gamma)} = \lim_{n\to\infty} \frac{D_n}{\inf_{\gamma\in\mathcal{D}_{D_n}^{0,\lambda}} T(\gamma)}.
$$

Since $\frac{2|x|}{D \min_y f(y)} \to 0$ as $D \to \infty$, (2.21) implies

$$
\begin{aligned}
\limsup_{D\to\infty} \frac{D}{\inf_{\gamma\in\mathcal{D}_D^{0,\lambda}} T(\gamma)} & \leq \liminf_{n\to\infty} \frac{D_n}{\inf_{\gamma\in\mathcal{D}_{D_n}^{x,\lambda}} T(\gamma)} \leq \\
& \leq \limsup_{D\to\infty} \frac{D}{\inf_{\gamma\in\mathcal{D}_D^{x,\lambda}} T(\gamma)}, \quad \forall x \in \mathbb{R}^N.
\end{aligned}
$$

The converse inequality follows in a similar manner, so we have proved

$$\limsup_{D\to\infty} \frac{D}{\inf_{\gamma\in\mathcal{D}_D^{0,\lambda}} T(\gamma)} = \limsup_{D\to\infty} \frac{D}{\inf_{\gamma\in\mathcal{D}_D^{x,\lambda}} T(\gamma)}, \quad \forall x \in \mathbb{R}^N.$$

from which we reach our assertion.

(ii) Let $\xi = \frac{\lambda}{|\lambda|}$ and

$$L = \liminf_{D\to\infty} \frac{1}{D} \inf_{\gamma\in\mathcal{D}_D^{0,\lambda}} T(\gamma) = \liminf_{D\to\infty} \frac{G(0, D\xi)}{D}.$$

Fix some $\varepsilon > 0$. By the definition of lim inf, there exists some $d_\varepsilon \geq \frac{3\sqrt{N}}{\varepsilon \min_x f(x)}$ for which

$$|L - \frac{G(0, d_\varepsilon\xi)}{d_\varepsilon}| \leq \frac{\varepsilon}{3}.$$

Pick some integer k with $k \geq \frac{3}{\varepsilon \min_x f(x)}$. Let $D_\varepsilon = kd_\varepsilon$ and choose some arbitrary D with $D > D_\varepsilon$.

Obviously, there has to exist some integer m, with $m \geq k$, for which $D \in (md_\varepsilon, (m+1)d_\varepsilon]$. Then Lemma 2 implies

$$G(0, D\xi) \leq G(0, md_\varepsilon\xi) + \frac{D - md_\varepsilon}{\min_x f(x)} \leq G(0, md_\varepsilon\xi) + \frac{md_\varepsilon}{\min_x f(x)}.$$

Since $m \geq k$ and $k \geq \frac{3}{\varepsilon \min_x f(x)}$, this yields

$$\begin{aligned} \frac{G(0, D\xi)}{T} &\leq \frac{G(0, D\xi)}{md_\varepsilon} \leq \frac{G(0, md_\varepsilon\xi)}{md_\varepsilon} + \frac{1}{m \min_x f(x)} \leq \\ &\leq \frac{G(0, md_\varepsilon\xi)}{md_\varepsilon} + \frac{1}{k \min_x f(x)} \leq \frac{G(0, md_\varepsilon\xi)}{md_\varepsilon} + \frac{\varepsilon}{3}. \end{aligned} \tag{2.22}$$

On the other hand, we clearly have

$$G(0, md_\varepsilon\xi) \leq G(0, (m-1)d_\varepsilon\xi) + G((m-1)d_\varepsilon\xi, md_\varepsilon\xi). \tag{2.23}$$

Since $(m-1)d_\varepsilon \in \mathbb{R}^N$, there exists some $y \in \mathbb{Z}^N$ such that $|y - (m-1)d_\varepsilon| \leq \frac{\sqrt{N}}{2}$. Due to the periodicity of f, we have that

$$G(y, y + d_\varepsilon\xi) = G(0, d_\varepsilon\xi).$$

By Lemma 2 and this last equality, (2.23) becomes

$$\begin{aligned} G(0, md_\varepsilon\xi) &\leq G(0, (m-1)d_\varepsilon\xi) + G(y, y + d_\varepsilon\xi) + 2\frac{|y - (m-1)d_\varepsilon|}{\min_x f(x)} \leq \\ &\leq G(0, (m-1)d_\varepsilon\xi) + G(0, d_\varepsilon\xi) + \frac{\sqrt{N}}{\min_x f(x)}. \end{aligned}$$

Iterating this inequality, we obtain

$$G(0, md_\varepsilon\xi) \leq mG(0, d_\varepsilon\xi) + (m-1)\frac{\sqrt{N}}{\min_x f(x)}.$$

Recalling the two assumptions we made on d_ε,

$$\begin{aligned}\frac{G(0, md_\varepsilon\xi)}{md_\varepsilon} &\leq \frac{G(0, d_\varepsilon\xi)}{d_\varepsilon} + \frac{m-1}{m}\frac{\sqrt{N}}{d_\varepsilon \min_x f(x)} \leq \\ &\leq L + \frac{\varepsilon}{3} + \frac{\sqrt{N}}{d_\varepsilon \min_x f(x)} \leq L + \frac{2\varepsilon}{3}. \end{aligned} \tag{2.24}$$

Adding the inequalities (2.22) and (2.24), we get

$$\frac{G(0, D\xi)}{D} \leq L + \varepsilon = \liminf_{D\to\infty} \frac{G(0, D\xi)}{D} + \varepsilon, \quad \forall\, T > T_\varepsilon,$$

which finally allows us to conclude that

$$\liminf_{D\to\infty} \frac{G(0, D\xi)}{D} = L = \lim_{D\to\infty} \frac{G(0, D\xi)}{D}.$$

This equality is sufficient to establish our assertion. ■

We now present our main results.

Theorem 2 *If f is Lipschitz continuous, Y-periodic and $f > 0$, the effective Hamiltonian is given by*

$$\bar{H}(p) = \sup_\lambda \Big(|p| \cos(\lambda, p) \lim_{D\to\infty} \frac{D}{\inf_{\gamma\in\mathcal{D}_D^\lambda} T(\gamma)} \Big) = \lim_{D\to\infty} \sup_{\gamma\in\mathcal{D}_D} \frac{p\cdot d(\gamma)}{T(\gamma)}, \tag{2.25}$$

where $d(\gamma)$ denotes the distance vector between the two endpoints of γ and $\mathcal{D}_D$ is the set of all H^1 paths with $|d(\gamma)| = D$.

The effective Hamiltonian is an even function of p and varies linearly with its length $|p|$.

Proof: The first equality is a direct consequence of the lemmas above, while for the second one we need to prove that the limit can be interchanged with the supremum.

Since the expression inside the supremum depends only on the direction of λ, it is enough to consider only the unit length vectors ($\lambda \in \partial B_1(0)$). Let us pass to the limit (as $D \to \infty$) in the inequality

$$\sup_{\lambda\in\partial B_1(O)} \frac{Dp\cdot\lambda}{\inf_{\gamma\in\mathcal{D}_D^\lambda} T(\gamma)} \geq \frac{Dp\cdot\lambda}{\inf_{\gamma\in\mathcal{D}_D^\lambda} T(\gamma)}.$$

Since the right-hand term has a limit, we get

$$\liminf_{D\to\infty} \sup_{\lambda\in\partial B_1(O)} \frac{Dp\cdot\lambda}{\inf_{\gamma\in\mathcal{D}_D^\lambda} T(\gamma)} \geq \lim_{D\to\infty} \frac{Dp\cdot\lambda}{\inf_{\gamma\in\mathcal{D}_D^\lambda} T(\gamma)}.$$

This stays true for any λ, so it must be that

$$\liminf_{D\to\infty} \sup_{\lambda\in\partial B_1(O)} \frac{Dp\cdot\lambda}{\inf_{\gamma\in\mathcal{D}_D^\lambda} T(\gamma)} \geq \sup_{\lambda\in\partial B_1(0)} \lim_{D\to\infty} \frac{Dp\cdot\lambda}{\inf_{\gamma\in\mathcal{D}_D^\lambda} T(\gamma)}. \tag{2.26}$$

We now aim at the complementary inequality. By the definition of lim sup and the compactness of $\partial B_1(0)$ (note that the expression inside the supremum is continuous with respect to λ, by Lemma 2, so the supremum becomes a maximum), we capture two sequences $D_n \to \infty$ and $\{\lambda_n\}_{n\in\mathbb{N}} \in \partial B_1(0)$ such that

$$\limsup_{D\to\infty} \sup_{\lambda\in\partial B_1(0)} \frac{D\lambda\cdot p}{\inf_{\gamma\in\mathcal{D}_D^\lambda} T(\gamma)} = \lim_{n\to\infty} \frac{D_n\lambda_n\cdot p}{\inf_{\gamma\in\mathcal{D}_{D_n}^{\lambda_n}} T(\gamma)}.$$

Using again the compactness of $\partial B_1(0)$, we may assume that the sequence λ_n converges to some $\lambda \in \partial B_1(0)$ (restrict to a subsequence if not).

A direct application of Lemma 2 gives

$$\begin{aligned} &\inf_{\gamma\in\mathcal{D}_{D_n}^{\lambda_n}} T(\gamma) = G(0, D_n\lambda_n) \geq \\ \geq\ & G(0, D_n\lambda) - \frac{D_n|\lambda-\lambda_n|}{\min_x f(x)} = \inf_{\gamma\in\mathcal{D}_{D_n}^{\lambda}} T(\gamma) - \frac{D_n|\lambda-\lambda_n|}{\min_x f(x)}. \end{aligned}$$

Thus

$$\frac{\inf_{\gamma\in\mathcal{D}_{D_n}^{\lambda_n}} T(\gamma)}{D_n} \geq \frac{\inf_{\gamma\in\mathcal{D}_{D_n}^{\lambda}} T(\gamma)}{D_n} - \frac{|\lambda-\lambda_n|}{\min_x f(x)}$$

and, since $\lambda_n\cdot p \to \lambda\cdot p$ as $n\to\infty$,

$$\begin{aligned} &\limsup_{D\to\infty} \sup_{\lambda\in\partial B_1(0)} \frac{D\lambda\cdot p}{\inf_{\gamma\in\mathcal{D}_D^\lambda} T(\gamma)} = \lim_{n\to\infty} \frac{D_n\lambda_n\cdot p}{\inf_{\gamma\in\mathcal{D}_{D_n}^{\lambda_n}} T(\gamma)} \leq \\ \leq\ & \lim_{n\to\infty} \frac{D_n\lambda\cdot p}{\inf_{\gamma\in\mathcal{D}_{D_n}^{\lambda}} T(\gamma)} = \lim_{D\to\infty} \frac{D\lambda\cdot p}{\inf_{\gamma\in\mathcal{D}_D^\lambda} T(\gamma)} \leq \\ \leq\ & \sup_{\lambda\in\partial B_1(0)} \lim_{D\to\infty} \frac{D\lambda\cdot p}{\inf_{\gamma\in\mathcal{D}_D^\lambda} T(\gamma)}. \end{aligned}$$

This inequality and (2.26) conclude the proof. ■

Theorem 3 *The effective velocity behaves monotonically with respect to f.*

Proof: Using (2.25), we see that $f_1 \leq f_2$ implies

$$\int_\gamma \frac{dl}{f_1} \geq \int_\gamma \frac{dl}{f_2}, \quad \forall\ \gamma,$$

which yields

$$\sup_{\gamma\in\mathcal{D}_D} \frac{p\cdot d(\gamma)}{\int_\gamma \frac{dl}{f_1}} \leq \sup_{\gamma\in\mathcal{D}_D} \frac{p\cdot d(\gamma)}{\int_\gamma \frac{dl}{f_2}}, \quad \forall\ D,$$

hence $H_1(p) \leq H_2(p)$, $\forall p \in \mathbb{R}^N$. ■

Theorem 4 *If f is Lipschitz continuous, Y-periodic and $f > 0$, the effective Hamiltonian is given by*

$$\bar{H}(p) = \lim_{T\to\infty} \sup_{\gamma\in\mathcal{T}_T} \frac{p \cdot d(\gamma)}{T(\gamma)}, \tag{2.27}$$

where $\mathcal{T}_T$ is the set of all H^1 paths with $T(\gamma) = T$.

Proof: Define

$$S(T) = \sup_{\gamma\in\mathcal{T}_T} \frac{p \cdot d(\gamma)}{T(\gamma)}.$$

Fix some positive small ε. For any T, we may find some $\gamma_\varepsilon \in \mathcal{T}_T$ such that

$$S(T) - \frac{\varepsilon}{2} < \frac{p \cdot d(\gamma_\varepsilon)}{T(\gamma_\varepsilon)} \leq \sup_{\gamma\in\mathcal{D}_{|d(\gamma_\varepsilon)|}} \frac{p \cdot d(\gamma)}{T(\gamma)}. \tag{2.28}$$

Consider the path $\tilde{\gamma}$ described by $y(s)p$ for $s \in [0, T]$, where y is the solution of the initial value problem

$$\begin{cases} \dot{y}(s) = \frac{f(y(s)p)}{|p|} \\ y(0) = 0 \end{cases}.$$

It is easy to see that $\tilde{\gamma} \in \mathcal{T}_T$ and that

$$|d(\gamma)| = \int_\gamma dl = \int_0^T |\dot{y}(s)p| ds \geq T \min_x f(x).$$

We infer that $S(T)$ is bounded from below for any T:

$$S(T) \geq |p| \min_x f(x).$$

Plugging this into (2.28), we've found some $\gamma_\varepsilon \in \mathcal{T}_T$ such that

$$|d(\gamma_\varepsilon)| > \frac{T(|p| \min_x f(x) - \frac{\varepsilon}{2})}{|p|}. \tag{2.29}$$

Now, using (2.25), we find a positive D_ε such that

$$\sup_{\gamma\in\mathcal{D}_D} \frac{p \cdot d(\gamma)}{T(\gamma)} < \bar{H}(p) + \frac{\varepsilon}{2}, \quad \forall D \geq D_\varepsilon. \tag{2.30}$$

Let $T_\varepsilon = \frac{|p| D_\varepsilon}{|p| \min_x f(x) - \frac{\varepsilon}{2}}$. For any $T \geq T_\varepsilon$, it follows from (2.29) that

$$|d(\gamma_\varepsilon)| > \frac{T(|p| \min_x f(x) - \frac{\varepsilon}{2})}{|p|} \geq \frac{T_\varepsilon(|p| \min_x f(x) - \frac{\varepsilon}{2})}{|p|} = D_\varepsilon,$$

so (2.30) and (2.28) yield

$$S(T) < \bar{H}(p) + \varepsilon, \quad \forall T \geq T_\varepsilon.$$

Thus

$$\limsup_{T\to\infty} S(T) \leq \bar{H}(p). \tag{2.31}$$

We now aim at the converse inequality. Fix some small positive ε and use (2.25) to obtain D_ε for which

$$\bar{H}(p) - \varepsilon < \sup_{\gamma\in\mathcal{D}_{D_\varepsilon}} \frac{p\cdot d(\gamma)}{T(\gamma)}.$$

Then there exists some path $\gamma_\varepsilon \in \mathcal{D}_{D_\varepsilon}$ such that

$$\bar{H}(p) - \varepsilon < \frac{p\cdot d(\gamma_\varepsilon)}{T(\gamma_\varepsilon)} \leq S(T_\varepsilon),$$

where $T_\varepsilon = T(\gamma_\varepsilon)$. But

$$T(\gamma_\varepsilon) \geq \frac{\int_{\gamma_\varepsilon} dl}{\max_x f(x)} \geq \frac{|d(\gamma_\varepsilon)|}{\max_x f(x)} = \frac{D_\varepsilon}{\max_x f(x)},$$

so we've found some T_ε larger than $\frac{D_\varepsilon}{\max_x f(x)}$ for which

$$\bar{H}(p) - \varepsilon < S(T_\varepsilon).$$

This is enough to infer that

$$\limsup_{T\to\infty} S(T) \geq \bar{H}(p).$$

All we have now left to show is that the lim sup above is a full limit and this can be done as in the proof of Lemma 3 (ii). ■

Corollary 1 *An alternative representation for the effective Hamiltonian is*

$$\bar{H}(p) = \lim_{T\to\infty} \sup\Big(\frac{p\cdot(x(T)-x(0))}{T} | x \in H^1(0,T), |\dot{x}| = f(x)\Big). \tag{2.32}$$

Proof: For any path in $\mathcal{T}_T$, we choose the parametrization $x(s)$, $s \in [0,S]$, given by

$$\frac{ds}{dl} = \frac{1}{f(x(s))}.$$

Such parametrizations always lie on the interval $[0,t]$ since

$$S = \int_0^S ds = \int_\gamma \frac{dl}{f} = T(\gamma) = T$$

and they verify

$$|\dot{x}(s)| = \frac{dl}{ds} = f(x(s)).$$

Conversely, any $x \in H^1(0,T)$ that satisfies $|\dot{x}| = f(x)$ describes a path γ with

$$T(\gamma) = \int_\gamma \frac{dl}{f} = \int_0^T \frac{|\dot{x}(s)|}{f(x(s))} ds = T,$$

so (2.32) follows from Theorem 4. ■

One other variational principle for the effective Hamiltonian has been obtained by Concordel in [10]. While its proof is presented for Hamiltonians with superlinear growth as $|p| \to \infty$ and the result is false for Hamiltonians with sublinear growth (a simple counterexample is given by $H(x,p) = |p|^{\frac{1}{2}}$), the corollary above allows us to extend it to our case.

Theorem 5 *If f is Lipschitz continuous, Y-periodic and $f > 0$, the effective Hamiltonian is given by*

$$\bar{H}(p) = \lim_{T\to\infty} \sup_{x\in H^1(0,T)} \frac{1}{T} \int_0^T [p \cdot \dot{x}(t) - L(\dot{x}(t), x(t))]dt, \tag{2.33}$$

where L is the Lagrangian described in (2.10).

Proof: Denote by $S(p,T)$ the supremum occurring in the right-hand term of (2.33). Using (2.10),

$$S(p,T) = \sup\{\frac{1}{T}\int_0^T p \cdot \dot{x}(t)dt | x \in H^1(0,T), |\dot{x}| \leq f(x)\}.$$

Pick some $x \in H^1(0,T)$ with $|\dot{x}| \leq f(x)$ on $[0,T]$ and pose the following initial value problem on $[0,T]$:

$$\begin{cases} \frac{ds}{dt} = \frac{|\dot{x}(t)|}{f(x(t))} \\ s(0) = 0 \end{cases}$$

Since $|\dot{x}| \leq f(x)$ on $[0,T]$ and $s(0) = 0$,

$$T = \int_0^T dt \geq \int_0^T \frac{|\dot{x}(t)|}{f(x(t))} dt = \int_0^{s(T)} ds = s(T) = S,$$

and we have equality if and only if $|\dot{x}| = f(x)$ on $[0,T]$. Moreover, due to the strict positiveness of f, the function $s(t)$ is invertible, so we may define $y \in H^1(0,T)$ by

$$y(s) = \begin{cases} x(t(s)), & \text{if} \quad s \in [0,S] \\ x(T) + (s-S)\min_z f(z)p, & \text{if} \quad s \in [S,T] \end{cases}.$$

Then

$$\begin{aligned}\int_0^T p\cdot\dot{y}(s)ds &= \int_0^S p\cdot\dot{y}(s)ds+\int_S^T p\cdot\dot{y}(s)ds\\ &= \int_0^T p\cdot\dot{x}(t)dt+(T-S)\min_z f(z)p^2\geq\int_0^T p\cdot\dot{x}(t)dt\end{aligned}$$

and the inequality is strict unless $T=S$. All this leads to the conclusion that, for the evaluation of $S(p,T)$, it is sufficient to consider those functions $x\in H^1(0,T)$ with $|\dot{x}|=f(x)$ on $[0,T]$. Then

$$\begin{aligned}S(p,T) &= \sup\{\frac{1}{T}\int_0^T p\cdot\dot{x}(t)dt|x\in H^1(0,T),|\dot{x}|=f(x)\}\\ &= \sup\{\frac{p\cdot|x(T)-x(0)|}{T}|x\in H^1(0,T),|\dot{x}|=f(x)\},\end{aligned}$$

hence (2.32) implies (2.33). ■

Theorem 6 *If f is Lipschitz continuous, Y-periodic and $f>0$, the effective Hamiltonian is given by*

$$\bar{H}(p)=\lim_{P\to\infty}\sup_{\gamma\in\mathcal{P}_P}\frac{p\cdot d(\gamma)}{T(\gamma)}, \tag{2.34}$$

where $\mathcal{P}_P$ is the set of all H^1 paths with $p\cdot d(\gamma)=P$.

Proof: Define

$$S(P)=\sup_{\gamma\in\mathcal{P}_P}\frac{p\cdot d(\gamma)}{T(\gamma)}.$$

Fix some positive small ε. Using (2.25), we find a positive D_ε such that

$$\sup_{\gamma\in\mathcal{D}_D}\frac{p\cdot d(\gamma)}{T(\gamma)}<\bar{H}(p)+\frac{\varepsilon}{2},\quad\forall D\geq D_\varepsilon. \tag{2.35}$$

Let $P_\varepsilon=|p|D_\varepsilon$. For any $P\geq P_\varepsilon$, we may find some $\gamma_\varepsilon\in\mathcal{P}_P$ such that

$$S(P)-\frac{\varepsilon}{2}<\frac{p\cdot d(\gamma_\varepsilon)}{T(\gamma_\varepsilon)}<\sup_{\gamma\in\mathcal{D}_{|d(\gamma_\varepsilon)|}}\frac{p\cdot d(\gamma)}{T(\gamma)}. \tag{2.36}$$

But

$$|d(\gamma_\varepsilon)|\geq\frac{p\cdot d(\gamma_\varepsilon)}{|p|}=\frac{P}{|p|}\geq\frac{P_\varepsilon}{|p|}=D_\varepsilon,$$

so (2.35) and (2.36) yield

$$S(P)<\bar{H}(p)+\varepsilon,\quad\forall P\geq P_\varepsilon,$$

which implies

$$\limsup_{P\to\infty}S(P)\leq\bar{H}(p). \tag{2.37}$$

We now aim at the converse inequality. Fix some small positive ε and use (2.25) to obtain D_ε for which

$$\bar{H}(p) - \varepsilon < \sup_{\gamma \in \mathcal{D}_{D_\varepsilon}} \frac{p \cdot d(\gamma)}{T(\gamma)}.$$

Then there exists some path $\gamma_\varepsilon \in \mathcal{D}_{D_\varepsilon}$ such that

$$\bar{H}(p) - \varepsilon < \frac{p \cdot d(\gamma_\varepsilon)}{T(\gamma_\varepsilon)} \leq S(P_\varepsilon), \tag{2.38}$$

where $P_\varepsilon = p \cdot d(\gamma_\varepsilon)$. But

$$T(\gamma_\varepsilon) \geq \frac{\int_{\gamma_\varepsilon} dl}{\max_x f(x)} \geq \frac{|d(\gamma_\varepsilon)|}{\max_x f(x)} = \frac{D_\varepsilon}{\max_x f(x)},$$

so (2.38) gives

$$P_\varepsilon > (\bar{H}(p) - \varepsilon) \frac{D_\varepsilon}{\max_x f(x)}.$$

Thus, we have found some P_ε larger than $(\bar{H}(p) - \varepsilon)\frac{D_\varepsilon}{\max_x f(x)}$ for which

$$\bar{H}(p) - \varepsilon < S(P_\varepsilon).$$

This is enough to infer that

$$\limsup_{P \to \infty} S(P) \geq \bar{H}(p).$$

All we have now left to show is that the lim sup above is a full limit and this can be done as in the proof of Lemma 3 (ii). ■

Theorem 7 *The effective normal velocity is continuous with respect to variations of f in $C(\mathbb{R}^N)$.*

Proof: Consider two Y-periodic continuous functions f_1 and f_2 and set

$$m_i = \min_x f_i(x), M_i = \max_x f_i(x), m = \min(m_1, m_2), M = \max(M_1, M_2),$$
$$H_i(p) = \lim_{P \to \infty} \sup_{\gamma \in \mathcal{P}_P} \frac{P}{\int_\gamma \frac{dl}{f_i}}.$$

Assume that these two functions are close in the $C(\mathbb{R}^N)$ topology:

$$\|f_1 - f_2\| = \sup_{x \in Y} |f_1(x) - f_2(x)| < \varepsilon$$

for some small positive ε.

For fixed $|p|$ and P, we may get a bound for the supremum in (2.34) by considering the segment $[0, P\frac{p}{|p|}]$:

$$S(P) = \sup_{\gamma \in \mathcal{P}_P} \frac{P}{T(\gamma)} \geq |p| \min_x f(x).$$

Thus, for the evaluation of H_1 and H_2 above, we may restrict the classes $\mathcal{P}_P$ by imposing the suplimentary inequality

$$\int_\gamma dl \leq \frac{MP}{m|p|}.$$

Then, for any path $\gamma \in \mathcal{P}_P$, we have

$$|\frac{\int_\gamma \frac{dl}{f_1}}{P} - \frac{\int_\gamma \frac{dl}{f_2}}{P}| \leq \frac{\|\frac{1}{f_1} - \frac{1}{f_2}\| \int_\gamma dl}{P} \leq \frac{M\varepsilon}{|p|m^3}.$$

This implies

$$|\inf_{\gamma \in \mathcal{P}_P} \frac{\int_\gamma \frac{dl}{f_1}}{P} - \inf_{\gamma \in \mathcal{P}_P} \frac{\int_\gamma \frac{dl}{f_2}}{P}| \leq \frac{M\varepsilon}{|p|m^3}.$$

Since the inequality above is uniform with respect to P, it gets transported to the limit, proving our continuity assertion. ■

Remark 1 *Theorems 2, 3, 4, 5, 6 and 7 can easily be extended to the anisotropic case. More exactly, if we allow f to have some directional dependence ($f(x,p) = f(x, \frac{p}{|p|})$), the only modification in the formulae for the effective Hamiltonian (2.25), (2.27), (2.32) and (2.34) is that f should be replaced with*

$$\tilde{f}(x,q) = \sup_{\cos(p,q)>0} \frac{f(x,p)}{cos(p,q)}.$$

2.5 Some bounds

We now obtain some bounds that are sharper than the ones in (2.9).

To obtain a lower bound on F (which is connected to $\bar{v}_n$ through (2.14)), start with some λ with $|\lambda| > F(\lambda)$. Writing (2.18) for $\phi = 0$, we get

$$D < |\lambda| \int_0^D \frac{1}{f(\lambda t)} dt \leq |\lambda| \sup_{\phi \in H_0^1(0,D)} \int_0^D \frac{1}{f(\lambda t + \phi(t))} dt.$$

Since this is true for any λ with $|\lambda| > F(\lambda)$, we conclude that we must have

$$F(\lambda) \geq D(\int_0^D \frac{1}{f(\lambda t)} dt)^{-1} \geq D \inf_{\phi \in H_0^1(0,D)} (\int_0^D \frac{1}{f(\lambda t + \phi(t))} dt)^{-1}.$$

This relation holds for any D sufficiently large, so it yields the following bound on F:

$$\begin{aligned} F(\lambda) &\geq \limsup_{D\to\infty}(D(\int_0^D \frac{1}{f(\lambda t)}dt)^{-1}) \geq \\ &\geq \limsup_{D\to\infty}(D \inf_{\phi\in H_0^1(0,D)}(\int_0^D \frac{1}{f(\lambda t+\phi(t))}dt)^{-1}). \end{aligned} \tag{2.39}$$

For an upper bound, start with some λ with $|\lambda| < F(\lambda)$. By (2.13), $\bar{L}(\lambda) = 0$, so (2.15) implies that there exists a sequence $D_n \to \infty$ and $\phi_n \in H_0^1(0, D_n)$ such that $|\lambda + \dot{\phi_n}(t)| \leq f(\lambda t + \phi_n(t))$, a.e. in $[0, D_n]$. This yields

$$\begin{aligned} |\lambda| &= |\frac{1}{D_n}\int_0^{D_n}(\lambda+\dot{\phi}_n(t))dt| \leq \frac{1}{D_n}\int_0^{D_n}|\lambda+\dot{\phi}_n(t)|dt \leq \\ &\leq \frac{1}{D_n}\int_0^{D_n} f(\lambda t+\phi_n(t))dt \leq \frac{1}{D_n}\sup_{\phi\in H_0^1(0,D_n)}\int_0^{D_n} f(\lambda t+\phi(t))dt. \end{aligned}$$

This relation stays true for a subsequence $D_n \to \infty$, so we must have that

$$|\lambda| \leq \limsup_{D\to\infty}\frac{1}{D}\sup_{\phi\in H_0^1(0,D)}\int_0^D f(\lambda t+\phi(t))dt.$$

Since this holds for any λ with $|\lambda| < F(\lambda)$, we conclude that

$$F(\lambda) \leq \limsup_{D\to\infty}\frac{1}{D}\sup_{\phi\in H_0^1(0,D)}\int_0^D f(\lambda t+\phi(t))dt. \tag{2.40}$$

Using (2.14), (2.39) and (2.40) yield upper and lower bounds on $\bar{v}_n$ and $\bar{H}$.

2.6 Examples

In the previous sections, we needed to assume certain smoothness of f (Lipschitz continuity or even $W^{1,\infty}$ regularity for Proposition 1 to hold). However, some classical examples of composite materials provide a discontinuous f, while the expressions for the effective Hamiltonian that we've reached make sense for a larger class of normal velocity laws and the monotonicity indicated in Theorem 3 remains true.

We also needed the strict positivity of f. We note again, that the variational principles can continue to make sense in some examples even when f changes sign. Specifically, when regions of negative f are isolated within regions of positive f as in Example 3, these formulas give the effective velocity of the leading front.

Hence, to illustrate our results in some simple cases, we extend our formulas to all functions f for which they make sense.

Example 1 (revisited). Recall that the normal velocity law we looked at in Example 1 was (see (2.3))

$$f(x) = a\cos(\frac{\pi x_1}{2}), \quad \forall x \in \mathbb{R}^2,$$

where a is a positive constant. We make use of (2.25) to calculate $\bar{v}_n(e_2)$.

Note that the inequality

$$f(x) \leq a, \quad \forall x \in \mathbb{R}^2$$

provides the bound

$$\bar{v}_n(p) \leq a, \quad \forall p \in \mathbb{R}^2. \tag{2.41}$$

On the other hand, if we choose in (2.25) γ to be the vertical segment of length D parallel with e_2 and originating in 0, we get

$$\bar{H}(e_2) \geq a = a|e_2|. \tag{2.42}$$

We may now use (2.41) and (2.42) to infer that

$$\bar{v}_n(e_2) = a.$$

However, as we have seen in Section 2.2, this effective normal velocity obtained only gives the velocity with which certain segments of the front are propagating. We conclude that the formulas we obtained in Section 2.4 cannot be extended to all normal velocity laws v_n.

We now use (6) to calculate $\bar{v}_n(e_1)$. Note that, for any $P > 2$ any path γ that belongs to $\mathcal{P}_P$ has to intersect one of the lines $x_1 \in (2\mathbb{Z} - 1)$, hence it will contain a point where f vanishes. Thus the sup occurring in (6) is 0 for any $P > 2$, which implies that

$$\bar{v}_n(e_1) = 0.$$

As we have seen in Section 2.2, this is indeed the effective normal velocity in the e_1 direction, so our results have provided the correct answer.

Example 2 (revisited). The normal velocity law we considered in Example 2 was

$$f(x) = a\cos(\frac{\pi x_1}{2})\cos(\frac{\pi x_2}{2}), \quad \forall x \in \mathbb{R}^2,$$

where a is a positive constant.

We use (6) to calculate $\bar{v}_n(p)$ for some $p \in \mathbb{R}^2$. Using the same line of reasoning as in the previous example, for any $P > 2\sqrt{2}$, any path γ that belongs to $\mathcal{P}_P$ will contain a point where f vanishes, so

the sup occurring in (6) is 0 for any $P > 2\sqrt{2}$, which implies that

$$\bar{v}_n(p) = 0, \quad \forall p \in \mathbb{R}^2.$$

This again agrees with the conclusion we arrived at in Section 2.

Example 3 (revisited). The normal velocity law we considered in Example 3 was (see (2.4))

$$f(x) = \begin{cases} |x - (\frac{1}{2}, \frac{1}{2})|, & \text{if} \quad x \in B_{\frac{1}{4}}(\frac{1}{2}, \frac{1}{2}) \\ \frac{1}{4}, & \text{if} \quad x \in Y_2 \setminus B_{\frac{1}{4}}(\frac{1}{2}, \frac{1}{2}) \end{cases}.$$

The inequality

$$f(x) \leq \frac{1}{4}, \quad \forall x \in \mathbb{R}^2,$$

provides the bound

$$\bar{v}_n(p) \leq \frac{1}{4}, \quad \forall p \in \mathbb{R}^2. \tag{2.43}$$

Now choose in (2.25) γ to be the vertical segment of length D parallel with e_2 and originating in 0 and get

$$\bar{H}(e_2) \geq \frac{1}{4} = \frac{1}{4}|e_2|. \tag{2.44}$$

From (2.43) and (2.44) we get

$$\bar{v}_n(e_2) = \frac{1}{4}.$$

Comparing with our observations in Section 2, we see that our formula was able to ignore the traces that the front leaves around the points where f vanishes and to pick up the velocity with which the leading part is propagating.

Example 4. Set $N = 2$ and consider a laminated composite with the normal velocity law

$$f(x) = \begin{cases} v_1, & \text{if} \quad x \in [0, \mu] \times [0, 1] \\ v_2, & \text{if} \quad x \in (\mu, 1) \times [0, 1] \end{cases},$$

extended by periodicity to all $\mathbb{R}^2$, where $v_1 > v_2 > 0$, $\mu \in (0, 1)$.

The first step is to compute $F(\lambda)$ for $\lambda \in \partial B_1(0)$. For this, we will use

$$F(\lambda) = \lim_{D \to \infty} \frac{D}{\inf_{\gamma \in \mathcal{D}_D^{0,\lambda}} T(\gamma)}.$$

By symmetry, it is enough to consider those λ's with $\lambda_1 > 0$ and $\lambda_2 \geq 0$. To evaluate the limit above, we choose to pick the sequence $D_n = \frac{n}{\lambda_1}$ (we will deal with the case $\lambda_1 = 0$ separately). In all the regions where f is constant, calculating the infimum occurring in the expression of F reduces to minimizing the distance between the two end points, hence the optimal path will be the connecting

segment. We thus see that all minimizers are piecewise linear. To understand what laws they have to obey in the points where f presents jumps, let us look at the case $n = 1$. Denote h to be the height at which the path crosses the vertical line $x_1 = \mu$. Then

$$T(\gamma) = \frac{\sqrt{\mu^2 + h^2}}{v_1} + \frac{\sqrt{(1-\mu)^2 + (\frac{\lambda_2}{\lambda_1} - h)^2}}{v_2}.$$

At the optimal h, the derivative of this expression should vanish, thus

$$\frac{h}{v_1\sqrt{\mu^2 + h^2}} = \frac{h - \frac{\lambda_2}{\lambda_1}}{v_2\sqrt{(1-\mu)^2 + (\frac{\lambda_2}{\lambda_1} - h)^2}},$$

which is nothing else but the refraction law for the angles made by the optimal path with the horizontal line $x_2 = h$ at the crossing point. Denote them by θ_1 and θ_2 and let θ be the argument of λ to conclude that

$$G(0, (1, \frac{1}{\cos\theta})) = \frac{1}{\cos\theta(\frac{\mu}{v_1\cos\theta_1} + \frac{1-\mu}{v_2\cos\theta_2})}.$$

For $n > 1$, the optimal path will have to obey the refraction law at every jump point of f. But the only path that satisfies this is the one constructed by n repetitions of the two-segments trajectory obtained for $n = 1$, hence

$$F(\lambda) = F(\cos\theta, \sin\theta) = \frac{1}{\cos\theta(\frac{\mu}{v_1\cos\theta_1} + \frac{1-\mu}{v_2\cos\theta_2})}, \tag{2.45}$$

where θ_1 and θ_2 are determined by

$$\begin{cases} \mu\tan\theta_1 + (1-\mu)\tan\theta_2 = \tan\theta \\ \frac{v_1}{\sin\theta_1} = \frac{v_2}{\sin\theta_2} \end{cases}. \tag{2.46}$$

In particular, if $\theta = 0$, then $\theta_1 = \theta_2 = 0$, so

$$F(e_1) = (\frac{\mu}{v_1} + \frac{1-\mu}{v_2})^{(-1)}.$$

It is easy to check that $F(\cos\theta, \sin\theta)\cos\theta \leq F(e_1)$ and thus

$$\bar{v}_n(e_1) = (\frac{\mu}{v_1} + \frac{1-\mu}{v_2})^{(-1)}. \tag{2.47}$$

One way to verify this is the explicit construction of a shape preserving interface moving in the e_1 direction. This is nothing else but a vertical line and indeed it will travel with average speed given by (2.47). By the comparison principle for Hamilton Jacobi equations, any front initially caught between two vertical lines will be trapped between them for good and forced to move in the e_1

direction with the same average velocity.

If $\lambda_1 = 0$ ($\lambda = e_2$), we may write

$$F(\lambda) = \lim_{D\to\infty} \frac{D}{\inf_{\gamma\in\mathcal{D}_D^{y,\lambda}} T(\gamma)},$$

with $y = (\frac{\mu}{2}, 0)$, and easily get $F(e_2) = v_1$. Using (2.46) and the inequality $v_1 > v_2$ we get

$$\frac{\tan\theta}{\frac{\mu}{v_1\cos\theta_1} + \frac{1-\mu}{v_2\cos\theta_2}} \le v_1 \frac{\tan\theta}{\frac{\mu}{\cos\theta_1} + \frac{1-\mu}{\cos\theta_2}} \le v_1 \frac{\tan\theta}{\frac{\mu\sin\theta_1}{\cos\theta_1} + \frac{(1-\mu)\theta_2}{\cos\theta_2}} = v_1,$$

which is nothing else but $F(\cos\theta, \sin\theta)\sin\theta \le F(e_2)$, and thus

$$\bar{v}_n(e_2) = v_1.$$

This again can be verified by an explicit construction of a periodic shape preserving front

$$x_2(x_1) = \begin{cases} 0 & \text{if} \quad x_1 \in [0, \mu] \\ (\mu - x_1)\cot\phi & \text{if} \quad x_1 \in [\mu, \frac{1+\mu}{2}] \\ (x_1 + \mu - 1)\cot\phi & \text{if} \quad x_1 \in [\frac{1+\mu}{2}, 1] \end{cases},$$

with $\phi \in (0, \frac{\pi}{2})$ determined by

$$\sin\phi = \frac{v_2}{v_1}, \tag{2.48}$$

which indeed moves in the e_2 direction with speed v_1.

Note that this last construction can be generalized to yield fronts moving in the direction $(\cos\theta, \sin\theta)$ with speed $v_1\sin\theta$, for angles θ close to $\frac{\pi}{2}$:

$$x_2(x_1) = \begin{cases} 0 & \text{if} \quad x_1 \in [0, \mu] \\ (\mu - x_1)\cot\phi & \text{if} \quad x_1 \in [\mu, 1-l] \\ (x_1 + \mu - 1)\cot\phi - \cot\theta & \text{if} \quad x_1 \in [1-l, 1] \end{cases},$$

with ϕ still given by (2.48) and

$$l = \frac{1 - \mu - \frac{v_2}{\sqrt{v_1^2 - v_2^2}}\cot\theta}{2}.$$

This type of construction stays possible as long as $l > 0$, i.e.,

$$\cot\theta < (1-\mu)\sqrt{\frac{v_1^2}{v_2^2} - 1}. \tag{2.49}$$

All this suggests that the function $F(\cos\theta, \sin\theta)$ has such a steep decrease near the maximal value at $\theta = \frac{\pi}{2}$ that $\bar{v}_n(\cos\theta, \sin\theta)$ is given by $v_1\sin\theta$ for angles θ that satisfy (2.49).

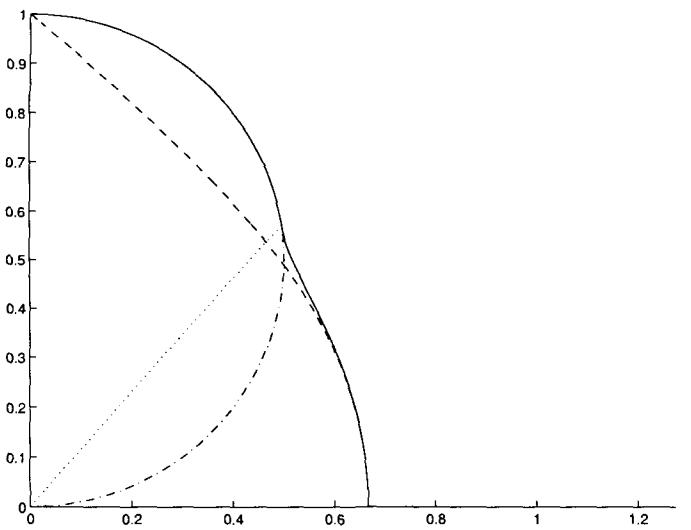

Figure 2.3: Polar plot of the effective normal velocity for a laminate

The system (2.46) can be solved numerically and then F and $\bar{v}_n$ can be calculated from (2.45) and (2.14), respectively. If we fix the three parameters of the problem: $\mu = 0.5$, $v_1 = 1$, $v_2 = 0.5$, we arrive at the values plotted in Figure 2.3. The solid and the dashed lines are the calculated polar plots of v_n and F, respectively, the dash-dot line represents the polar plot of $v_1 \sin\theta$, while the dotted line pictures the smallest angle in the first quadrant that satisfies (2.49). As predicted by the construction, we notice a perfect agreement of the solid and dash-dot lines, for θ between the dotted line and the vertical axis.

These types of constructions may be easily generalized to higher dimensions.

One conclusion is that, for laminated composites, homogenization of isotropic media may give birth to anisotropic ones. This stays true for the chess-board case, as will be seen in the following example.

Example 5. Fix $N = 2$ and consider a checkerboard composite with the normal velocity law

$$f(x) = \begin{cases} v_1, & \text{if} \quad x \in ([0, \frac{1}{2}] \times [\frac{1}{2}, 1]) \cup ([\frac{1}{2}, 1] \times [0, \frac{1}{2}]) \\ v_2, & \text{otherwise} \end{cases},$$

extended by periodicity to all $\mathbb{R}^2$, where $v_1 > v_2 > 0$. Following an example worked out by Acerbi and Buttazzo in [3], we also impose $v_1 \geq 2v_2$; this will allow us to deduce a closed formula for the effective normal velocity.

We may leave aside the case $\lambda_1 = 0$ since it can be straightaway noticed that

$$F(e_2) = \lim_{D \to \infty} \frac{G(0, De_2)}{D} = v_1. \tag{2.50}$$

As in the laminate case, we choose the sequence $D_n = \frac{n}{|\lambda_1|}$ and write that

$$F(\lambda) = \lim_{n\to\infty} \frac{G(0, D_n\lambda)}{D_n} = \lim_{n\to\infty} \frac{D_n}{\inf_{\gamma\in\mathcal{D}_{D_n}^{0,\lambda}} T(\gamma)}, \quad \forall\lambda \in \partial B_1(0). \tag{2.51}$$

Denote by γ_n a minimizer for the infimum occurring above. In all the regions where f is constant, we are left to minimize the distance between the two end points, hence the optimal path will be the connecting segment. We thus see that γ_n is piecewise linear.

Assume for the moment that γ_n contains segments on which the normal velocity equals w. We may construct another path $\tilde{\gamma}_n$ by avoiding the region where $f = w$ and taking a roundabout way that lies on the boundary of the $\frac{1}{2}$-edged square. Since it is possible to choose this roundabout way such that its length is at most twice the length of the straight segment and $v_1 \geq 2v_2$, we are in this way constructing an at-least-as-fast path.

We conclude that γ_n has to be a piecewise linear path contained in the region where $f = v_1$. Moreover, any segment included in γ_n has to be vertical with length $\frac{1}{2}$, horizontal with length $\frac{1}{2}$ or diagonal with length $\frac{\sqrt{2}}{2}$ (with the possible exception of the last one, since $\frac{2n\lambda_2}{\lambda_1}$ does not necessarily have to be an integer). It is then easy to see that the length of γ_n has to satisfy the suplimentary inequality

$$\int_{\gamma_n} dl \geq \frac{n}{|\lambda_1|}((\sqrt{2}-1)\min(|\lambda_1|,|\lambda_2|) + \max(|\lambda_1|,|\lambda_2|)) \tag{2.52}$$

and thus

$$F(\lambda) \leq \frac{v_1}{(\sqrt{2}-1)\min(|\lambda_1|,|\lambda_2|) + \max(|\lambda_1|,|\lambda_2|)}. \tag{2.53}$$

On the other hand, if z is the point of $\mathbb{Z}^2$ closest to $\frac{2n\lambda_2}{\lambda_1}$, we may consider the path γ_n' composed by the adjacent segments $[0, \frac{1}{2}(\min(z_1,z_2), \min(z_1,z_2))]$, $[\frac{1}{2}(\min(z_1,z_2), \min(z_1,z_2)), \frac{z}{2}]$ and $[\frac{z}{2}, \frac{n\lambda}{\lambda_1}]$. We get

$$F(\lambda) \geq \lim_{n\to\infty} \frac{D_n}{T(\gamma_n')} = \frac{v_1}{(\sqrt{2}-1)\min(|\lambda_1|,|\lambda_2|) + \max(|\lambda_1|,|\lambda_2|)}$$

and, by (2.53),

$$F(\lambda) = \frac{v_1}{(\sqrt{2}-1)\min(|\lambda_1|,|\lambda_2|) + \max(|\lambda_1|,|\lambda_2|)}, \quad \forall\lambda \in \partial B_1(0).$$

Using (2.14),

$$\bar{v}_n(p) = \sup_{\lambda\in\partial B_1(0)} \frac{v_1 \cos(\lambda, p)}{(\sqrt{2}-1)\min(|\lambda_1|,|\lambda_2|) + \max(|\lambda_1|,|\lambda_2|)}.$$

Since F is not a constant, neither is $\bar{v}_n$, thus again homogenization of an isotropic medium gave birth to an anisotropic one. This is easily noticed in Figure 2.4, which pictures the polar plots of F (dashed line) and $\bar{v}_n$ (solid line) for the case $v_1 = 1$.

If we drop the restriction $v_1 \geq 2v_2$, we may still argue that the resulting F is not a constant.

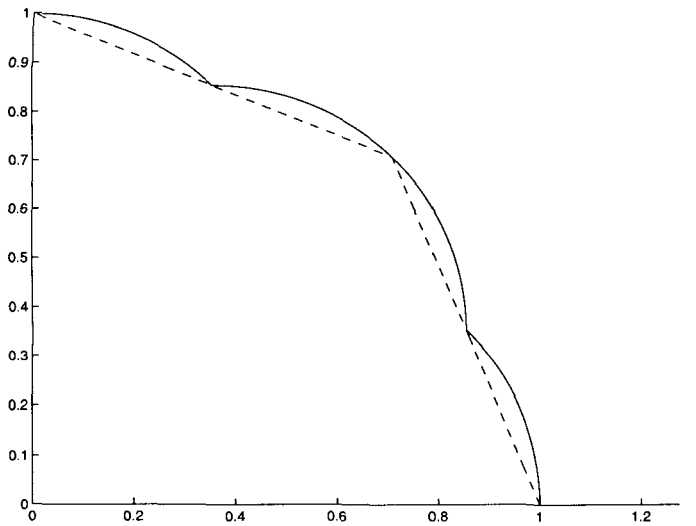

Figure 2.4: Polar plot of the effective normal velocity for the checkerboard example

Indeed, if it were a constant, then (2.50) imposes that $F = v_1$. Since $f \leq v_2$ and any $\gamma \in \mathcal{D}_D^{0,\lambda}$ satisfies $\int_\gamma dl \geq D$, (2.51) yields

$$F(\lambda) \leq v_1 \lim_{n\to\infty} \frac{D_n}{\inf_{\gamma\in\mathcal{D}_{D_n}^{0,\lambda}} \int_\gamma dl} \leq v_1$$

and equality is possible only if there exists a sequence of paths $\gamma_n \in \mathcal{D}_{D_n}^{0,\lambda}$ contained in the region where $f = v_1$ for which $\frac{D_n}{\int_\gamma dl} \to 1$. But (2.52) rules out this possibility unless $\lambda_1 = 0$ or $\lambda_2 = 0$ or $|\lambda_1| = |\lambda_2|$.

We may extend all this to the micro-geometry where the squares on which f is constant get replaced with rectangles congruent to $[0, a_1] \times [0, a_2]$; the corresponding restriction on the two normal velocities is $v_1 \geq \frac{a_1+a_2}{a_2} v_2$. Then

$$\bar{v}_n(p) = \sup_{\lambda\in\partial B_1(0)} \frac{v_1 \cos(\lambda, p)}{\frac{\sqrt{a_1^2+a_2^2}-a_1}{a_2}|\lambda_2| + |\lambda_1|},$$

where we have reiterated the coordinates such that $\frac{|\lambda_1|}{a_1} \geq \frac{|\lambda_2|}{a_2}$.

One other possible extension is to higher dimensions. For the case when $v_1 \geq 2v_2$ we get

$$\bar{v}_n(p) = \sup_{\lambda\in\partial B_1(0)} \frac{v_1 \cos(\lambda, p)}{|\lambda_1| + \sum_{i=2}^N (\sqrt{i} - \sqrt{i-1})|\lambda_i|},$$

where $\{\lambda_i\}_{i=1}^N$ have been reiterated such that $|\lambda_i| \leq |\lambda_j|$ for $i > j$.

Example 6. In a similar manner we may treat a packed-square composite suggested by Con-

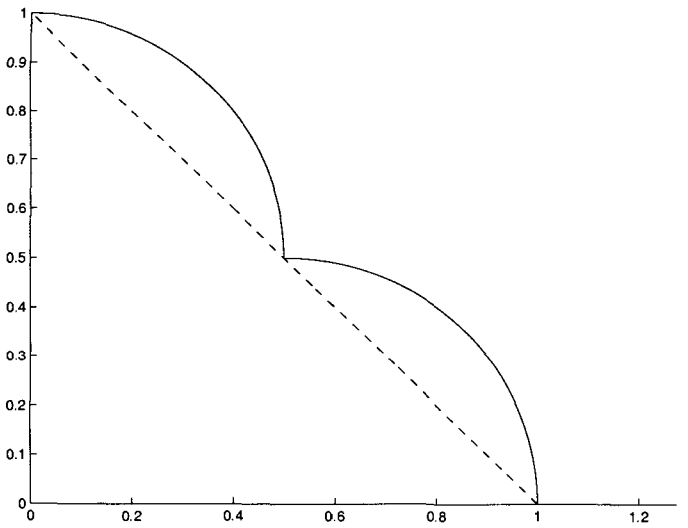

Figure 2.5: Polar plot of the effective normal velocity for the packed squares example

cordel in [11]. Consider a normal velocity law defined on $\mathbb{R}^N$ by

$$f(x) = \begin{cases} v_1, & \text{if } \exists 1 \leq i \leq N \text{ such that } x_j \in \mathbb{Z}, \forall j \neq i \\ v_2, & \text{otherwise} \end{cases},$$

with $v_1 \geq 2v_2 > 0$. Intuitively, this places a grid (obtained by periodically repeating the coordinate planes) with fast normal velocity v_1 in a space with slow normal velocity v_2.

For $\lambda_1 \neq 0$, any minimizer $\gamma_n \in \mathcal{D}_{D_n}^{0,\lambda}$ (where $D_n = \frac{n}{|\lambda_1|}$) will again be piecewise linear, while the inequality satisfied by v_1 and v_2 prevents it from entering the slower speed regions, so that it will be composed only of unit length segments parallel with one of the unit vectors e_i (with the possible exception of the last segment, which may have any length). Then γ_n has to satisfy

$$\int_{\gamma_n} dl \geq \frac{n}{|\lambda_1|} \sum_{i=1}^{N} |\lambda_i|.$$

Constructions analogous to the $\tilde{\gamma}_n$ from the previous example hold and we get

$$\bar{v}_n(p) = \sup_{\lambda \in \partial B_1(0)} \frac{v_1 \cos(\lambda, p)}{\sum_{i=1}^{N} |\lambda_i|}. \tag{2.54}$$

Figure 2.5 pictures the polar plots of F (dashed line) and $\bar{v}_n$ (solid line) for the case $v_1 = 1$.

If the unit cube gets replaced with the parallelepiped $\prod_{i=1}^{N}[0, a_i]$ and $v_1 \geq \frac{a+b}{a} v_2$, where a and b ($a \leq b$) are the smallest two edges of the parallelepiped, (2.54) still holds. Also, it can be proved that the resulting medium is anisotropic even if we drop the requirement $v_1 \geq \frac{a+b}{a} v_2$.

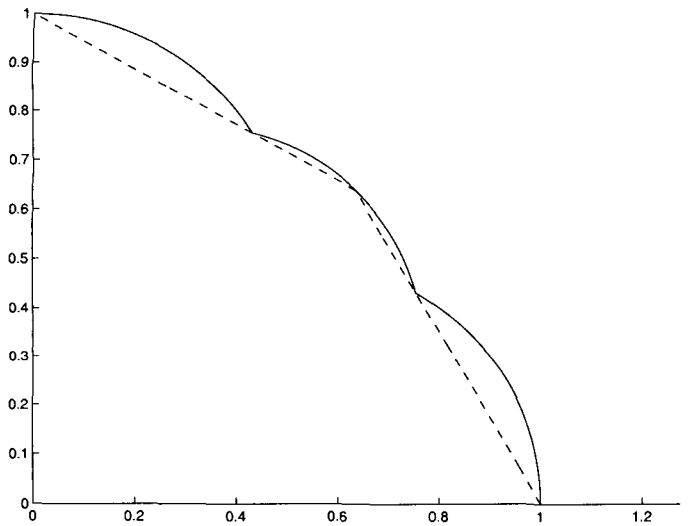

Figure 2.6: Polar plot of the effective normal velocity for the touching disks example

This example may be easily generalized to the case when $f(x)$ equals v_1 whenever k of the coordinates of x are integer (for some k between 1 and $N-1$) and v_2 otherwise.

Example 7. Set $N = 2$ and consider a normal velocity law defined on $[0,1)^2$ by

$$f(x) = \begin{cases} v_1, & \text{if } (x_1 - \frac{1}{2})^2 + (x_2 - \frac{1}{2})^2 < \frac{1}{4} \\ v_2, & \text{otherwise} \end{cases}$$

extended by periodicity to all $\mathbb{R}^2$, where $v_1 \geq \frac{\pi}{2} v_2 > 0$.

The inequality satisfied by v_1 and v_2 prevents minimizers from entering the slower speed regions. Then, for $\lambda_1 \neq 0$, any optimal path $\gamma_n \in \mathcal{D}_{D_n}^{0,\lambda}$ (where $D_n = \frac{n}{|\lambda_1|}$) will be mainly made up by horizontal or vertical unit length segments and quarters of the $\frac{1}{2}$-rayed circle. Thus γ_n has to satisfy

$$\int_{\gamma_n} dl \geq \frac{n}{|\lambda_1|}(\min(|\lambda_1|, |\lambda_2|)(\frac{\pi}{2} - 1) + \max(|\lambda_1|, |\lambda_2|)).$$

Constructions analogous to the $\tilde{\gamma}_n$ from the second example hold and we get

$$\bar{v}_n(p) = \sup_{\lambda \in \partial B_1(0)} \frac{v_1 \cos(\lambda, p)}{\min(|\lambda_1|, |\lambda_2|)(\frac{\pi}{2} - 1) + \max(|\lambda_1|, |\lambda_2|)}.$$

Figure 2.6 pictures the polar plots of F (dashed line) and $\bar{v}_n$ (solid line) for the case $v_1 = 1$.

This example may easily be generalized to the micro-geometry where, instead of a slower speed circle inscribed in the unit square, we have a slower speed ellipse inscribed in the rectangle $[0,a] \times [0,b]$. Also, it can be proved that the resulting homogenized medium is anisotropic even if we drop the requirement $v_1 \geq \frac{\pi}{2} v_2$.

Chapter 3

Effective motion of a curvature driven interface through a heterogeneous medium

3.1 Introduction

This chapter deals with the evolution of fronts propagating with a normal velocity that depends on the position and the mean curvature of the front. The motivation for such a study comes from the normal velocity law that we arrived at in Chapter 1 (see (1.7)). If we assume that the elastic term that depends on the interface is negligible, we are left with a normal velocity law of the form

$$v_n = -f(x) - c\kappa, \tag{3.1}$$

where f is a function that depends on the position only, c is a positive constant (representing the density of the interfacial energy) and κ is the mean curvature of the interface. In particular, if f is heterogeneous on a scale small compared to the domain, then the evolution of the front may be very complicated. It is of interest then to ask if one can define an average or overall front and its propagation; one that captures the essential macroscopic features and ignores the exact microscopic details. This is the issue studied in this chapter.

As in the previous chapter, we write the problem in terms of the level set formulation. If we assume that there exists a smooth function $h : \mathbb{R}^N \times [0,T) \to \mathbb{R}$ such that our front coincides with its zero level set at all times, a simple calculation yields

$$n = \frac{\nabla h}{|\nabla h|}, \ \kappa = \operatorname{div} \frac{\nabla h}{|\nabla h|}$$

and

$$v_n = -\frac{1}{|\nabla h|}\frac{\partial h}{\partial t};$$

so our normal velocity law implies that h satisfies the following equation:

$$\frac{\partial h}{\partial t} = f(x)|\nabla h| + c|\nabla h|\mathrm{div}\frac{\nabla h}{|\nabla h|}. \tag{3.2}$$

To this equation one has to attach the initial condition

$$h(x,0) = h_0(x) \quad \text{in} \quad \mathbb{R}^N,$$

where h_0 is a function chosen such that its zero level set coincides with the initial position of the front, and appropriate boundary or far field conditions.

If the medium in which the front is propagating is periodic with unit cell $[0,\varepsilon]^N$, the corresponding problem is

$$\begin{cases} \frac{\partial h^\varepsilon}{\partial t} = f(\frac{x}{\varepsilon})|\nabla h^\varepsilon| + \varepsilon c|\nabla h^\varepsilon|\mathrm{div}\frac{\nabla h^\varepsilon}{|\nabla h^\varepsilon|} & \text{in} \quad \mathbb{R}^N \times [0,T) \\ h^\varepsilon(x,0) = h_0(x) & \text{in} \quad \mathbb{R}^N \end{cases}, \tag{3.3}$$

with f continuous and periodic with period $Y_N = [0,1]^N$. Our aim is to study the homogenization of this phenomenon, i.e., to capture its limit behavior when the structure of the medium becomes infinitely fine ($\varepsilon \to 0$).

There are, unfortunately, serious open mathematical issues concerning (3.3). In particular, existence, uniqueness and comparison principles remain open. We shall not address these issues in this study, but proceed with what we believe are reasonable assumptions in this regard.

We show in Section 3.2, following the methods of Evans [13] that, as $\varepsilon \to 0$, the solution of (3.3) converges uniformly to the solution of

$$\begin{cases} \frac{\partial h}{\partial t} = \bar{f}(\frac{\nabla h}{|\nabla h|})|\nabla h| & \text{in} \quad \mathbb{R}^N \times [0,T) \\ h(x,0) = h_0(x) & \text{in} \quad \mathbb{R}^N \end{cases}, \tag{3.4}$$

where $\bar{f}$ is determined by solving a suitable periodic problem on the unit cell (3.24). This implies that the average or overall interface propagates with normal velocity

$$v_n = \bar{f}(n),$$

where n is the normal to the interface. So, the normal velocity depends on the orientation of the interface but not on the position or the mean curvature. In short, the average interface undergoes an anisotropic geometric motion.

We also show that if f is strictly positive (or strictly negative), then the resulting $\bar{f}$ leads to (3.4) being a well posed mathematical problem. If f takes both signs, then $\bar{f}$ may be such that (3.4) is ill-posed. This corresponds to the interface being trapped. We explore this and other issues with

various examples in Section 3.3.

We notice from our examples that the effective behavior is easily characterized when the curvature coefficient c is quite large. We study this limit in Section 3.4 and provide an explicit characterization for $\bar{f}$ in this case.

3.2 A homogenization result

Note that the partial differential equation in (3.3) can also be written as

$$\frac{\partial h^\varepsilon}{\partial t} + F(\varepsilon\nabla^2 h^\varepsilon, \nabla h^\varepsilon, \frac{x}{\varepsilon}) = 0,$$

where

$$F(A, p, x) = -f(x)|p| - c\langle I - \frac{p \otimes p}{|p|^2}, A\rangle. \tag{3.5}$$

The operator F defined above is degenerate elliptic, in the sense that

$$F(X, p, x) \geq F(Y, p, x) \quad \text{if} \quad Y \geq X \quad \text{(i.e. if } Y - X \text{ is positive semidefinite).}$$

Also, it can be easily checked that F is a geometric operator, in the sense that it has the following scaling invariance

$$F(\lambda X + \sigma p \otimes p, \lambda p, x) = \lambda F(X, p, x), \quad \text{for all} \quad \lambda > 0,\ \sigma \in \mathbb{R}.$$

We now study the homogenization of the problem

$$\begin{cases} \frac{\partial u^\varepsilon}{\partial t} + F(\varepsilon\nabla^2 u^\varepsilon, \nabla u^\varepsilon, \frac{x}{\varepsilon}) = 0 & \text{in} \quad \mathbb{R}^N \times [0, T) \\ u^\varepsilon(x, 0) = u_0(x) & \text{in} \quad \mathbb{R}^N \end{cases}, \tag{3.6}$$

where F is a geometric and degenerate elliptic operator, Lipschitz continuous and periodic in the variable x with unit cell $Y_N = [0, 1]^N$. This more general problem includes our front propagation problem (3.3) as a particular case.

We start by gaining some insight with a formal asymptotic treatment. For this, it is natural to begin with the expansion (see [5] for a systematic presentation of such ansatz)

$$u^\varepsilon(x, t) = u^0(x, t) + \varepsilon u^1(\frac{x}{\varepsilon}, t) + o(\varepsilon).$$

Plugging this expansion into (3.6) and identifying the terms in front of powers of ε^0, we find

$$u^0_t(x, t) + F(\nabla^2_y u^1(y, t), \nabla_x u^0(x, t) + \nabla_y u^1(y, t), y) = 0,$$

where $y = \frac{x}{\varepsilon}$. This can be looked at as a partial differential equation for the corrector u^1; its solvability condition provides a constraint between the partial derivatives of the average u^0:

$$u_t^0 + \bar{F}(\nabla u^0) = 0,$$

with $\bar{F}$ determined by the condition that a periodic solution v of

$$F(\nabla_y^2 v(y), p + \nabla_y v(y), y) = \bar{F}(p)$$

exists.

There are important difficulties when approaching this problem in a more rigorous manner: several key existence, uniqueness, regularity and comparison results have not yet been proved. To overcome this difficulty, we shall make the following assumptions:

Assumption A1. *There exists a unique continuous viscosity solution of the problem*

$$\begin{cases} \frac{\partial u}{\partial t} + F(\nabla^2 u, \nabla u, x) = 0 & \text{in} \quad \mathbb{R}^N \times [0,T) \\ u(x,0) = u_0(x) & \text{in} \quad \mathbb{R}^N \end{cases}.$$

Assumption A2. *For any $p_0 \in \mathbb{R}^N$ and for any $\delta \in (0,1)$ there exists a unique continuous viscosity solution of the problem*

$$\delta u + F(\nabla^2 u, \nabla u + p_0, x) = 0. \tag{3.7}$$

Assumption A3. (uniform regularity) *The solution of (3.7) is Holder continuous in x and its Holder coefficient is bounded with respect to δ for $\delta \in (0,1)$.*

Assumption A4. *The comparison principle for periodic solutions of geometric degenerate elliptic equations holds: if u^1 and u^2 are solutions of the same geometric degenerate elliptic equation with initial data u_0^1 and respectively u_0^2, then $u_0^1 \geq u_0^2$ implies $u^1 \geq u^2$.*

Assumption A5. *The comparison principle for initial and boundary value problems for geometric degenerate parabolic equations on bounded domains holds.*

All five assumptions listed above are very natural and some results that are very close to them have already been established (see [8], [9] and [14]). Using **A1** - **A5** above, we now proceed to proving the homogenization theorem for (3.6), following the work of Evans in [13].

Theorem 8 *If F is a degenerate elliptic and geometric operator, Lipschitz continuous and periodic in the variable x with unit cell $Y_N = [0,1]^N$, the viscosity solution of problem (3.6) converges uniformly (as $\varepsilon \to 0$) on $\mathbb{R}^N \times [0,T)$ to the viscosity solution of the Hamilton-Jacobi initial value*

problem

$$\begin{cases} \frac{\partial u}{\partial t} + \bar{F}(\nabla u) = 0 & in \quad \mathbb{R}^N \times [0,T) \\ u^\varepsilon(x,0) = u_0(x) & in \quad \mathbb{R}^N \end{cases}, \tag{3.8}$$

where the Hamiltonian $\bar{F}(p)$ is uniquely determined by the requirement that there exists a periodic viscosity solution v to the following degenerate elliptic equation:

$$F(\nabla^2 v(y), \nabla v(y) + p, y) = \bar{F}(p). \tag{3.9}$$

Relation (3.9) is also called the cell problem.

Proof: Consider the approximating problem

$$\delta w^\delta(y) + F(\nabla_y^2 w^\delta(y), \nabla_y w^\delta(y) + p, y) = 0, \tag{3.10}$$

for some $p \in \mathbb{R}^N$ and some $\delta \in (0,1)$. By assumption **A2**, (3.10) also has a unique continuous viscosity solution w^δ. Moreover, the periodicity of F and the uniqueness of the solution w^δ imply that w^δ has to be periodic with the same unit cell $Y_N = [0,1]^N$.

In any point where w^δ attains its maximum, its Hessian $\nabla_y^2 w^\delta$ is negative semidefinite, so the degenerate ellipticity of F implies that

$$\delta w^\delta(y) = -F(\nabla_y^2 w^\delta(y), \nabla_y w^\delta(y) + p, y) \leq F(0,p,y) \leq \|F(0,p,\cdot)\|_{L^\infty(Y_N)}$$

whenever y is a maximum of w^δ. In a similar manner it can be argued that

$$\delta w^\delta(y) \geq -\|F(0,p,\cdot)\|_{L^\infty(Y_N)}$$

whenever w^δ reaches its minimum. Hence we proved that

$$\sup_{0<\delta<1} \|\delta w^\delta\|_{L^\infty(Y_N)} \leq \|F(0,p,\cdot)\|_{L^\infty(Y_N)}.$$

Using this and **A3**, we conclude that there exists a subsequence $\delta_j \to 0$ such that $v^{\delta_j} \to v$ uniformly in $\mathbb{R}^N$ and $\delta_j w^{\delta_j} \to -\lambda$ uniformly in $\mathbb{R}^N$, where the function v^δ is defined by $v^\delta(y) = w^\delta(y) - \min_{Y_N} w^\delta$ and λ is some constant. Thus we can pass to the limit $\delta \to 0$ in (3.10) to get

$$F(\nabla_y^2 v(y), D_y v(y) + p, y) = \lambda. \tag{3.11}$$

We now want to prove the uniqueness of the constant λ for which a function v that satisfies (3.11) exists. Assume by contradiction that there exists a second pair $(\tilde{v}, \tilde{\lambda})$ that satisfies (3.11),

with $\tilde{v}$ a periodic function and $\tilde{\lambda} > \lambda$. By adding a constant if necessary, we may also assume that $v > \tilde{v}$. Then, for some ε small enough, we have that

$$\varepsilon\tilde{v} + F((\nabla_y^2\tilde{v}(y), D_y\tilde{v}(y) + p, y) > \theta > \varepsilon v + F(D_y^2 v(y), D_y v(y) + p, y)$$

for some constant θ. Thus $\tilde{v}$ is a periodic super-solution of the equation

$$F(\nabla_y^2 v(y), D_y v(y) + p, y) + \varepsilon v - \theta = 0$$

and v is a periodic sub-solution of the same equation. Using **A4** we arrive at $\tilde{v} > v$, in contradiction with our assumption that $v > \tilde{v}$. Thus the constant λ for which a periodic solution v to (3.11) exists is unique and we may denote it by $\bar{F}(p)$. All we have now left to prove is that the viscosity solution of problem (3.6) converges uniformly (as $\varepsilon \to 0$) on $\mathbb{R}^N \times [0,T)$ to the viscosity solution of the Hamilton Jacobi initial value problem (3.8).

Since F is degenerate elliptic and parabolic, **A1** gives the existence of a unique continuous viscosity solution u^ε on $\mathbb{R}^N \times [0,T]$. Let us define the function $u^* : \mathbb{R}^N \times [0,T) \to \mathbb{R}$ by

$$u^*(x,t) = \limsup_{\varepsilon \to 0, z \to x, s \to t} u^\varepsilon(z,s).$$

We claim that

$$\frac{\partial u^*}{\partial t}(x,t) + \bar{F}(\nabla u^*(x,t)) \leq 0 \tag{3.12}$$

in viscosity sense. Indeed, consider a function $\phi \in C^\infty(\mathbb{R}^N \times [0,T))$ such that $u^* - \phi$ has a strict local maximum at the point (x_0, t_0), with

$$u^*(x_0,t_0) = \phi(x_0,t_0). \tag{3.13}$$

We shall assume by contradiction that

$$\frac{\partial \phi}{\partial t} + \bar{F}(\nabla\phi) = \theta \quad \text{at} \quad (x_0,t_0), \tag{3.14}$$

where θ is some positive constant. By the definition of $\bar{F}$, there exists a Y-periodic viscosity solution v to the problem

$$F(\nabla_y^2 v(y), \nabla v(y) + \nabla_x\phi(x_0,t_0), y) = \bar{F}(\nabla_x\phi(x_0,t_0)). \tag{3.15}$$

Define the function ϕ^ε by

$$\phi^\varepsilon(x,t) = \phi(x,t) + \varepsilon v(\frac{x}{\varepsilon}).$$

We claim that

$$\frac{\partial \phi}{\partial t}(x,t_0) + F(\varepsilon \nabla^2 \phi^\varepsilon(x,t_0), \nabla \phi^\varepsilon(x,t_0), \frac{x}{\varepsilon}) \geq \frac{\theta}{2} \tag{3.16}$$

in viscosity sense, in some ball $B(x_0,r)$ centered in x_0 with small enough radius r. To prove this, fix some $\psi \in C^\infty(\mathbb{R}^N \times [0,T))$ such that $\phi^\varepsilon - \psi$ has a minimum at $(x_1,t_0) \in B(x_0,r) \times t_0$ with

$$\phi^\varepsilon(x_1,t_0) = \psi(x_1,t_0).$$

Then the application $y \longmapsto v(y) - \eta(y)$ has a minimum at $y_1 = \frac{x_1}{\varepsilon}$, where

$$\eta(y) = \frac{1}{\varepsilon}(\psi(\varepsilon y,t_0) - \phi(\varepsilon y,t_0)).$$

Since v is a viscosity solution of (3.15), this implies that

$$F(\nabla_y^2 \eta(y), \nabla_y \eta(y) + \nabla_x \phi(x_0,t_0), y) \geq \bar{F}(\nabla_x \phi(x_0,t_0)),$$

thus, using also (3.14),

$$\frac{\partial \phi}{\partial t}(x_0,t_0) + F(\varepsilon \nabla^2 \psi(x_1,t_0) - \varepsilon \nabla^2 \phi(x_1,t_0), \nabla \psi(x_1,t_0) - \nabla \phi(x_1,t_0) + \nabla \phi(x_0,t_0), \frac{x_1}{\varepsilon}) \geq \theta.$$

Using the Lipschitz continuity of F and the fact that

$$\frac{\partial \phi}{\partial t}(x_1,t_0) = \frac{\partial \phi^\varepsilon}{\partial t}(x_1,t_0) = \frac{\partial \psi}{\partial t}(x_1,t_0),$$

we infer that

$$\frac{\partial \psi}{\partial t} + F(\varepsilon \nabla^2 \psi, \nabla \psi, \frac{x_1}{\varepsilon}) \geq \frac{\theta}{2} \quad \text{at} \quad (x_1,t_0).$$

Since the choice of the function $\psi \in C^\infty(\mathbb{R}^N \times [0,T))$ was arbitrary, the argument above establishes (3.16).

Since $\phi \in C^\infty(\mathbb{R}^N \times [0,T))$, inequality (3.16) implies that

$$\frac{\partial \phi}{\partial t}(x,t) + F(\varepsilon \nabla^2 \phi^\varepsilon(x,t), \nabla \phi^\varepsilon(x,t), \frac{x}{\varepsilon}) \geq \frac{\theta}{4} \quad \text{in} \quad B(x_0,r) \times [t_0 - r', t_0 + r']$$

for some r' small enough. But u^ε is a viscosity solution of (3.6), so the comparison principle **A5** yields

$$\max_{B(x_0,r) \times B(t_0,r')} (u^\varepsilon - \phi^\varepsilon) \leq \max_{\partial(B(x_0,r) \times B(t_0,r'))} (u^\varepsilon - \phi^\varepsilon).$$

In the limit $\varepsilon \to 0$ this inequality becomes

$$(u^* - \phi^\varepsilon)(x_0, t_0) \leq \max_{\partial(B(x_0,r)\times B(t_0,r'))} (u^* - \phi^\varepsilon),$$

which contradicts (3.13). This proof by contradiction establishes (3.12).

Also, using the continuity of u^ε and the definition of u^*, the initial condition in (3.6) implies

$$u^*(x_0, 0) = u_0(x) \quad \text{in} \quad \mathbb{R}^N. \tag{3.17}$$

Then the comparison principle for (3.8), along with (3.12) and (3.17), gives

$$u^* \leq u.$$

Similarly it can be proved that

$$u \leq u_* = \liminf_{\varepsilon \to 0, z \to x, s \to t} u^\varepsilon(s, z)$$

and since we obviously have $u_* \leq u^*$, we conclude that $u = u^* = u_*$.

Hence u^ε converges uniformly (as $\varepsilon \to 0$) to u, the solution of (3.8). ■

We now proceed to show that certain properties of the operator F are inherited by the limit Hamiltonian $\bar{F}$.

Theorem 9 *If the operator F in (3.6) satisfies*

$$\lim_{|p| \to \infty} F(0, p, y) = \infty \quad \textit{uniformly in} \quad y,$$

then the same holds for the homogenized Hamiltonian $\bar{F}$:

$$\lim_{|p| \to \infty} \bar{F}(p) = \infty.$$

Proof: We refer to the approximating problem (3.10) in the proof of Theorem 8. Writing (3.10) in a point y_0 where w^δ attains its maximum we get

$$\delta w^\delta(y_0) + F(0, p, y_0) \leq 0. \tag{3.18}$$

For any $M > 0$, if p is large enough, (3.18) implies that

$$-\delta w^\delta \geq M.$$

But $-\delta w^\delta \to \bar{F}(p)$ uniformly as $\delta \to 0$, so the inequality above proves the theorem. ■

Theorem 10 *If the operator F in (3.6) is Lipschitz continuous in p in the ball $B(0,L)$ and its Lipschitz constant is C_L, then the same holds for the homogenized Hamiltonian $\bar{F}$.*

Proof: Fix p and $\hat{p}$ in $B(0,L)$ and let $\hat{w}$ be a solution of the equation

$$\delta\hat{w}^\delta + F(\nabla_y^2\hat{w}^\delta, \nabla_y\hat{w}^\delta + \hat{p}, y) = 0.$$

Then

$$\delta\hat{w}^\delta + F(\nabla_y^2\hat{w}^\delta, \nabla_y\hat{w}^\delta + p, y) \geq -C_L|\hat{p} - p|,$$

so $\hat{w}$ is a super-solution of the equation

$$\delta w^\delta + F(\nabla_y^2 w^\delta, \nabla_y w^\delta + p, y) + C_L|\hat{p} - p| = 0. \tag{3.19}$$

We now refer to the approximating problem (3.10) in the proof of Theorem 8. If w^δ is a solution to (3.10), then $w^\delta - \frac{1}{\delta}C_L|\hat{p} - p|$ is a solution to (3.19) and then the comparison principle **A4** implies that

$$\delta\hat{w}^\delta - \delta w^\delta \geq -C_L|\hat{p} - p|.$$

As $\delta \to 0$, this yields

$$-\bar{F}(\hat{p}) + \bar{F}(p) \geq -C_L|\hat{p} - p|. \tag{3.20}$$

In a similar manner it can be proved that

$$\bar{F}(\hat{p}) - \bar{F}(p) \leq C_L|\hat{p} - p|,$$

which, together with (3.20), establishes that $\bar{F}$ is Lipschitz continuous in p in $B(0,L)$ and that its Lipschitz constant is C_L. ■

Theorem 11 *If the operator F in (3.6) is convex with respect to its first two variables, then the homogenized Hamiltonian $\bar{F}$ is convex in p.*

Proof: Fix $p, q \in \mathbb{R}^N$, $x \in \mathbb{R}^N$ and let v^p, v^q and $v^{(p+q)/2}$ be the Y_N-periodic viscosity solutions of the following cell problems:

$$\begin{cases} F(\nabla^2 v^p(y), \nabla v^p(y) + p, y) = \bar{F}(p) \\ F(\nabla^2 v^q(y), \nabla v^q(y) + q, y) = \bar{F}(q) \\ F(\nabla^2 v^{(p+q)/2}(y), \nabla v^{(p+q)/2}(y) + \frac{p+q}{2}, y) = \bar{F}(\frac{p+q}{2}) \end{cases}.$$

By subtracting a constant from $v^{(p+q)/2}$ if necessary, we may also assume that

$$v^{(p+q)/2} < \frac{1}{2}(v^p + v^q) \quad \text{in} \quad \mathbb{R}^N. \tag{3.21}$$

We shall assume by contradiction that

$$\bar{F}(\frac{p+q}{2}) > \frac{1}{2}(\bar{F}(p) + \bar{F}(q)). \tag{3.22}$$

We now make the claim that

$$F(\nabla^2 \frac{v^p + v^q}{2}(y), \nabla \frac{v^p + v^q}{2}(y) + \frac{p+q}{2}, y) \leq \frac{1}{2}(\bar{F}(p) + \bar{F}(q)) \quad \text{in} \quad \mathbb{R}^N. \tag{3.23}$$

To prove this, let $w = \frac{1}{2}(v^p + v^q)$ and $w_\varepsilon = \eta_\varepsilon * w$, where η_ε is the mollifier with support in the ball $B(0,\varepsilon)$, i.e., an infinitely many times differentiable function $\eta_\varepsilon \geq 0$ such that

$$\eta_\varepsilon(x) = \eta_\varepsilon(|x|), \quad \int_0^\varepsilon \eta_\varepsilon(x) x dx = 1, \quad \eta_\varepsilon(x) = 0 \text{ if } x \geq \varepsilon.$$

Then

$$\begin{aligned}
& F(\nabla^2 w_\varepsilon(y), \nabla w_\varepsilon(y) + \frac{p+q}{2}, y) \\
\leq & \int_{B(y,\varepsilon)} \eta_\varepsilon(y-z) F(\nabla^2 w(z), \nabla w(z) + \frac{p+q}{2}, y) dz \\
= & \int_{B(y,\varepsilon)} \eta_\varepsilon(y-z) F(\nabla^2 w(z), \nabla w(z) + \frac{p+q}{2}, z) dz + o(1) \\
\leq & \frac{1}{2} \int_{B(y,\varepsilon)} \eta_\varepsilon(y-z) F(\nabla^2 v^p(z), \nabla v^p(z) + p, z) dz \\
& + \frac{1}{2} \int_{B(y,\varepsilon)} \eta_\varepsilon(y-z) F(\nabla^2 v^q(z), \nabla v^q(z) + q, z) dz + o(1) \\
= & \frac{1}{2}\bar{F}(p) + \frac{1}{2}\bar{F}(q) + o(1)
\end{aligned}$$

as $\varepsilon \to 0$. In the limit $\varepsilon = 0$, we get (3.23).

But (3.22) and (3.23) imply, by **A4**, that

$$\frac{1}{2}(v^p + v^q) \leq v^{(p+q)/2},$$

which contradicts (3.21). ■

We now specialize to F defined by the interface propagation problem (3.5). Theorem 8 tells us that its viscosity solution converges uniformly (as $\varepsilon \to 0$) on $\mathbb{R}^N \times [0,T)$ to the viscosity solution of the Hamilton Jacobi initial value problem (3.8), with $\bar{F}(p)$ uniquely determined by the requirement

that there exists a periodic viscosity solution v to the following cell problem:

$$-f(x)|\nabla v + p| - c(\delta_{ij} - \frac{(v_{x_i} + p_i)(v_{x_j} + p_j)}{|\nabla v + p|^2})v_{x_i x_j} = \bar{F}(p). \tag{3.24}$$

Proposition 2 *For F defined by (3.5) we have that*

$$\bar{F}(p) = \bar{f}(\frac{p}{|p|})|p|.$$

Proof: Let us define $\bar{f}(p)$ by

$$\bar{f}(p) = \frac{\bar{F}(p)}{|p|} \quad \text{for} \quad p \neq 0.$$

If v is a periodic viscosity solution for (3.24) corresponding to a vector p:

$$-f(x)|\nabla v + p| - c(\delta_{ij} - \frac{(v_{x_i} + p_i)(v_{x_j} + p_j)}{|\nabla v + p|^2})v_{x_i x_j} = \bar{f}(p)|p|,$$

and α is some positive constant, it can easily be seen that

$$-f(x)|\nabla(\alpha v) + \alpha p| - c(\delta_{ij} - \frac{(\alpha v_{x_i} + \alpha p_i)(\alpha v_{x_j} + \alpha p_j)}{|\nabla(\alpha v) + \alpha p|^2})\alpha v_{x_i x_j} = \bar{f}(p)|\alpha p|,$$

hence αv is a periodic viscosity solution for the cell problem with the constant $\bar{f}(p)|\alpha p|$ in the right-hand side. By the uniqueness of $\bar{F}$ (which is equivalent to the uniqueness of $\bar{f}$), it follows that

$$\bar{f}(p) = \bar{f}(\alpha p), \quad \forall \alpha > 0,$$

thus the homogenized Hamiltonian has the form

$$\bar{F}(p) = \bar{f}(\frac{p}{|p|})|p|.$$

■

We conclude that the effective motion of a curvature driven interface through a heterogeneous medium is an anisotropic geometric one, similar to the effective motion studied in Chapter 2.

3.3 Examples

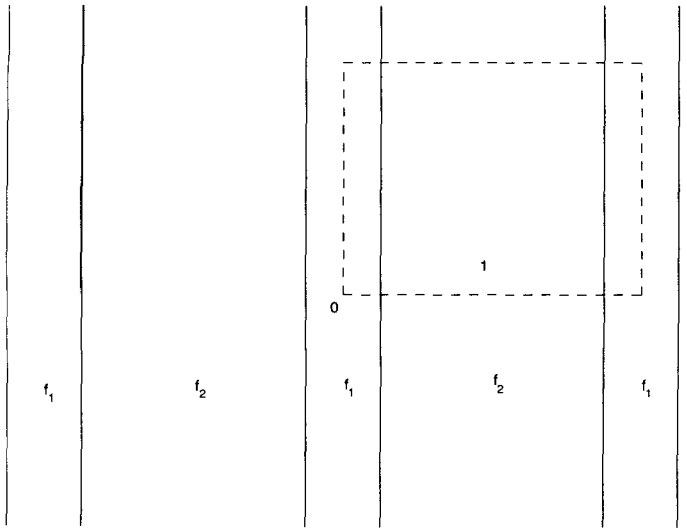

Figure 3.1: Laminated material

3.3.1 Laminates

Assume that the function $f(x)$ has only two possible values f_1 and f_2 in alternating stripes with volume fractions μ and $1-\mu$ respectively, as shown in Figure 3.1. More exactly, let

$$f(x_1,x_2) = \begin{cases} f_1 & \text{if} \quad x_1 \in [0,\frac{\mu}{2}] \cup [1-\frac{\mu}{2},1] \\ f_2 & \text{if} \quad x_1 \in (\frac{\mu}{2},1-\frac{\mu}{2}) \end{cases},$$

with f extended by periodicity outside the strip $x_1 \in [0,1]$. We assume that $f_1 > f_2$ without loss of generality.

We study the propagation of an interface whose average normal is in the x_2 direction. We claim that if we find a self-similar front $\mathcal{F}$, $[0,1]$-periodic in x_1, that propagates by uniform translation in the x_2 direction, then the translation velocity will be the effective normal velocity in this upwards x_2 direction. Indeed, any other front that has effective velocity parallel to x_2 can be initially trapped between two copies of $\mathcal{F}$ and then, by the comparison principle, it will stay trapped in between them; it follows that its effective velocity has to be the same as the effective velocity of $\mathcal{F}$.

We begin by trying to find a self similar front $\mathcal{F}$ that can also be written as the graph $x_2 = g(x_1)$ of a $[0,1]$-periodic function g. We make the choice that $f_1 > f_2$ (by translating the periodicity cell with $\frac{1}{2}$ in the x_1 direction if need be). If v denotes the constant upwards-translation velocity of $\mathcal{F}$, then its normal velocity and curvature at any point are

$$v_n = (0,v)\cdot n = \frac{v}{\sqrt{1+g'(x_1)^2}}, \quad \kappa = -\frac{g''(x_1)}{\sqrt{1+g'(x_1)^2}^3}.$$

Plugging this in our normal velocity formula $v_n = f - c\kappa$, we get

$$\frac{v}{\sqrt{1+z(x_1)^2}} = f(x_1) + c\frac{z'(x_1)}{\sqrt{1+z(x_1)^2}^3}, \tag{3.25}$$

where $z(x_1) = g'(x_1)$. This equation can also be written as

$$v\cos u(x_1) = f(x_1) + cu'(x_1)\cos u(x_1),$$

in the new unknown function $u(x_1) = \arctan z(x_1)$. The variables in this ordinary differential equation can be separated

$$\frac{du\cos u}{v\cos u - f} = \frac{dx_1}{c} \tag{3.26}$$

in all the regions where f is constant.

Due to the periodicity of f and g and due to the symmetry of f with respect to the axis $x_1 = \frac{1}{2}$, the front $\mathcal{F}$ has critical points at $x_1 = 0$ and $x_1 = \frac{1}{2}$. This means that

$$u(0) = u(\frac{1}{2}) = 0. \tag{3.27}$$

We now consider the case $v \neq 0$ (the case $v = 0$ is treated separately in Section 3.3.3). We can obtain two values for $u(\frac{\mu}{2})$, by integrating (3.26) with starting points $x_1 = 0$ (forward) and $x_1 = 1/2$ (backward), respectively:

$$\begin{cases} u(\frac{\mu}{2}) + \frac{2f_1}{\sqrt{v^2-f_1^2}}\operatorname{arctanh}\frac{(f_1+v)\tan\frac{u(\frac{\mu}{2})}{2}}{\sqrt{v^2-f_1^2}} = \frac{\mu v}{2c} \\ u(\frac{\mu}{2}) + \frac{2f_2}{\sqrt{v^2-f_2^2}}\operatorname{arctanh}\frac{(f_2+v)\tan\frac{u(\frac{\mu}{2})}{2}}{\sqrt{v^2-f_2^2}} = \frac{(\mu-1)v}{2c} \end{cases}. \tag{3.28}$$

This is a system of two algebraic equations in two unknowns, v and $u(\frac{\mu}{2})$. While it cannot be solved exactly due to its transcendental nature, it is possible to use common numerical techniques for obtaining the values of the function $v = v(f_1, f_2, \mu, c)$.

Figure 3.2 shows the dependence $v = v(c)$ for fixed values of f_1 $(= 1)$ and μ $(= \frac{1}{2})$ and for various f_2 varying from $-.05$ to $.95$ (the uppermost graph is for the highest value of the parameter f_2). For each value of f_2, v decreases monotonically with c, reaches the limit $\max(f_1, f_2) = 1$ as $c \to 0$ and the average $\frac{1}{2}(f_1 + f_2)$ as $c \to \infty$. We note that the former limit is consistent with the case $c = 0$ (Example 1 in Section 2.4) and we shall study the latter in greater detail later.

Note that the plots in Figure 3.2 do not start from the value $c = 0$. When we solve the system (3.28), we can only accept solutions that satisfy $u \in [-\frac{\pi}{2}, \frac{\pi}{2}]$, else the assumption of a graph breaks down. We find that this breaks down for c small enough. The minimal value c_m of c for which the construction above is possible can be obtained by solving the system (3.28) in the unknowns v and

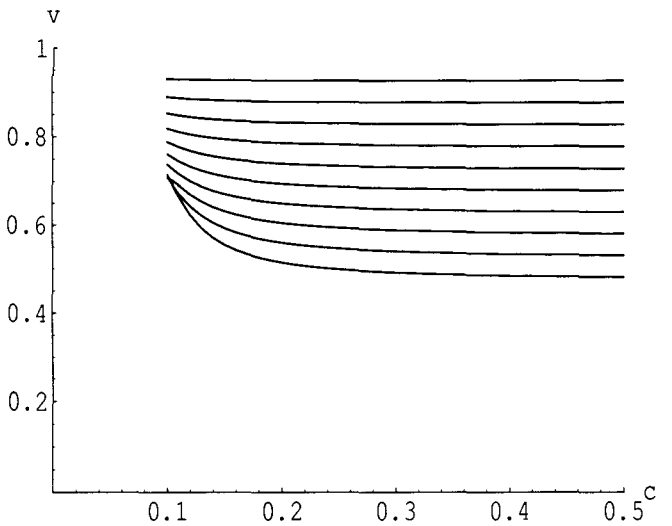

Figure 3.2: The function $v = v(c)$ for various values of f_2

c with $u(\frac{\mu}{2}) = -\frac{\pi}{2}$ fixed. Table 3.1 contains a list of values of c_m calculated numerically for various f_2.

For $c < c_m$, it is no longer possible to construct self similar fronts with periodicity 1. It turns out, however, that we can do so with periodicity N, a large enough integer. Proceeding as before, the system corresponding to (3.28) is

$$\begin{cases} u(N\frac{\mu}{2}) + \frac{2f_1}{\sqrt{v^2-f_1^2}}\operatorname{arctanh}\frac{(f_1+v)\tan\frac{u(N\frac{\mu}{2})}{2}}{\sqrt{v^2-f_1^2}} = N\frac{\mu v}{2c} \\ u(N\frac{\mu}{2}) + \frac{2f_2}{\sqrt{v^2-f_2^2}}\operatorname{arctanh}\frac{(f_2+v)\tan\frac{u(N\frac{\mu}{2})}{2}}{\sqrt{v^2-f_2^2}} = N\frac{(\mu-1)v}{2c} \end{cases}.$$

After we replace $u(N\frac{\mu}{2})$ with $-\frac{\pi}{2}$, we notice that we obtain the same system as before, except that c is now multiplied with $\frac{1}{N}$. It follows that

$$c_m(N) = \frac{1}{N}c_m(1),$$

which means that we are able to construct self-similar interfaces for any values of f_1, f_2 and c, provided that we choose a large enough number of cells.

We now turn to the limit $c \to \infty$. Setting $c = \infty$ in (3.28) gives $u(\frac{\mu}{2}) = 0$ and v is indeterminate. Therefore, we assume the asymptotic expansion

$$\begin{aligned} c &= \frac{1}{\epsilon} \\ u(\frac{\mu}{2}) &\sim \epsilon u_0 + o(\epsilon) \\ v &\sim v_0 + o(1) \end{aligned}$$

f_2	c_m for unit cell $[0,1]^2$
0.95	0.0328
0.85	0.0381
0.75	0.0576
0.65	0.0751
0.55	0.0791
0.45	0.0772
0.35	0.0814
0.25	0.0866
0.15	0.0903
0.05	0.0981
-0.05	0.1192
-0.15	0.1361
-0.25	0.1512
-0.35	0.1653
-0.45	0.1790
-0.55	0.1924
-0.65	0.2054
-0.75	0.2183
-0.85	0.2311
-0.95	0.2437

Table 3.1: List of values of c_m as f_2 varies

as $\epsilon \to 0$. The algebraic system (3.28) then becomes

$$\begin{cases} \frac{u(\frac{\mu}{2})}{\epsilon} + \frac{2f_1}{\epsilon\sqrt{v^2-f_1^2}}\operatorname{arctanh}\frac{(f_1+v)\tan\frac{u(\frac{\mu}{2})}{2}}{\sqrt{v^2-f_1^2}} = \frac{\mu v}{2} \\ \frac{u(\frac{\mu}{2})}{\epsilon} + \frac{2f_2}{\epsilon\sqrt{v^2-f_2^2}}\operatorname{arctanh}\frac{(f_2+v)\tan\frac{u(\frac{\mu}{2})}{2}}{\sqrt{v^2-f_2^2}} = \frac{(\mu-1)v}{2} \end{cases}.$$

In the limit $\epsilon \to 0$ we can use L'Hopital's rule for the second term in the left-hand side of both equations to get

$$\begin{cases} u_0 + \frac{f_1(f_1+v_0)}{v_0^2-f_1^2}u_0 = \frac{\mu v_0}{2} \\ u_0 + \frac{f_2(f_2+v_0)}{v_0^2-f_2^2}u_0 = \frac{(\mu-1)v_0}{2} \end{cases}.$$

Dividing the two equations we are left with an equation in v_0:

$$\frac{1+\frac{f_1}{v_0-f_1}}{\frac{f_2}{v_0-f_2}} = \frac{\mu}{\mu-1},$$

which has as solution

$$v_0 = \mu f_1 + (1-\mu)f_2 = \int_0^1 f(x_1)\,dx_1,$$

as suggested by Figure 3.2. We shall return to this limit in the general case in Section 3.4.

The self-similar fronts not only allow us to calculate the values of the effective normal velocity but they also seem to act as attractors in the space of solutions for (3.2). This was observed by means

of a numerical simulation built on a 64×64 grid. We use a semi-implicit scheme when discretizing (3.2):

$$\frac{h^{n+1} - h^n}{\Delta t} = f\ P + c|\nabla h^n|\ \text{div}\ \frac{\nabla h^{n+1}}{|\nabla h^n|},$$

where

$$P = \begin{cases} \sqrt{\max(p_-^x, 0)^2 + \min(p_+^x, 0)^2 + \max(p_-^y, 0)^2 + \min(p_+^y, 0)^2} & \text{if } f > 0 \\ \sqrt{\min(p_-^x, 0)^2 + \max(p_+^x, 0)^2 + \min(p_-^y, 0)^2 + \max(p_+^y, 0)^2} & \text{if } f \leq 0 \end{cases},$$

$$p_-^x = \frac{1}{\Delta x} D_x^- \phi_{i,j}^n + \frac{1}{2\Delta x}\ \text{minmod}\ (D_x^- D_x^+ \phi_{i,j}^n, D_x^- D_x^+ \phi_{i-1,j}^n),$$

$$p_+^x = \frac{1}{\Delta x} D_x^- \phi_{i+1,j}^n + \frac{1}{2\Delta x}\ \text{minmod}\ (D_x^- D_x^+ \phi_{i+1,j}^n, D_x^- D_x^+ \phi_{i,j}^n),$$

$$p_-^y = \frac{1}{\Delta x} D_y^- \phi_{i,j}^n + \frac{1}{2\Delta x}\ \text{minmod}\ (D_y^- D_y^+ \phi_{i,j}^n, D_y^- D_y^+ \phi_{i,j-1}^n),$$

$$p_+^y = \frac{1}{\Delta x} D_y^- \phi_{i,j+1}^n + \frac{1}{2\Delta x}\ \text{minmod}\ (D_y^- D_y^+ \phi_{i,j+1}^n, D_y^- D_y^+ \phi_{i,j}^n),$$

$$\text{minmod}\ (u, v) = \begin{cases} \text{sign}(u)\ \min(|u|, |v|) & \text{if } uv > 0 \\ 0 & \text{if } uv \leq 0 \end{cases},$$

$$D_x^- \phi_{i,j} = \phi_{i,j} - \phi_{i-1,j} \quad \text{(backward)},$$

$$D_x^+ \phi_{i,j} = \phi_{i+1,j} - \phi_{i,j} \quad \text{(forward)}.$$

For the rest of the spatial derivatives, we simply use centered difference operators. We solve the resulting linear system by means of a conjugate gradient method. Since we wish to avoid large gradients in the level set function, we keep it close to the signed distance function to the interface by using, after each time step, a reinitialization procedure developed by Sussman, Smereka and Osher in [26].

Figure 3.3 shows several snapshots of the initially flat front moving in the laminate with the parameters

$$\mu = \frac{1}{2}, f_1 = 1, f_2 = 0, c = 1,$$

taken at every 50 time steps (we used the time step $\Delta t = 0.0001$).

We see how this initially flat interface rapidly approaches the self-similar shape. It subsequently starts a uniform upward translation. This is elaborated in Figure 3.4, which shows snapshots of the same simulation taken every 500 time steps.

Figures 3.5 and 3.6 depict the evolution of an initially flat interface for the laminate with the parameters

$$\mu = \frac{1}{2}, f_1 = 1, f_2 = -0.6, c = 4$$

and the snapshots are taken at every 100 and every 2000 time steps respectively (again, the used time

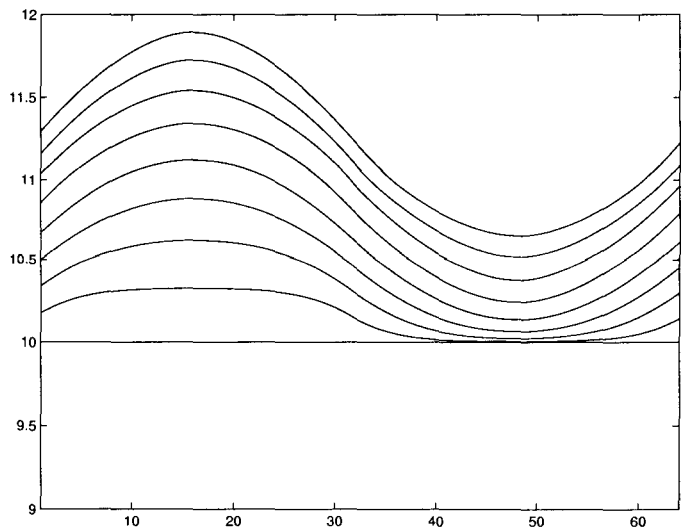

Figure 3.3: Motion of a curvature driven interface in a laminate. The figure shows snapshots of an initially flat interface at every 50 time steps.

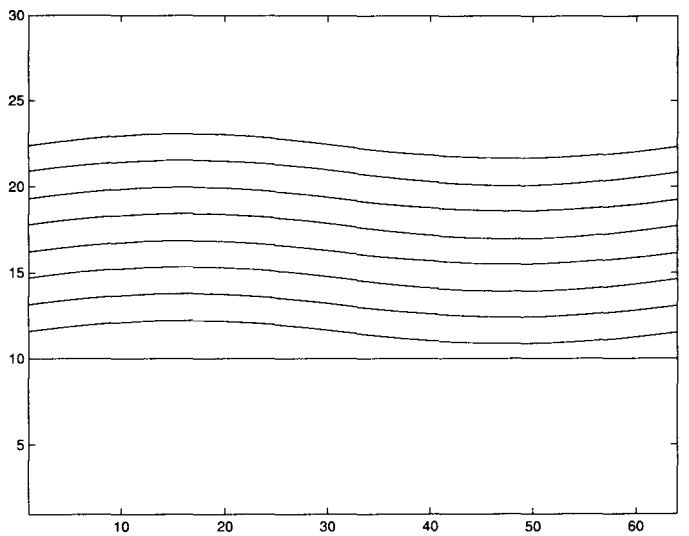

Figure 3.4: Self-similar motion of a curvature driven interface in a laminate. The figure shows snapshots of an initially flat interface at every 500 time steps.

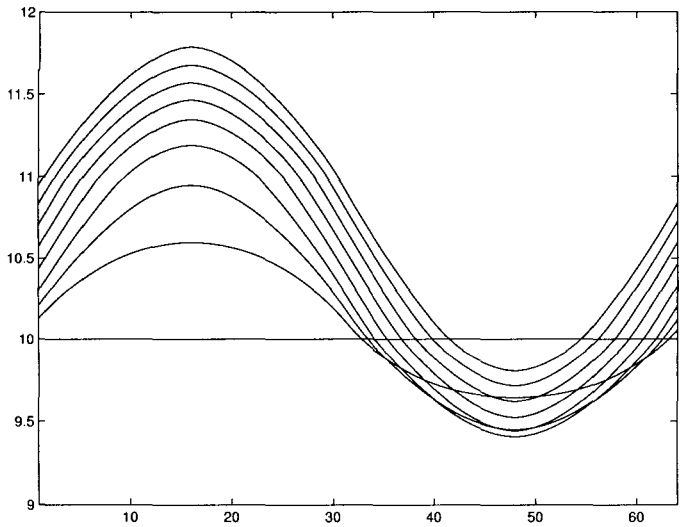

Figure 3.5: Motion of a curvature driven interface in a laminate with both positive and negative values for v_n. The figure shows snapshots of an initially flat interface at every 100 time steps.

step is $\Delta t = 0.0001$). It can be noticed how the front initially moves downwards in the part where f is negative and then eventually assumes the self similar shape and starts translating upwards.

In both these cases, the effective normal velocity (which can be calculated from the distance between the level sets) agrees with the one obtained from (3.28).

3.3.2 Other geometries

For mediums which do not have a laminate-type normal velocity law, self similar interfaces do not generally exist. However, Theorem 8 suggests the existence of interfaces which are self similar to the extent that they assume the same shape after being propagated over one periodicity cell of f. In certain situations, these self-similar interfaces seem to act as attractors, in the sense that interfaces that start with any initial data approach them as time evolves.

As an example, consider the normal velocity law

$$f = 10 + 5\sin(4\pi x)\sin(4\pi y) = 10 + 5\sin(4\pi\frac{i}{n})\sin(4\pi\frac{j}{n}).$$

Figure 3.7 depicts the evolution of an initially flat interface positioned at the height $j = 10$ with a 64×64 grid laid on the periodicity cell. The snapshots are taken at every 100 time steps (with $\Delta t = 0.0001$). In the lower half of the unit square, the left part is faster than the right so the front assumes a shape similar to the one observed in the laminate examples. However, as the interface approaches the height $j = 32$, the interface starts to flatten. In the upper half of the unit square, the situation is reversed: the right part of the interface will be faster than the left and then it again

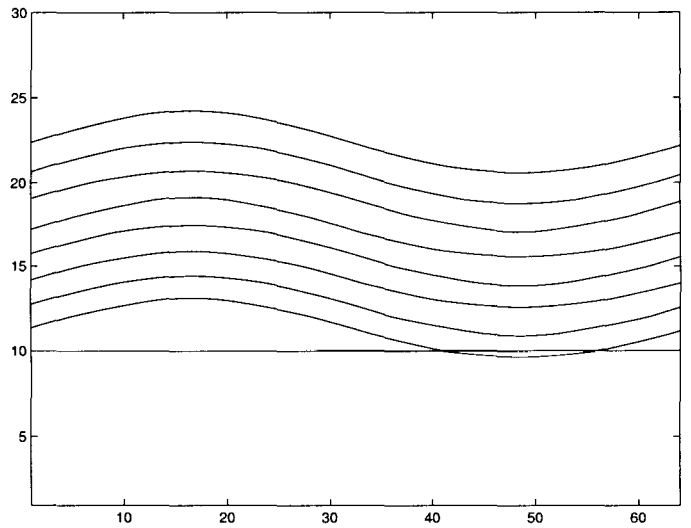

Figure 3.6: Self-similar motion of a curvature driven interface in a laminate with both positive and negative values for v_n. The figure shows snapshots of an initially flat interface at every 2000 time steps.

starts to flatten as it approaches the upper boundary of the periodicity cell.

3.3.3 Trapping

Of particular interest are the interfaces that are trapped, i.e., interfaces which evolve to a stationary position. We begin with a laminate and seek conditions when one has a stationary interface with average normal in the x_2 direction. We assume, as before, that the interface is a graph. We then have to solve

$$du \cos u = -\frac{f}{c} dx,$$

subject to (3.27). We obtain

$$u(x_1) = \begin{cases} \arcsin \frac{-f_1 x_1}{c} & \text{for} \quad x_1 \in [0, \frac{\mu}{2}] \\ \arcsin \frac{f_2(\frac{1}{2} - x_1)}{c} & \text{for} \quad x_1 \in [\frac{\mu}{2}, \frac{1}{2}] \end{cases} . \tag{3.29}$$

For this to make sense, we need to impose that

$$c > \frac{|f_1|\mu}{2}, \quad c > \frac{|f_2|(1-\mu)}{2};$$

these are the conditions for the existence of the self similar interface $\mathcal{F}$ with periodicity 1. If c is smaller, we can proceed with periodicity N as before. The continuity of u at $x_1 = \frac{\mu}{2}$ gives

$$\arcsin \frac{-f_1 \mu}{2c} = \arcsin \frac{f_2(1-\mu)}{2c},$$

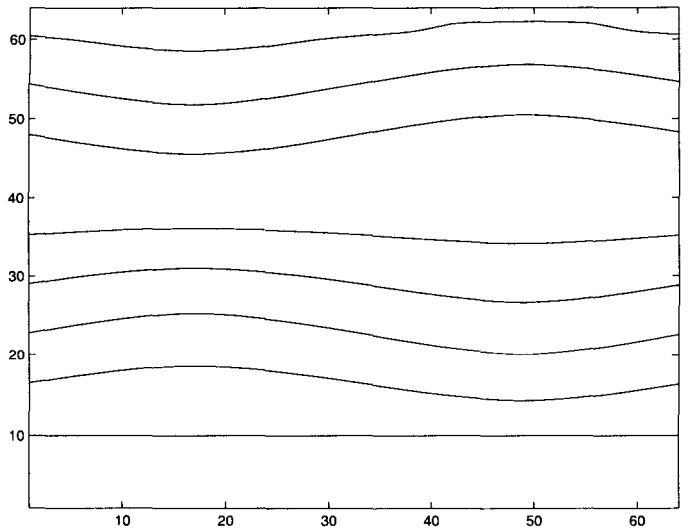

Figure 3.7: Motion of a curvature driven interface in a medium with a sinusoidal normal velocity law. The figure shows snapshots of an initially flat interface at every 100 time steps.

which implies

$$\int_0^1 f(x_1)\, dx_1 = \mu f_1 + (1-\mu) f_2 = 0.$$

Thus we can construct a stationary front when the average of f is zero. We note that the converse is also true: if the average of f is positive (negative), then the average velocity is positive (negative) for $c = \infty$ and therefore positive (negative) for any $c \geq 0$ by the monotonicity of the effective velocity with c.

Similar trapping conditions can also be deduced for other geometries. For example, consider the case of a two-dimensional medium with $f > 0$ constant and circular inclusions of radius r with $f < 0$ constant. In particular, consider $f : [0,1]^2 \to \mathbb{R}$ defined by

$$f(x_1, x_2) = \begin{cases} f_1 & \text{if } (x_1 - \frac{1}{2})^2 + (x_2 - \frac{1}{2})^2 > r^2 \\ f_2 & \text{if } (x_1 - \frac{1}{2})^2 + (x_2 - \frac{1}{2})^2 < r^2 \end{cases},$$

with f extended by periodicity outside the square $[0,1]^2$, where $r \in [0, \frac{1}{2})$, $f_1 > 0$ and $f_2 < 0$ are constants.

Stationary fronts can be constructed using the same method as in the laminate if

$$f_1 \leq \frac{c}{r} \leq -f_2. \tag{3.30}$$

Again, using of the comparison principle, we conclude that no other front is be able to break through these stationary barriers, so the effective normal velocity in the e_2 direction is null.

The trapping conditions in (3.30) are sharp in the following sense: If the first inequality is not

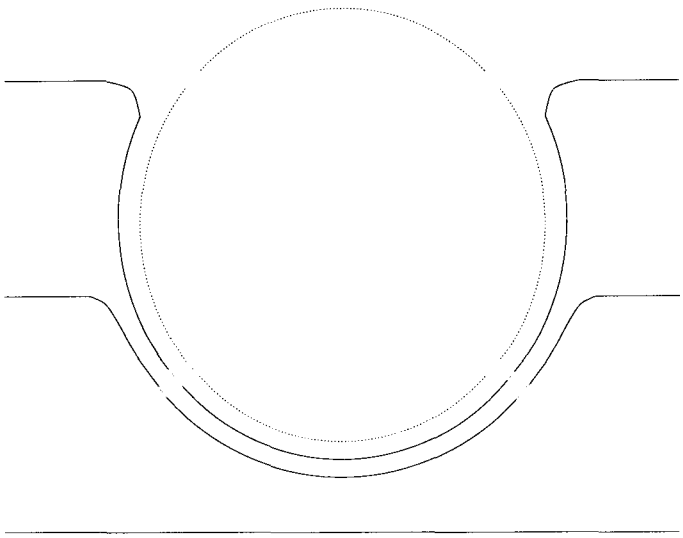

Figure 3.8: Propagation of a front by looping around a slow-velocity inclusion. The dotted line shows the frontier of the obstacle, while the continuous lines capture the shape of the interface at three different moments.

satisfied, then the curvature is not penalized enough and the front is able to propagate by looping around the slow-speed inclusions (see Figure 3.8); if the second inequality is not satisfied, then the resistance to phase change inside the inclusion is not large enough and the curvature that the front has when hitting the obstacle will allow it to continue propagating by cutting through the inclusions (see Figure 3.9).

3.4 Large c asymptotics for the effective normal velocity

We saw in our study of laminates that one can obtain a simple characterization of the effective normal velocity when the curvature coefficient c becomes very large. We now generalize this result to other microstructures. Heuristically, as c becomes large, the curvature is severely penalized so the interface evolves to become flat in the limit $c \to \infty$. We thus obtain a one-dimensional problem: a flat interface propagating normal to itself. Therefore, following Bhattacharya [6] (also see Abeyaratne, Chu and James [1]), the effective velocity is the harmonic mean of its instantaneous normal velocity. We shall see that this instantaneous normal velocity is given by the average of f over the interface. We thus obtain the characterization (3.43) below.

We begin with the two-dimensional case. We first prove that, for c large enough, any sufficiently smooth interface in $\mathbb{R}^2$ that is initially a graph remains so. Assume that the initial interface can be described as the graph $y = g(x)$ of a $[0,1]$ - periodic function $g(\cdot,0) : \mathbb{R} \to \mathbb{R}$. As we've seen in the

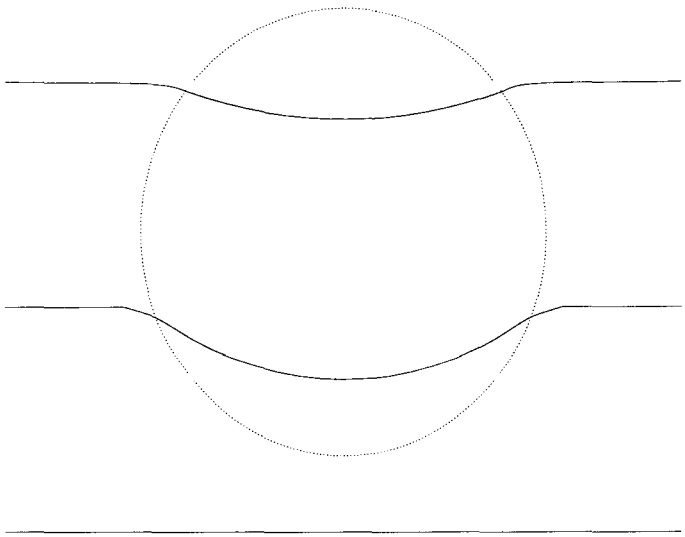

Figure 3.9: Propagation of a front by cutting through a slow-velocity inclusion. The dotted line shows the frontier of the obstacle, while the continuous lines capture the shape of the interface at three different moments.

previous section (see (3.25)), the equation of motion for the function g is

$$\frac{g_t(x,t)}{\sqrt{1+g_x(x,t)^2}} = f(x,g(x,t)) + c\frac{g_{xx}(x,t)}{\sqrt{1+g_x(x,t)^2}^3}$$

as long as the interface can be written as a graph. By scaling time $s = ct$ we can rewrite this as

$$g_s = k\sqrt{1+g_x^2}, \tag{3.31}$$

where

$$k(x,s) = \frac{f(x,g(x,s))}{c} - \kappa(x,g(x,s)) = \frac{f(x,g(x,s))}{c} + \frac{g_{xx}}{(1+g_x^2)^{\frac{3}{2}}}. \tag{3.32}$$

Differentiating (3.31) with respect to x, we get the following expression for g_{xs}:

$$g_{xs} = k_x\sqrt{1+g_x^2} + k\frac{g_x g_{xx}}{\sqrt{1+g_x^2}}. \tag{3.33}$$

But, from (3.32),

$$g_{xx} = (k - \frac{f}{c})(1+g_x^2)^{\frac{3}{2}}. \tag{3.34}$$

Plugging this into (3.33), we get that

$$g_{xs} = k_x\sqrt{1+g_x^2} + k(k - \frac{f}{c})g_x(1+g_x^2). \tag{3.35}$$

Differentiating (3.35) with respect to x and replacing all second order spatial derivatives g_{xx} with

the right-hand side of (3.34), we get the following expression for g_{xxs}:

$$\begin{aligned} g_{xxs} &= k_{xx}\sqrt{1+g_x^2} + 2k_x g_x (k - \frac{f}{c})(1+g_x^2) + \\ &+ k(k_x - \frac{f_x + f_y g_x}{c}) g_x (1+g_x^2) + k(k - \frac{f}{c})^2 (1+3g_x^2)(1+g_x^2)^{\frac{3}{2}}. \end{aligned} \tag{3.36}$$

We now differentiate (3.32) with respect to s and obtain

$$k_s = \frac{f_y g_s}{c} + \frac{g_{xxs}}{(1+g_x^2)^{\frac{3}{2}}} - \frac{3}{2}(k - \frac{f}{c}) \frac{2 g_x g_{xs}}{1+g_x^2},$$

which, after replacing the g_{xs} and g_{xxs} with the expressions obtained in (3.35) and (3.36) and some algebraic manipulation, becomes

$$k_s = \frac{k_{xx}}{\sqrt{1+g_x^2}} + \frac{f}{c}\frac{g_x}{\sqrt{1+g_x^2}} k_x + k(k - \frac{f}{c})^2 + k\frac{f_y - f_x g_x}{c\sqrt{1+g_x^2}}. \tag{3.37}$$

We may choose the initial data for the interface to be such that

$$k(x, g(x,0)) \geq 0.$$

Then (3.37) enforces this inequality to stay valid at all times. Indeed, let s_1 be the first point in time when the function k assumes the value 0 in some point x_1. If x_1 is an isolated zero point of k, then we have

$$k_x(x_1, s_1) = 0, k_{xx}(x_1, t_1) > 0$$

and then (3.37) gives that $k_s(x_1, s_1) > 0$. If x_1 is not an isolated zero point of k, then

$$k_x(x_1, s_1) = k_{xx}(x_1, s_1) = 0$$

and then (3.37) gives that $k_s(x_1, s_1) = 0$. It follows that, indeed, k does not ever assume negative values.

By (3.32), the positivity of k implies

$$\frac{d}{dx}\frac{g_x}{\sqrt{1+g_x^2}} \geq -\frac{f(x,g)}{c},$$

thus

$$g_x^2 (1 - (\int_x^{x_0} \frac{f(x,g)}{c}\, dx)^2) \leq (\int_x^{x_0} \frac{f(x,g)}{c}\, dx)^2, \tag{3.38}$$

for all $x < x_0$, where x_0 is a point where g assumes its maximum value. Moreover, a similar inequality

will hold for $x < x_0$. Assuming that c is large enough such that

$$(\int_{x_1}^{x_2} \frac{f(x,g)}{c}\, dx)^2 \leq 1 \tag{3.39}$$

for any x_1 and x_2, (3.38) and its correspondent for values of x with $x < x_0$ will provide finite bounds on g_x. These bounds ensure, in particular, that the interface will be such that it can be written as the graph of the function g at all times.

It also follows that we are able to use the governing equation for g

$$g_t = f(x,g)\sqrt{1+g_x^2} + c\frac{g_{xx}}{1+g_x^2}$$

at all times. Integrating with respect to x, this yields

$$(\int_{x_1}^{x_2} g(x,t)\, dx)_t = \int_{x_1}^{x_2} f(x,g(x,t))\, dx + c \arctan g_x|_{x_1}^{x_2}.$$

Choosing x_1 and x_2 ends of an interval of periodicity for g, the last term in the right-hand side vanishes and we are left with

$$(\int_{x_1}^{x_2} g(x,t)\, dx)_t = \int_{x_1}^{x_2} f(x,g(x,t))\, dx, \tag{3.40}$$

which says that, at any time, the instantaneous effective speed of the interface equals the average of the values of f along the front.

We now estimate the effective normal velocity for the case when the constant interfacial energy c is very large. If c is large enough such that (3.39) holds, (3.38) implies that

$$|g_x| \leq m = m(c) = \frac{\max|f|}{\sqrt{c^2 - \max|f|}},$$

and thus, for every $x_0 \in [0,1]$,

$$|g(x_0,t) - \bar{g}(t)| \leq m(c) \tag{3.41}$$

holds, where

$$\bar{g}(t) = \int_0^1 g(x,t)dx.$$

This expresses the fact that, as $c \to \infty$, curvature becomes more and more penalized so the front becomes flatter and flatter. Using (3.40), (3.41) and the Lipschitz property of f,

$$\begin{aligned} |\bar{g}_t - \int_0^1 f(x,\bar{g}(x))dx| &= |\int_0^1 f(x,g(x,t))dx - \int_0^1 f(x,\bar{g}(x))dx| \leq \\ &\leq \int_0^1 |f(x,g(x,t)) - f(x,\bar{g}(t))|dx \leq \end{aligned}$$

$$\leq \int_0^1 L|g(x,t) - \bar{g}(t)|dx \leq \int_0^1 Lm(c)dx \leq Lm(c).$$

Thus, at any instant of time, the velocity equals $\int_0^1 f(x, \bar{g}(x))dx$, up to an error of order $o(\frac{1}{c})$. Then, as long as $\int_0^1 f(x,y)\ dx$ never vanishes, the speed with which the average front $\bar{g}(t)$ travels over one periodicity interval $[0,1]$ will be

$$(\int_0^1 \frac{1}{\int_0^1 f(x,y)\ dx} dy)^{(-1)}, \tag{3.42}$$

up to an error of order $o(\frac{1}{c})$. Since (3.41) ensures that the front $\mathcal{F}$ stays close to its average (given by $\bar{g}(t)$), (3.42) will also be the limit as $c \to \infty$ of the effective normal velocity of $\mathcal{F}$.

If the function f is such that $\int_0^1 f(x,y)\ dx$ vanishes for some y, then the front will be trapped once it reaches that position and we have that $V(e_2) = 0$.

To write this in a more compact manner, we shall make the following two notations in $\mathbb{R}^N$: let $< \cdot >_{p^\perp}$ denote the average of a Y_N-periodic function g on the $(N-1)$-dimensional hyperplane that is orthogonal to p and let $\langle \cdot \rangle$ denote the usual one-dimensional average. We have proved the following result:

Proposition 3 *For a periodic interface in $\mathbb{R}^2$ with effective normal e_2 and moving with the normal velocity law (3.1), where f is a $[0,1]^2$-periodic function, its effective normal velocity has the limit*

$$V(e_2) = \bar{f}(e_2) = \langle \langle f \rangle_{e_2^\perp}^{-1} \rangle^{(-1)} \tag{3.43}$$

as $c \to \infty$, as long as $\langle f \rangle_{e_2^\perp}$ never vanishes. If $\langle f \rangle_{e_2^\perp}$ assumes the value 0, then $\bar{f}(e_2) = 0$.

We now extend this result to $\mathbb{R}^N$ through an asymptotic analysis on the degenerate parabolic equation in problem (3.3):

$$\frac{\partial h^\varepsilon}{\partial t} = f(\frac{x}{\varepsilon})|\nabla h^\varepsilon| + \varepsilon c|\nabla h^\varepsilon| \mathrm{div} \frac{\nabla h^\varepsilon}{|\nabla h^\varepsilon|}, \tag{3.44}$$

as $c \to \infty$ fast enough so that we also have $\varepsilon c \to \infty$. We make the following ansatz for h^ε:

$$h^\varepsilon(x,t) = u^\varepsilon(x,t) + \frac{1}{c} v^\varepsilon(x,t) + o(\frac{1}{c}).$$

Plugging this in (3.44) and separating the terms multiplied by c, we get that the c^1 order problem is

$$|\nabla u^\varepsilon| \mathrm{div} \frac{\nabla u^\varepsilon}{|\nabla u^\varepsilon|} = 0.$$

Hence u^ε is either a constant (which we exclude, because we want the zero level set of h^ε to be $N-1$-dimensional and not void or the whole space) or a function the level sets of which have zero mean curvature everywhere. Adding the periodicity conditions that we have for h^ε (and thus for u^ε

also), this implies that u^ε needs to have all level sets flat, thus it has to be a function of one spatial variable only. With proper choice of initial conditions for h^ε, we may assume that

$$u^\varepsilon(x,t) = u^\varepsilon(x_N,t). \tag{3.45}$$

Next, by separating the terms that are not multiplied by any power of c, we get that the c^0 order problem is

$$\begin{aligned}\frac{\partial u^\varepsilon}{\partial t} &= f(\frac{x}{\varepsilon})|\nabla u^\varepsilon| - \varepsilon|\nabla u^\varepsilon|\mathrm{div}\frac{\nabla v^\varepsilon}{|\nabla u^\varepsilon|} - \varepsilon\frac{\nabla u^\varepsilon\cdot\nabla v^\varepsilon}{|\nabla u^\varepsilon|}\ \mathrm{div}\frac{\nabla u^\varepsilon}{|\nabla u^\varepsilon|} + \\ &+ \varepsilon|\nabla u^\varepsilon|\mathrm{div}(\frac{\nabla u^\varepsilon\cdot\nabla v^\varepsilon}{|\nabla u^\varepsilon|^3}\nabla u^\varepsilon).\end{aligned}$$

Taking into account that

$$\mathrm{div}\frac{\nabla u^\varepsilon}{|\nabla u^\varepsilon|} = 0,$$

the c^0 order problem becomes

$$\begin{aligned}\frac{\partial u^\varepsilon}{\partial t} &= f(\frac{x}{\varepsilon})|\nabla u^\varepsilon| - \varepsilon\triangle v^\varepsilon + \varepsilon\frac{\nabla u^\varepsilon\cdot(D^2u^\varepsilon\nabla v^\varepsilon)}{|\nabla u^\varepsilon|^2} + \\ &+ \varepsilon\frac{\nabla u^\varepsilon\cdot\nabla v^\varepsilon}{|\nabla u^\varepsilon|}\mathrm{div}\frac{\nabla u^\varepsilon}{|\nabla u^\varepsilon|} + \varepsilon\frac{\nabla v^\varepsilon\cdot(D^2u^\varepsilon\nabla u^\varepsilon)}{|\nabla u^\varepsilon|^2} + \\ &+ \varepsilon\frac{\nabla u^\varepsilon\cdot(D^2v^\varepsilon\nabla u^\varepsilon)}{|\nabla u^\varepsilon|^2} - 2\varepsilon\frac{\nabla u^\varepsilon\cdot\nabla v^\varepsilon}{|\nabla u^\varepsilon|^4}\nabla u^\varepsilon\cdot(D^2u^\varepsilon\nabla u^\varepsilon).\end{aligned}$$

Using (3.45), this reduces to

$$\frac{\partial u^\varepsilon}{\partial t}(x_N,t) = f(\frac{x}{\varepsilon})|\nabla u'(x_N)| - \varepsilon(\triangle v^\varepsilon(x,t) + v_{x_Nx_N}(x,t)).$$

We can get rid of the last term by integrating over $Y^\varepsilon_{(N-1)} = [0,\varepsilon]^{(N-1)}$ in the first $(N-1)$ variables and obtain

$$\frac{\partial u^\varepsilon}{\partial t}(x_N,t) = \tilde{f}(\frac{x_N}{\varepsilon})|\frac{du^\varepsilon}{dx_N}(x_N)|, \tag{3.46}$$

where

$$\tilde{f}(x_N) = \int_{[0,1]^{(N-1)}} f(x)\ dx_1...dx_{N-1}.$$

We notice that the equation (3.46) is of the Hamilton Jacobi type. If $\tilde{f}(x_N)$ has constant sign, we can use the homogenization results proved in [6] and in Chapter 2 to argue that its solution u^ε converges uniformly (as $\varepsilon\to 0$) to the solution u of

$$\frac{\partial u}{\partial t}(x_N,t) = \bar{f}\ |u'(x_N)|,$$

where $\bar{f}$ can be calculated by means of the variational principle derived in Theorem 2:

$$\bar{f} = \lim_{D\to\infty} \sup_{I\in\mathcal{I}_D} \frac{D}{\int_I \frac{dx_N}{\tilde{f}(x_N)}},$$

where $\mathcal{I}_D$ is the set of all intervals of length D.

If $\tilde{f}(x_N)$ does not have constant sign, it was shown in [6] that the resulting effective velocity is null.

Since $c \to \infty$ fast enough so that we also have $\varepsilon c \to \infty$, u will also be the limit of h^ε. Hence large c limit of the effective normal velocity in the e_N direction is

$$\bar{v}_n(e_N) = \lim_{D\to\infty} \sup_{I\in\mathcal{I}_D} \frac{D}{\int_I \frac{dx_N}{\int_{[0,1]^{(N-1)}} f(x)\, dx_1 \ldots dx_{N-1}}}. \tag{3.47}$$

If $d = d(D)$ is the largest integer smaller than D, then any interval $I \in \mathcal{I}_D$ is the reunion of d periodicity cells $[0,1]$ with an interval of length $D - d(D)$, so we can rewrite (3.47) as

$$\begin{aligned}\bar{v}_n(e_N) &= \lim_{D\to\infty} \frac{D}{d\int_0^1 \frac{dx_N}{\int_{[0,1]^{(N-1)}} f\, dx_1 \ldots dx_{N-1}} + \inf_{I\in\mathcal{I}_d} \int_I \frac{dx_N}{\int_{[0,1]^{(N-1)}} f\, dx_1 \ldots dx_{N-1}}} = \\ &= \Big(\int_0^1 \frac{dx_N}{\int_{[0,1]^{(N-1)}} f\, dx_1 \ldots dx_{N-1}}\Big)^{(-1)},\end{aligned}$$

which gives the generalization of (3.43).

Chapter 4

The effect of precipitates on the motion of a twin boundary

4.1 Introduction

In the present chapter we study the effect of precipitates on the motion of an interface or phase boundary in a solid, such as shape memory alloys capable of martensitic phase transitions. Shape memory alloys are able to assume various different phases: a high-symmetry, high-temperature phase (called austenite) and several symmetry-related low-symmetry, low-temperature phases (called variants of martensites). The interfaces that separate two martensitic phases or variants are called twin boundaries and it is their presence and mobility that makes the shape memory effect possible.

The motivation for our study is given by the commercially important shape memory alloy NiTi. This alloy is very ductile and therefore it is usually precipitate hardened: by annealing an alloy which is slightly rich in Ti, it is possible to obtain NiTi shape memory alloys with a small volume fraction of Ni_3Ti_4 precipitates. It has been observed that this raises the yield strength of the alloy while, at the same time, it does not affect too much the shape memory effect or the mobility of the twin/phase boundaries. It also only slightly depresses the transformation temperature. Thus these precipitates have quite a significant effect on plasticity (or mobility of dislocations) but no significant effect on phase transformation (or motion of twin/phase boundaries). The increase of yield strength by precipitates is quite well understood (see for example [22]). The precipitates pin the underlying dislocation and make it more difficult for them to move. So why do they not pin the twin/phase boundary? This question motivates this chapter.

A heuristic explanation for this phenomenon is that the precipitates have the symmetry of the austenite (cubic in this case). Therefore, they are equally (energetically) disliked by all variants of martensite, and hence they do not produce any systematic preference of one martensitic variant over the other. Further, their effect is very localized and their concentration very dilute. Therefore, they do not produce any systematic or long range effect on the motion of the phase boundary.

We have seen in Chapter 1 that, in the context of linear elasticity, the normal velocity of the phase boundary can be written as a sum of four terms: the first term is a constant, the second term contains the influence of the inclusions and independent of the interface, the third term is given by the position of the interface and independent of the inclusions, while the fourth term is the product of the interfacial energy with the mean curvature of the interface. The previous chapters have considered this problem in simplified setup and derived formulas for an effective normal velocity when the second term is heterogeneous on a scale small compared to the domain. In this chapter we study the effect of precipitates, including the key elastic term that depends on the interface. Rather than focusing on the issue of homogenization, we try to expose the effect of the precipitates through simulation of certain examples. Section 4.2 specializes the problem to the case of an anti-plane shear deformation and also contains an estimate of the effect of the inclusions in the two-dimensional case. Sections 4.3 and 4.4 present a numerical method that allows us to simulate of the propagation of the phase boundary. Section 4.5 contains the results of certain simulations, which in particular show that the precipitate inclusions indeed have only a short range effect on the motion of the twin boundary. Finally, Section 4.6 considers the effect of a dilute dispersion of precipitates on the overall kinetics of phase boundaries.

4.2 Anti-plane shear deformation

We now specialize the model proposed in Chapter 1 to a body which occupies the whole three-dimensional space and undergoes anti-plane shear deformations, where the displacement is parallel to a fixed axis and independent of the axial coordinate. We calculate the driving force and normal velocity (1.7) explicitly for an interface propagating through a region containing circular precipitates in an attempt to understand the effect of precipitates on kinetics.

In anti-plane shear, we may regard the displacement as a scalar function u on a plane. The strain may be regarded as the vector ∇u. We assume that all phases and precipitates are isotropic and (by scaling the applied stress if necessary) take the elastic modulus equal to 1. Thus the energy is

$$W(\nabla u) = \frac{1}{2}|\nabla u - \xi_k|^2,$$

where ξ_k are the transformation strains corresponding to the various phases of the solid, and the stress is given by

$$\sigma = \nabla u - \xi_k. \tag{4.1}$$

The linear momentum balance (1.3) reduces to

$$\sigma_{\alpha,\alpha} = 0 \tag{4.2}$$

at all points where u is smooth. At points where u is not smooth, the linear momentum balance reduces to continuity of traction:

$$[\![\sigma_\alpha]\!] n_\alpha = 0. \tag{4.3}$$

In the following we will denote by ξ_1 and ξ_2 the transformation strains of the phases separated by Γ and by ξ_0 the transformation strain of the phase in each inclusion. We assume that Γ and the boundaries of all inclusions A_i consist of a finite number of regular arcs (in the sense of Kellogg - see [18]) and that they do not have corners. The equilibrium equations (4.2) then imply that u is a harmonic function, while (4.3) dictates the jump conditions on Γ and on the boundary of each ξ_0-phase inclusion A_i:

$$\begin{aligned}
&\Delta u = 0 \quad \text{in} \quad \mathbb{R}^2 \setminus (\Gamma \cup \bigcup_i \partial A_i) \\
&u^+_{,\alpha} - u^-_{,\alpha} = (\xi_{2\beta} - \xi_{1\beta}) n_\beta n_\alpha \quad \text{on } \Gamma, \\
&u^+_{,\alpha} - u^-_{,\alpha} = (\xi_{0\beta} - \xi_{2\beta}) n_\beta n_\alpha \quad \text{on } \partial A_i, \quad \text{for all } A_i \text{ inside } \Gamma, \\
&u^+_{,\alpha} - u^-_{,\alpha} = (\xi_{0\beta} - \xi_{1\beta}) n_\beta n_\alpha \quad \text{on } \partial A_i, \quad \text{for all } A_i \text{ outside } \Gamma.
\end{aligned} \tag{4.4}$$

To this set of equations we have to add the far field conditions which contain the applied stress $\tilde{\sigma}$:

$$u \to \tilde{\sigma}_\alpha x_\alpha \quad \text{as} \quad x \to \infty. \tag{4.5}$$

In two dimensions, this problem (4.4) & (4.5) is analytically solvable in terms of logarithmic potentials, following Rosakis [23]. Some results that will prove useful are summarized by Rosakis' Lemma 4.1 in [23] and will be repeated here for the reader's convenience. If we define the logarithmic potential of a region $D \subset \mathbb{R}^2$ by

$$\phi^D(x) = \frac{1}{2\pi} \int_D \log|x - z| da_z,$$

we have that

$$\Delta \phi^D = \begin{cases} 1 & \text{on } D \\ 0 & \text{on } \mathbb{R}^2 \setminus D \end{cases},$$

$$\phi^D_{,\alpha}(x) = \frac{1}{2\pi} \int_D \frac{x_\alpha - z_\alpha}{|x - z|^2} dA_z = -\frac{1}{2\pi} \int_{\partial D} \log|x - z| n_\alpha(z) ds_z$$

and

$$\phi^D_{,\alpha}(x) \to 0 \quad \text{as} \quad |x| \to \infty.$$

Further, if we set

$$\psi^D_{\alpha\beta}(x) = \frac{1}{2\pi} \int_{\partial D} \frac{z_\beta - x_\beta}{|x - z|^2} n_\alpha(z) ds_z,$$

then

$$\phi^D_{,\alpha\beta} = \psi^D_{\alpha\beta} \quad \text{on } \mathbb{R}^2 \setminus \partial D$$

and

$$\phi^{D\pm}_{,\alpha\beta}(x) = \lim_{x^\pm \to x} \phi^D_{,\alpha\beta}(x^\pm) = \psi^D_{\alpha\beta}(x) \pm \frac{1}{2} n_\alpha(x) n_\beta(x), \tag{4.6}$$

where $x^+ \in D$, $x^- \in \mathbb{R}^2 \setminus D$ and $x \in \partial D$.

Using this result, we find the solution to our problem (4.4) and (4.5) to be

$$\begin{aligned} u(x) &= (\xi_2 - \xi_1) \cdot \nabla \phi^0(x) + \sum_i (\xi_0 - \xi_{s(i)}) \cdot \nabla \phi^i(x) + \tilde{\sigma} \cdot x \\ &= \frac{\xi_2 - \xi_1}{2\pi} \cdot \int_\Gamma \log|x - z| n(z) ds_z + \sum_i \frac{\xi_{s(i)} - \xi_0}{2\pi} \cdot \int_{\partial A_i} \log|x - z| n(z) ds_z + \tilde{\sigma} \cdot x, \end{aligned} \tag{4.7}$$

where $s(i) = 1$ if A_i is outside Γ and $s(i) = 2$ for the inclusions A_i inside Γ, ϕ^0 is the logarithmic potential of the interior of Γ and ϕ^i is the logarithmic potential of the interior of A_i.

Therefore, in anti-plane shear, the normal velocity (1.7) yields

$$v_n = \frac{1}{2}(\xi_2^2 - \xi_1^2) - (\xi_2 - \xi_1) \cdot \left(\sum_{i=1}^N \nabla^2 \phi^i(x)(\xi_0 - \xi_{s(i)}) \right) - (\xi_2 - \xi_1) \cdot \langle \nabla^2 \phi^0(x)(\xi_2 - \xi_1) \rangle - c\kappa. \tag{4.8}$$

Note that the influence of the inclusions are described by the sum in parentheses. We henceforth concentrate only on this:

$$V = -(\xi_2 - \xi_1) \cdot \left(\sum_{i=1}^N \nabla^2 \phi^i(x)(\xi_0 - \xi_{s(i)}) \right) = -\sum_{i=1}^N (\xi_{2\alpha} - \xi_{1\alpha}) \psi^i_{\alpha\beta}(x)(\xi_{0\beta} - \xi_{s(i)\beta}). \tag{4.9}$$

In order to estimate this quantity explicitly, we assume that the inclusions A_i are all circles of radius R centered at the positions z_i. Then

$$\begin{aligned} \psi^i_{11}(x) &= \frac{R}{2\pi} \int_0^{2\pi} \frac{R\cos\theta - y_{i1}}{y_{i1}^2 + y_{i2}^2 + R^2 - 2R(y_{i1}\cos\theta + y_{i2}\sin\theta)} \sin\theta d\theta \\ &= \frac{R}{2\pi} \int_0^{2\pi} \frac{R\cos\theta - y_{i1}}{y_i^2 + R^2 - 2R|y_i|\cos(\theta - \alpha_i)} \sin\theta d\theta, \end{aligned}$$

where $y_i = x - z_i$ and α_i is the argument of y_i.

Changing variables $t = \frac{\pi}{2} + \alpha_i - \theta$, we get

$$\begin{aligned} \psi^i_{11}(x) &= \frac{R}{2\pi} \int_{\alpha_i - \frac{3\pi}{2}}^{\alpha_i + \frac{\pi}{2}} \frac{R\sin(t - \alpha_i) - y_{i1}}{y_i^2 + R^2 - 2R|y_i|\sin t} \cos(\alpha_i - t) dt \\ &= -\frac{R^2 \cos\alpha_i \sin\alpha_i}{2\pi} I_{c2} - \frac{R^2 \sin^2\alpha_i}{2\pi} I_{cs} + \frac{R^2 \cos^2\alpha_i}{2\pi} I_{cs} + \frac{R^2 \cos\alpha_i \sin\alpha_i}{2\pi} I_{s2} - \\ &\quad - \frac{R y_{i1} \cos\alpha_i}{2\pi} I_{c1} - \frac{R y_{i1} \sin\alpha_i}{2\pi} I_{s1}, \end{aligned} \tag{4.10}$$

where

$$I_{c1} = \int_{\alpha_i - \frac{3\pi}{2}}^{\alpha_i + \frac{\pi}{2}} \frac{\cos t}{y_i^2 + R^2 - 2R|y_i| \sin t} dt,$$
$$I_{s1} = \int_{\alpha_i - \frac{3\pi}{2}}^{\alpha_i + \frac{\pi}{2}} \frac{\sin t}{y_i^2 + R^2 - 2R|y_i| \sin t} dt,$$
$$I_{c2} = \int_{\alpha_i - \frac{3\pi}{2}}^{\alpha_i + \frac{\pi}{2}} \frac{\cos^2 t}{y_i^2 + R^2 - 2R|y_i| \sin t} dt,$$
$$I_{s2} = \int_{\alpha_i - \frac{3\pi}{2}}^{\alpha_i + \frac{\pi}{2}} \frac{\sin^2 t}{y_i^2 + R^2 - 2R|y_i| \sin t} dt$$

and

$$I_{cs} = \int_{\alpha_i - \frac{3\pi}{2}}^{\alpha_i + \frac{\pi}{2}} \frac{\cos t \sin t}{y_i^2 + R^2 - 2R|y_i| \sin t} dt.$$

To calculate these integrals, we use the following identities:

$$\int \frac{\cos t}{y_i^2 + R^2 - 2R|y_i| \sin t} dt = -\frac{1}{2R|y_i|} \log(y_i^2 + R^2 - 2R|y_i| \sin t)$$

and

$$\int \frac{dt}{y_i^2 + R^2 - 2R|y_i| \sin t} = \frac{2}{y_i^2 - R^2} \arctan \frac{(y_i^2 + R^2) \tan \frac{t}{2} - 2R|y_i|}{y_i^2 - R^2}$$

for $|y_i| > R$ (which translates to the fact that Γ does not intersect any of the A_i's). We obtain

$$\begin{aligned}
I_{c1} &= -\frac{1}{2R|y_i|} \log(y_i^2 + R^2 - 2R|y_i| \sin t) \,|_{\alpha_i - \frac{3\pi}{2}}^{\alpha_i + \frac{\pi}{2}} = 0, \\
I_{s1} &= -\frac{1}{2R|y_i|} \int_{\alpha_i - \frac{3\pi}{2}}^{\alpha_i + \frac{\pi}{2}} \frac{y_i^2 + R^2 - 2R|y_i| \sin t - (y_i^2 + R^2)}{y_i^2 + R^2 - 2R|y_i| \sin t} dt \\
&= -\frac{1}{2R|y_i|} \int_{\alpha_i - \frac{3\pi}{2}}^{\alpha_i + \frac{\pi}{2}} dt + \frac{y_i^2 + R^2}{2R|y_i|} \int_{\alpha_i - \frac{3\pi}{2}}^{\alpha_i + \frac{\pi}{2}} \frac{dt}{y_i^2 + R^2 - 2R|y_i| \sin t} = \frac{\pi}{R|y_i|}, \\
I_{s2} &= -\frac{1}{2R|y_i|} \int_{\alpha_i - \frac{3\pi}{2}}^{\alpha_i + \frac{\pi}{2}} \frac{(y_i^2 + R^2 - 2R|y_i| \sin t) \sin t - (y_i^2 + R^2) \sin t}{y_i^2 + R^2 - 2R|y_i| \sin t} dt \\
&= -\frac{1}{2R|y_i|} \int_{\alpha_i - \frac{3\pi}{2}}^{\alpha_i + \frac{\pi}{2}} \sin t \, dt + \frac{y_i^2 + R^2}{2R|y_i|} I_{s1} = \frac{\pi(y_i^2 + R^2)}{2R^2 y_i^2}, \\
I_{c2} &= \int_{\alpha_i - \frac{3\pi}{2}}^{\alpha_i + \frac{\pi}{2}} \frac{1 - \sin^2 t}{y_i^2 + R^2 - 2R|y_i| \sin t} dt = \int_{\alpha_i - \frac{3\pi}{2}}^{\alpha_i + \frac{\pi}{2}} \frac{dt}{y_i^2 + R^2 - 2R|y_i| \sin t} - I_{s2} \\
&= \frac{2}{y_i^2 - R^2} \arctan \frac{(y_i^2 + R^2) \tan \frac{t}{2} - 2R|y_i|}{y_i^2 - R^2} \,|_{\alpha_i - \frac{3\pi}{2}}^{\alpha_i + \frac{\pi}{2}} - I_{s2} = -\frac{\pi(y_i^2 + R^2)}{2R^2 y_i^2}
\end{aligned}$$

and

$$I_{cs} = -\frac{1}{2R|y_i|} \int_{\alpha_i - \frac{3\pi}{2}}^{\alpha_i + \frac{\pi}{2}} \frac{(y_i^2 + R^2 - 2R|y_i| \sin t) \cos t - (y_i^2 + R^2) \cos t}{y_i^2 + R^2 - 2R|y_i| \sin t} dt$$

$$= -\frac{1}{2R|y_i|}\int_{\alpha_i-\frac{3\pi}{2}}^{\alpha_i+\frac{\pi}{2}} \cos t\ dt + \frac{y_i^2+R^2}{2R|y_i|} I_{c1} = 0.$$

Plugging all these results in (4.10), we get

$$\begin{aligned}\psi_{11}^i(x) &= \frac{R^2\cos\alpha_i\sin\alpha_i}{2\pi}\ \frac{\pi(y_i^2+R^2)}{2R^2y_i^2} + \frac{R^2\cos\alpha_i\sin\alpha_i}{2\pi}\ \frac{\pi(y_i^2+R^2)}{2R^2y_i^2} - \\ &- \frac{Ry_{i1}\sin\alpha_i}{2\pi}\ \frac{\pi}{R|y_i|} = \frac{R^2\sin 2\alpha_i}{4y_i^2}.\end{aligned}$$

Similarly,

$$\begin{aligned}\psi_{12}^i(x) &= \frac{R}{2\pi}\int_0^{2\pi} \frac{R\sin\theta - y_{i2}}{y_i^2+R^2-2R|y_i|\cos(\theta-\alpha_i)}\sin\theta d\theta \\ &= \frac{R}{2\pi}\int_{\alpha_i-\frac{3\pi}{2}}^{\alpha_i+\frac{\pi}{2}} \frac{R\cos(\alpha_i-t)-y_{i2}}{y_i^2+R^2-2R|y_i|\sin t}\cos(\alpha_i-t)dt \\ &= \frac{R^2\cos^2\alpha_i}{2\pi}I_{c2} + \frac{R^2\cos\alpha_i\sin\alpha_i}{2\pi}I_{cs} + \frac{R^2\cos\alpha_i\sin\alpha_i}{2\pi}I_{cs} + \frac{R^2\sin^2\alpha_i}{2\pi}I_{s2} - \\ &- \frac{Ry_{i2}\cos\alpha_i}{2\pi}I_{c1} - \frac{Ry_{i2}\sin\alpha_i}{2\pi}I_{s1} \\ &= -\frac{R^2\cos^2\alpha_i}{2\pi}\ \frac{\pi(y_i^2+R^2)}{2R^2y_i^2} + \frac{R^2\sin^2\alpha_i}{2\pi}\ \frac{\pi(y_i^2+R^2)}{2R^2y_i^2} - \frac{Ry_{i2}\sin\alpha_i}{2\pi}\frac{\pi}{R|y_i|} \\ &= -\frac{1}{4}(\frac{R^2}{y_i^2}\cos 2\alpha_i + 1), \\ \psi_{21}^i(x) &= \frac{R}{2\pi}\int_0^{2\pi} \frac{R\cos\theta - y_{i1}}{y_i^2+R^2-2R|y_i|\cos(\theta-\alpha_i)}\cos\theta d\theta \\ &= \frac{R}{2\pi}\int_{\alpha_i-\frac{3\pi}{2}}^{\alpha_i+\frac{\pi}{2}} \frac{R\sin(t-\alpha_i)-y_{i1}}{y_i^2+R^2-2R|y_i|\sin t}\sin(t-\alpha_i)dt \\ &= \frac{R^2\cos^2\alpha_i}{2\pi}I_{s2} - \frac{R^2\sin\alpha_i\cos\alpha_i}{2\pi}I_{cs} - \frac{R^2\sin\alpha_i\cos\alpha_i}{2\pi}I_{cs} + \frac{R^2\sin^2\alpha_i}{2\pi}I_{c2} - \\ &- \frac{Ry_{i1}\cos\alpha_i}{2\pi}I_{s1} - \frac{Ry_{i1}\sin\alpha_i}{2\pi}I_{c1} \\ &= \frac{R^2\cos^2\alpha_i}{2\pi}\ \frac{\pi(y_i^2+R^2)}{2R^2y_i^2} - \frac{R^2\sin^2\alpha_i}{2\pi}\ \frac{\pi(y_i^2+R^2)}{2R^2y_i^2} - \frac{Ry_{i1}\cos\alpha_i}{2\pi}\frac{\pi}{R|y_i|} \\ &= \frac{1}{4}(\frac{R^2}{y_i^2}\cos 2\alpha_i - 1)\end{aligned}$$

and

$$\begin{aligned}\psi_{22}^i(x) &= \frac{R}{2\pi}\int_0^{2\pi} \frac{R\sin\theta - y_{i2}}{y_i^2+R^2-2R|y_i|\cos(\theta-\alpha_i)}\cos\theta d\theta \\ &= \frac{R}{2\pi}\int_{\alpha_i-\frac{3\pi}{2}}^{\alpha_i+\frac{\pi}{2}} \frac{R\cos(\alpha_i-t)-y_{i2}}{y_i^2+R^2-2R|y_i|\sin t}\sin(t-\alpha_i)dt \\ &= \frac{R^2\cos^2\alpha_i}{2\pi}I_{cs} - \frac{R^2\sin\alpha_i\cos\alpha_i}{2\pi}I_{c2} + \frac{R^2\sin\alpha_i\cos\alpha_i}{2\pi}I_{s2} - \frac{R^2\sin^2\alpha_i}{2\pi}I_{cs} - \\ &- \frac{Ry_{i2}\cos\alpha_i}{2\pi}I_{s1} + \frac{Ry_{i2}\sin\alpha_i}{2\pi}I_{c1}\end{aligned}$$

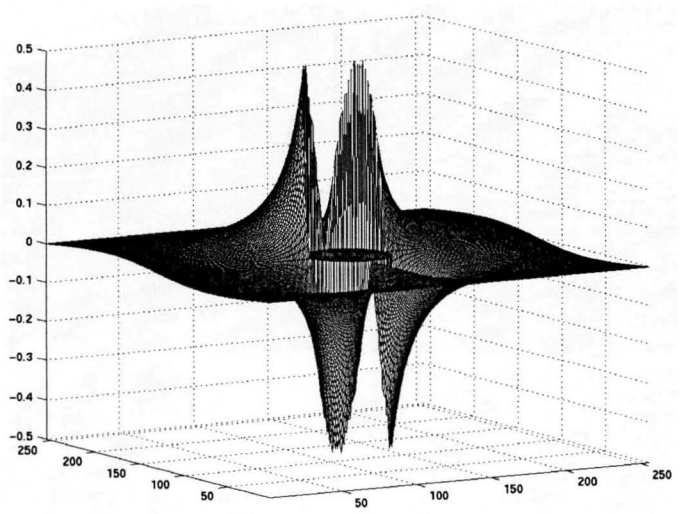

Figure 4.1: Plot of the influence of the inclusions on the normal velocity

$$= \frac{R^2 \sin\alpha_i \cos\alpha_i}{\pi} \frac{\pi(y_i^2 + R^2)}{2R^2 y_i^2} - \frac{R y_{i2} \cos\alpha_i}{2\pi} \frac{\pi}{R|y_i|}$$
$$= \frac{R^2 \sin 2\alpha_i}{4y_i^2}.$$

Substituting these values for $\psi^i_{\alpha\beta}(x)$ in (4.9), we obtain

$$V = -\frac{1}{4}\sum_{i=1}^{N}\left((\xi_{21}-\xi_{11})\frac{R^2\sin 2\alpha_i}{y_i^2}(\xi_{01}-\xi_{s(i)1}) - (\xi_{21}-\xi_{11})(\frac{R^2}{y_i^2}\cos 2\alpha_i + 1)(\xi_{02}-\xi_{s(i)2})\right)$$
$$- \frac{1}{4}\sum_{i=1}^{N}\left((\xi_{22}-\xi_{12})(\frac{R^2}{y_i^2}\cos 2\alpha_i - 1)(\xi_{01}-\xi_{s(i)1}) + (\xi_{22}-\xi_{12})\frac{R^2\sin 2\alpha_i}{y_i^2}(\xi_{02}-\xi_{s(i)2})\right).$$

Figure 4.1 shows V according to the formula above for the case when $\xi_0 = 0$, $\xi_1 = (0, 0.1)$, $\xi_2 = (0, -0.1)$ and the inclusions have radius 0.1 and form a periodic 15×15 lattice with period $[0,1]^2$, centered at the point $(0.5, 0.5)$. The calculation was performed with the help of a 256×256 grid laid on the unit cell. The values for ξ_0, ξ_1, ξ_2 are chosen to mimic a situation in NiTi, where one has martensitic variants which are symmetry related (ξ_1 and ξ_2) and precipitates which posses the symmetry of the austenite. Notice that V has lobes close to the precipitates but dies off away from it. Therefore, we conclude that the precipitates would affect the phase boundaries only when they get close to it but have no long range or systemic effect. The shape of V that we observe in Figure 4.1 is in agreement with the shape of a phase boundary in the vicinity of an inclusion which we shall observe in Figure 4.3.

4.3 The level set formulation

We now proceed towards studying the evolution of the phase boundary as it encounters obstacles. An efficient tool in problems that deal numerically with free boundaries is the level set method, described by Osher and Sethian in [21]. We assume that there exists a level set function $\phi : \mathbb{R}^2 \times [0,T) \to \mathbb{R}$ such that our twin boundary coincides with its zero level set at all times and

$\phi > 0$ in the regions of phase with deformation strain ξ_1 (and appropriate inclusions),

$\phi < 0$ in the regions of phase with deformation strain ξ_2 (and appropriate inclusions).

Since the obstacles are fixed, we use a level set function only for the twin boundary Γ. Then

$$n = \frac{\nabla\phi}{|\nabla\phi|}, \quad v_n = -\frac{\frac{\partial\phi}{\partial t}}{|\nabla\phi|},$$

so our normal velocity law implies that ϕ satisfies the following equation:

$$\frac{\partial\phi}{\partial t} = v_n|\nabla\phi|. \tag{4.11}$$

To this equation one has to attach the initial condition

$$\phi(x,0) = \phi_0(x) \quad \text{in} \quad \mathbb{R}^2, \tag{4.12}$$

where ϕ_0 is a function chosen such that its zero level set coincides with the initial position of the front, and appropriate boundary or far field conditions. If Γ_0 denotes the set of all points in the initial front, a common choice for ϕ_0 is

$$\phi_0(x) = \min(d(x,\Gamma_0), 1),$$

where $d(x,\Gamma_0)$ is the distance from x to Γ_0.

However, to use this level set formulation, we notice in (4.11) that we need a normal velocity field v_n defined everywhere and not only along the twin boundary. To overcome this difficulty, we shall use a relaxation proposed by Hou, Rosakis and LeFloch in [16].

First, we define a regularization of the energy function W. For $0 \le h \le 1$, let $\hat{W}(\nabla u, h)$ be a function such that

$$\begin{cases} \hat{W}(\nabla u, h) = \frac{1}{2}|\nabla u - \xi_0| & \text{in } \bigcup_i A_i \\ \\ \hat{W}(\nabla u, 0) = \frac{1}{2}|\nabla u - \xi_2|, \quad \hat{W}(\nabla u, 1) = \frac{1}{2}|\nabla u - \xi_1| & \text{outside } \bigcup_i A_i \end{cases}. \tag{4.13}$$

One possible choice for such a regularization is

$$\hat{W}(\nabla u, h) = \begin{cases} \frac{1}{2}|\nabla u - \xi_0| & \text{in } \bigcup_i A_i \\ \\ \frac{1}{2}|\nabla u - \xi_2| - h(\frac{1}{2}|\nabla u - \xi_2| - \frac{c}{2}|\nabla u - \xi_1|) & \text{outside } \bigcup_i A_i \end{cases} . \tag{4.14}$$

If $H : \mathbb{R} \to \mathbb{R}$ is the Heaviside step function

$$H(x) = \begin{cases} 1, & \text{if } x > 0 \\ 0, & \text{if } x < 0 \end{cases},$$

then, due to (4.13), $\hat{W}(\nabla u, H(\phi))$ describes the stored energy W.

For each $\varepsilon > 0$, let $H_\varepsilon : \mathbb{R} \to \mathbb{R}$ be a regularized Heaviside function, i.e., a smooth monotonically nondecreasing function with

$$H_\varepsilon(x) = \begin{cases} 1, & \text{if } x > \varepsilon \\ 0, & \text{if } x < -\varepsilon \end{cases},$$
$$H'_\varepsilon(x) > 0 \quad \text{for } |x| < \varepsilon.$$

A possible choice for the regularized Heaviside function is

$$H_\varepsilon(x) = \begin{cases} 0, & \text{if } x < -\varepsilon \\ \frac{x+\varepsilon}{2\varepsilon} + \frac{1}{2\pi}\sin\frac{\pi x}{\varepsilon} & \text{if } |x| \le \varepsilon \\ 1, & \text{if } x > \varepsilon \end{cases} . \tag{4.15}$$

The corresponding regularized Dirac delta is defined by

$$\delta_\varepsilon(x) = H'_\varepsilon(x). \tag{4.16}$$

In particular, if H_ε is defined by (4.15), then the regularized Dirac delta function is

$$\delta_\varepsilon(x) = \begin{cases} 0, & \text{if } |x| > \varepsilon \\ \frac{1}{2\varepsilon} + \frac{1}{2\varepsilon}\cos\frac{\pi x}{\varepsilon} & \text{if } |x| \le \varepsilon \end{cases} .$$

We can then define the regularized stored energy function W_ε by

$$W_\varepsilon(\nabla u, \phi) = \hat{W}(\nabla u, H_\varepsilon(\phi)). \tag{4.17}$$

This will replace the interfacial discontinuity Γ with a transition layer

$$\Gamma_\varepsilon = \{x : |\phi(x,t)| < \varepsilon\},$$

with width of order 2ε. The regularized stress is defined in analogy with (4.1):

$$\sigma_\varepsilon(\gamma,\phi) = \frac{\partial}{\partial\gamma} W_\varepsilon(\gamma,\phi). \tag{4.18}$$

We now enforce global versions of the momentum balance (4.2) and dissipation inequality, but with W and σ replaced with their regularized versions W_ε and σ_ε. Since we are in the quasi-static case, the momentum balance reduces to

$$\nabla \cdot \sigma_\varepsilon = 0, \tag{4.19}$$

while the regularized dissipation rate is

$$\Delta_\varepsilon(t) = -\int_{\mathbb{R}^2} \frac{\partial W_\varepsilon}{\partial\phi}\ \phi_t\ dx.$$

If we define the regularized driving traction by

$$f_\varepsilon = -\frac{\partial \hat{W}}{\partial h}(\nabla u, H_\varepsilon(\phi)), \tag{4.20}$$

then we can use (4.11), (4.16) and (4.17) to rewrite $\Delta_\varepsilon(t)$ as

$$\Delta_\varepsilon(t) = \int_{\mathbb{R}^2} f_\varepsilon\ v_n\ \delta_\varepsilon(\phi)\ |\phi|\ dx. \tag{4.21}$$

Note that the regularized driving traction is a globally defined field, whereas f is only defined on the interface Γ. Its definition (4.20) is motivated by a comparison of (4.21) with (1.4). Indeed, if ϕ vanishes on Γ and θ is some smooth field, it was proved in [7] that

$$\int_{\mathbb{R}^2} \theta\delta(\phi)|\nabla\phi| dx = \int_\Gamma \theta dl.$$

This shows that (4.21) is a regularized version of (1.4).

We can now extend the assumption $v_n = f_\varepsilon$ to the whole space to obtain a globally defined function v_n. Substituting it into (4.11) yields

$$\frac{\partial\phi}{\partial t} = f_\varepsilon|\nabla\phi| \quad \text{in } \mathbb{R}^2. \tag{4.22}$$

Equations (4.19) and (4.22) comprise a system of two coupled partial differential equations for u and ϕ. Attached to the initial condition (4.12) and appropriate boundary (or far-field) conditions, they define the regularized problem.

4.4 Finite difference discretization associated to the regularized level set formulation for a periodic structure

We now present a numerical method to obtain the evolution of the twin boundary in a periodic structure. We assume that the inclusions are periodically arranged with unit cell $[0,1]^2$. We also assume that the initial data ϕ_0 is $[0,1]^2$-periodic and the initial twin boundary is chosen such that it does not intersect any of the inclusions. We seek periodic solutions to (4.19) and (4.22).

We can write the solution to (4.19) with the help of the $[0,1]^2$-periodic Green function G for Laplace's equation. Recall that

$$G(x,z) = G(x-z) = \sum_m -\frac{1}{m^2} e^{2\pi i\ m\cdot(x-z)} = \sum_m -\frac{1}{m^2}\cos(2\pi i\ m\cdot(x-z)),$$

where the sums are taken over all $m \in \mathbb{Z}^2$ with $m \neq 0$.

Plugging (4.17) and (4.18) into (4.19) we conclude

$$\nabla \cdot \frac{\partial \hat{W}(\nabla u, H_\varepsilon(\phi))}{\partial \gamma} = 0.$$

The linearity of this equation allows us to write its solution as the sum of two terms, one being the solution u_0 to

$$\nabla \cdot \frac{\partial(|\nabla u - \xi_2| - H_\varepsilon(\phi)(|\nabla u - \xi_2| - |\nabla u - \xi_1|))}{\partial \gamma} = 0 \tag{4.23}$$

and the other one being the sum u_{incl} of all potentials associated to the inclusions:

$$u_{incl}(x) = \sum_i (\xi_0 - \xi_{s(i)}) \cdot \frac{1}{2\pi} \int_{A_i} \nabla G(x-z)\, dz.$$

The sum above is taken over all inclusions in $[0,1]^2$ and $s(i)$ equals 1 or 2, depending on which of the phases the inclusion is surrounded by. Written in terms of the convolution product,

$$u_{incl}(x) = \sum_i (\xi_0 - \xi_{s(i)}) \cdot \frac{1}{2\pi} \chi_i * \nabla G,$$

where $\chi_i : [0,1]^2 \to \mathbb{R}$ is the characteristic function associated to the inclusion A_i:

$$\chi_i(x) = \begin{cases} 1, & \text{if } x \in A_i \\ 0, & \text{otherwise} \end{cases}.$$

A short calculation shows that (4.23) may be written as

$$\nabla \cdot (\nabla u - \xi_2) + H_\varepsilon(\phi) \cdot (\nabla \cdot (\nabla u - \xi_2) - \nabla \cdot (\nabla u - \xi_1)) + H'_\varepsilon(\phi)\nabla\phi \cdot ((\nabla u - \xi_2) - (\nabla u - \xi_1)) = 0,$$

$$\Delta u + H'_\varepsilon(\phi)\nabla\phi \cdot (\xi_1 - \xi_2) = 0,$$

so its solution u_0 can also be expressed in terms of the periodic Green function G:

$$u_0(x) = (\xi_1 - \xi_2) \cdot (H'_\varepsilon(\phi)\nabla\phi) * G.$$

Hence the solution to (4.19) is

$$u(x) = (\xi_1 - \xi_2) \cdot (\delta_\varepsilon(\phi)\nabla\phi) * G + \sum_i (\xi_0 - \xi_{s(i)}) \cdot \frac{1}{2\pi}\chi_i * \nabla G, \tag{4.24}$$

where the sum is taken over all inclusions in $[0,1]^2$.

We shall now describe the finite difference discretization for this two-dimensional periodic problem. An $N \times N$ grid is laid on the periodicity cell $[0,1]^2$ with grid spacing $h = \frac{1}{N}$. Denote by $u^n_{i,j}$ the approximation of $u(x_i, y_j, t_n)$ and by $\phi^n_{i,j}$ the approximation of $\phi(x_i, y_j, t_n)$, where $x_i = ih$ $(i = 1, ..., N)$, $y_j = jh$ $(j = 1, ..., N)$, $t_n = n\Delta t$ (n nonnegative integer) and Δt is the time step.

We also introduce the following notations for the difference operators

$$\begin{aligned} D^0_x f_{i,j} &= f_{i+1,j} - f_{i-1,j} \quad \text{(centered)}, \\ D^-_x f_{i,j} &= f_{i,j} - f_{i-1,j} \quad \text{(backward)}, \\ D^+_x f_{i,j} &= f_{i+1,j} - f_{i,j} \quad \text{(forward)}. \end{aligned}$$

The operators D^0_y, D^-_y and D^+_y are defined similarly.

At each time step, the solution u^n to (4.19) is calculated using (4.24). The convolution products appearing in the right-hand side of (4.24) are conveniently fast calculated with the help of the fast Fourier transform.

Once we have u^n, we proceed to the calculation of the driving force f^n, using centered-difference discretizations of (4.14) and (4.20).

Next, we employ a fifth order WENO (weighted essentially non oscillatory) scheme, introduced by Jiang and Peng in Section 2.2 of [17], to discretize equation (4.22) describing the evolution of the

level set function ϕ. Define

$$\begin{aligned}
\phi_x^-(i,j) &= \frac{1}{12h}(-D_x^+\phi_{i-2,j} + 7D_x^+\phi_{i-1,j} + 7D_x^+\phi_{i,j} - D_x^+\phi_{i+1,j}) \\
&- \phi^{WENO}(\frac{D_x^-D_x^+\phi_{i-2,j}}{h}, \frac{D_x^-D_x^+\phi_{i-1,j}}{h}, \frac{D_x^-D_x^+\phi_{i,j}}{h}, \frac{D_x^-D_x^+\phi_{i+1,j}}{h}), \\
\phi_x^+(i,j) &= \frac{1}{12h}(-D_x^+\phi_{i-2,j} + 7D_x^+\phi_{i-1,j} + 7D_x^+\phi_{i,j} - D_x^+\phi_{i+1,j}) \\
&+ \phi^{WENO}(\frac{D_x^-D_x^+\phi_{i+2,j}}{h}, \frac{D_x^-D_x^+\phi_{i+1,j}}{h}, \frac{D_x^-D_x^+\phi_{i,j}}{h}, \frac{D_x^-D_x^+\phi_{i-1,j}}{h}), \\
\phi_y^-(i,j) &= \frac{1}{12h}(-D_y^+\phi_{i,j-2} + 7D_y^+\phi_{i,j-1} + 7D_y^+\phi_{i,j} - D_y^+\phi_{i,j+1}) \\
&- \phi^{WENO}(\frac{D_y^-D_y^+\phi_{i,j-2}}{h}, \frac{D_y^-D_y^+\phi_{i,j-1}}{h}, \frac{D_y^-D_y^+\phi_{i,j}}{h}, \frac{D_y^-D_y^+\phi_{i,j+1}}{h}), \\
\phi_y^+(i,j) &= \frac{1}{12h}(-D_y^+\phi_{i,j-2} + 7D_y^+\phi_{i,j-1} + 7D_y^+\phi_{i,j} - D_y^+\phi_{i,j+1}) \\
&+ \phi^{WENO}(\frac{D_y^-D_y^+\phi_{i,j+2}}{h}, \frac{D_y^-D_y^+\phi_{i,j+1}}{h}, \frac{D_y^-D_y^+\phi_{i,j}}{h}, \frac{D_y^-D_y^+\phi_{i,j-1}}{h}),
\end{aligned}$$

where

$$\phi^{WENO}(a,b,c,d) = \frac{1}{3}\omega_0(a-2b+c) + \frac{1}{6}(\omega_2 - \frac{1}{2})(b-2c+d)$$

and the weights ω_0, ω_2 are defined as

$$\omega_0 = \frac{\alpha_0}{\alpha_0+\alpha_1+\alpha_2}, \quad \omega_2 = \frac{\alpha_2}{\alpha_0+\alpha_1+\alpha_2},$$

$$\alpha_0 = \frac{1}{(\epsilon+IS_0)^2}, \quad \alpha_1 = \frac{6}{(\epsilon+IS_1)^2}, \quad \alpha_0 = \frac{3}{(\epsilon+IS_2)^2}, \tag{4.25}$$

$$IS_0 = 13(a-b)^2 + 3(a-3b)^2, \quad IS_0 = 13(b-c)^2 + 3(b+c)^2, \quad IS_0 = 13(c-d)^2 + 3(3c-d)^2.$$

To numerically compute the Hamiltonian in (4.22), we shall use the local Lax-Friedrichs flux. If $\mathcal{H}(\phi_x, \phi_y)$ denotes the Hamiltonian to be discretized, then

$$\mathcal{H}^{LLF}(\phi_x^+, \phi_x^-, \phi_y^+, \phi_y^-) = \mathcal{H}(\frac{\phi_x^+ + \phi_x^-}{2}, \frac{\phi_y^+ + \phi_y^-}{2}) - \alpha(\phi_x^+, \phi_x^-)\frac{\phi_x^+ - \phi_x^-}{2} - -\beta(\phi_y^+, \phi_y^-)\frac{\phi_y^+ - \phi_y^-}{2},$$

where

$$\alpha(\phi_x^+, \phi_x^-) = \max_{u\in\mathcal{I}(\phi_x^+,\phi_x^-), v\in[C,D]} |\mathcal{H}_{,1}(u,v)|, \beta(\phi_y^+, \phi_y^-) = \max_{v\in\mathcal{I}(\phi_y^+,\phi_y^-), u\in[A,B]} |\mathcal{H}_{,1}(u,v)|.$$

Here $\mathcal{H}_{,1}$ (respectively $\mathcal{H}_{,2}$) stands for the partial derivative of $\mathcal{H}$ with respect to ϕ_x (respectively ϕ_y), $[A,B]$ is the value range for $\phi_x^\pm$ and $\mathcal{I}(a,b) = [\min(a,b), \max(a,b)]$.

In our case, the numerical local Lax-Friedrichs flux reduces to

$$\mathcal{H}^{LLF}(\phi_x^+, \phi_x^-, \phi_y^+, \phi_y^-) = f^n|(\phi_x^0)^2 + (\phi_y^0)^2|,$$

where

$$\phi_x^0 = \min(\phi_x^+, \phi_x^-), \quad \phi_y^0 = \min(\phi_y^+, \phi_y^-).$$

Having this discretization of the right-hand side of (4.22), we proceed to updating the values of the level set function ϕ by numerically integrating it with respect to time, using a fourth order non-TVD (total variation diminishing) Runge Kutta scheme, described by Shu in [24].

In general, if we prescribe the initial value of the level set function ϕ to equal signed distance from the interface, it will not remain a distance function at later times. For large time computations it is desirable to keep ϕ as a distance function. This will ensure that the interface has a finite thickness of order ε at all times. In [26], an iterative procedure was proposed to reinitialize ϕ at each time step, so that it remains close to the signed distance function from the evolving interface. Specifically, given a level-set function $\phi^n = \phi(x, t_n)$ at fixed time t_n, one computes the solution of the initial value problem

$$\begin{cases} \phi_t = \operatorname{sgn}(\phi^n)(1 - |\nabla\phi|) \\ \phi(x, 0) = \phi^n(x) \end{cases} . \tag{4.26}$$

The solution converges rapidly in time to a function that has the same sign and the same zero level set as ϕ^n and also satisfies $|\nabla\phi| = 1$, so that it equals the signed distance from the interface. After ϕ evolves at each time step according to (4.22), it is reinitialized by solving (4.26) for a few time steps. Note that, when running the reinitialization procedure, the computational cell has to be extended to include several periodicity intervals since values of the signed distance function near the boundary may be dictated by points of the front outside the interval $[0, 1]^2$.

4.5 Numerical results

We now apply this numerical method to various examples. In each of these examples, the material is periodic with the unit square as the unit cell. We consider a medium with two phases labelled 1 and 2, and precipitates labelled 0. Since in practice the precipitate inclusions are small compared to the distances in between them, we choose them to be circles of small radius $r = .005$. The transformation strain of the phases ξ_1 and ξ_2 are chosen to be symmetry related with each other and ξ_0 is chosen to be zero. In each example below, we will choose the initial condition to be three horizontal bands in the unit cell: phase 1 - phase 2 - phase 1. This corresponds to an infinite number of infinitely long alternating bands as in the observed fine twins of martensite. The parameters ε (which gives the width of the numerical approximation to the front) and ϵ (which occurs in (4.25)) are chosen to be $\varepsilon = 0.01$ and $\epsilon = 10^{-6}$ respectively. All the simulations were run on a 256×256 grid laid on the unit cell $[0, 1]^2$.

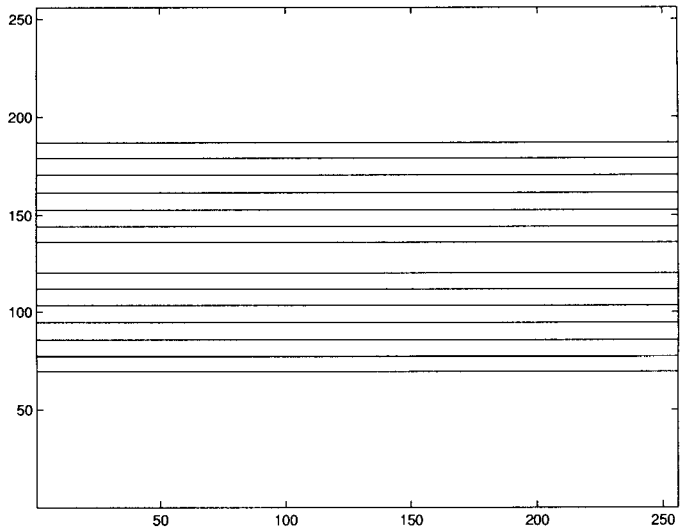

Figure 4.2: Evolution of phase boundaries in the case when there are no inclusions

Example 1. Assume

$$\xi_0 = (0,0), \quad \xi_1 = (0,0.1), \quad \xi_2 = (0,-0.1)$$

and that there are four inclusions present in the unit cell, with centers at the coordinates $(\frac{1}{2},\frac{1}{8})$, $(\frac{1}{2},\frac{3}{8})$, $(\frac{1}{2},\frac{5}{8})$ and $(\frac{1}{2},\frac{7}{8})$. The two horizontal phase boundaries are initially placed symmetrically with respect to the line $x_2 = \frac{1}{2}$ and the phase with deformation strain ξ_2 occupies the area in between them. For the example presented in Figures 4.2 and 4.3, the two interfaces are at the coordinates $j = 120$ and $j = 136$ respectively and the initial level set function is chosen to be the signed distance function. Note that the orientation of the interfaces is compatible with the transformation strain:

$$n = e_2 \parallel (\xi_1 - \xi_2).$$

However, the initial positions are not at equilibrium (which corresponds to equal volume fraction) and thus the driving traction (4.20) does not vanish. The kinetic relation $v_n = f$ forces the interfaces to move and the level set function changes according to (4.22). The coupling of u and ϕ in (4.19) and (4.22) drives the subsequent dynamics of the problem.

For the sake of comparison, Figure 4.2 shows the evolution of the phase boundaries in the case when there are no inclusions of phase 0. It presents a sequence of evolving configurations of the interfaces at $t = 0.0, 0.0002, 0.0004, 0.0006, 0.0008, 0.001, 0.0012$. The interfaces translate uniformly apart from each other until they reach the positions $x_2 = .25$ and $x_2 = .75$ respectively, when the two phases share equal volume fractions and the problem attains a state of equilibrium. This has

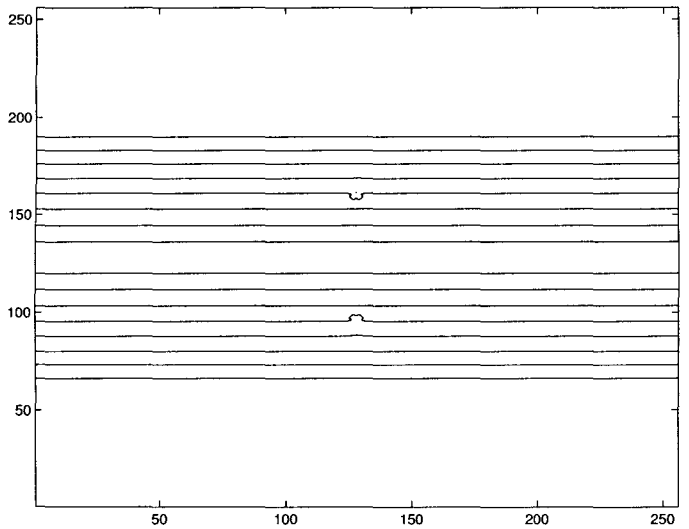

Figure 4.3: Evolution of phase boundaries in the case when there are inclusions

been also checked numerically by running a separate simulation with initial positions of the two horizontal phase boundaries placed at $x_2 = .25$ and $x_2 = .75$ respectively (the two interfaces remain fixed).

We now place the four inclusions of phase 0 and start with the same initial data. It turns out that the influence of the inclusions on the normal velocity is much smaller than the influence of the fact that the two phases do not have equal volume fraction. Therefore, the two phase boundaries are forced to pass through the inclusions with centers at $(\frac{1}{2}, \frac{3}{8})$ and $(\frac{1}{2}, \frac{5}{8})$ and grow till phase 2 occupies half of the unit cell. This is observed in Figure 4.3, which shows a sequence of evolving configurations of the interfaces at the same instances $t = 0.0, 0.0002, 0.0004, 0.0006, 0.0008, 0.001, 0.0012$. The phase boundaries loop around the two inclusions and they develop a disconnected shape which contains a leading front and a trace left around the obstacles, pictured separately in Figure 4.4. After looping around the inclusions, the leading parts continue to translate uniformly in the upward (and downward) direction until they reach the equilibrium positions at $x_2 = .25$ and $x_2 = .75$ respectively (the positions of the inclusions have been chosen symmetrically to the lines $x_2 = .25$ and $x_2 = .75$ so that the final equilibrium position does not change; this can again be checked numerically by running a simulation with initial positions of the two horizontal phase boundaries at $x_2 = .25$ and $x_2 = .75$).

Note that the shape of the phase boundary in the vicinity of the inclusion that we observe in Figure 4.3 is in agreement with the shape of V that we observed in Figure 4.1.

Figure 4.5 presents a comparison of the two cases, with and without inclusions. The interfaces are plotted at the same amount of elapsed time, by a dotted line for the case when there are no inclusions and by a continuous line for the case with obstacles. Note that the inclusions introduce a

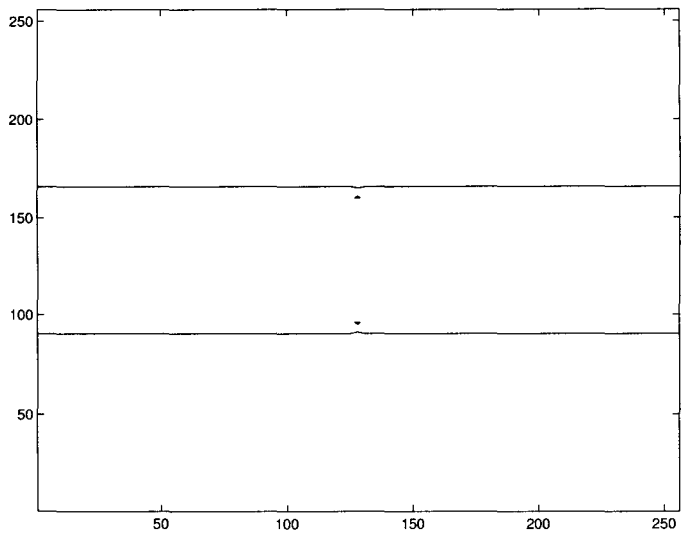

Figure 4.4: Shape of the phase boundaries after it loops around the inclusions

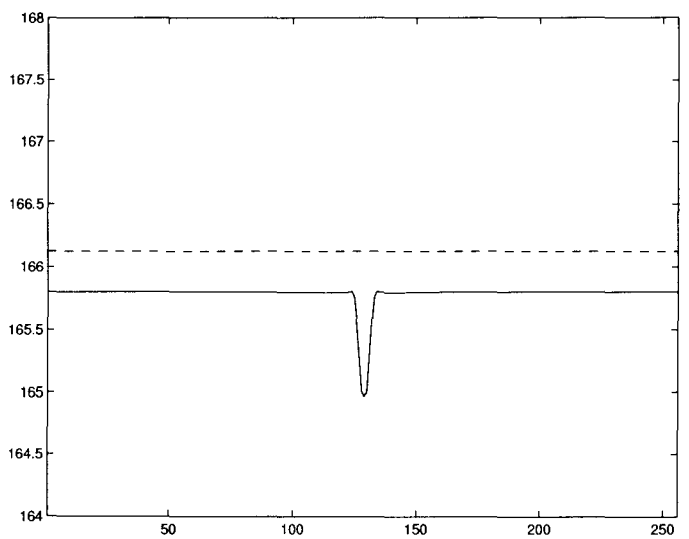

Figure 4.5: Comparison of the two phase boundaries (with and without inclusions)

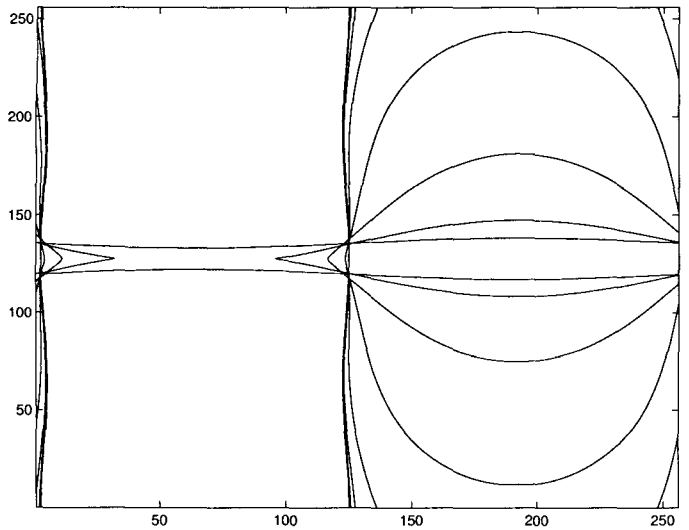

Figure 4.6: Evolution of phase boundaries with mismatched normal in the case when there are no inclusions

small delay in the evolution of the front (the vertical axis has been blown up so that the delay can be easier observed) and also affect its shape locally.

Example 2. While the inclusions seem to have little effect on the evolution of the phase boundaries in the first example, we now show how they can have a crucial effect when acting as instabilities. For this, we consider the same setting only with the three phases modified such that they have the transformation strains

$$\xi_0 = (0,0), \quad \xi_1 = (0.1,0), \quad \xi_2 = (-0.1,0).$$

Again, the two interfaces are initially placed horizontally at the coordinates $j = 120$ and $j = 136$ respectively and the initial level set function is chosen to be the signed distance function. Note now that the orientation of the interfaces is incompatible with the difference between the two transformation strains. If there are no precipitates and if the initial boundaries are perfectly straight, then the two phase boundaries seem to be in a state of unstable equilibrium and do not move. However, if their initial positions are perturbed, the system becomes unstable and evolves to the stable equilibrium, with equal volume fraction and phase boundaries with correct (matched) normal.

Figure 4.6 shows a sequence of evolving configurations of the interfaces for the case when the shape of the two initial phase boundaries was sinusoidally perturbed. The instances when the snapshots are taken are $t = 0.0, 0.002, 0.004, 0.006, 0.008, 0.01, 0.012, 0.014, 0.016, 0.018$. Once the simulation is started, the thinner side of phase 2 starts shrinking as its wider part starts growing. When $t = 0.5$ it has already transformed into a bubble which continues to grow in the e_2 direction

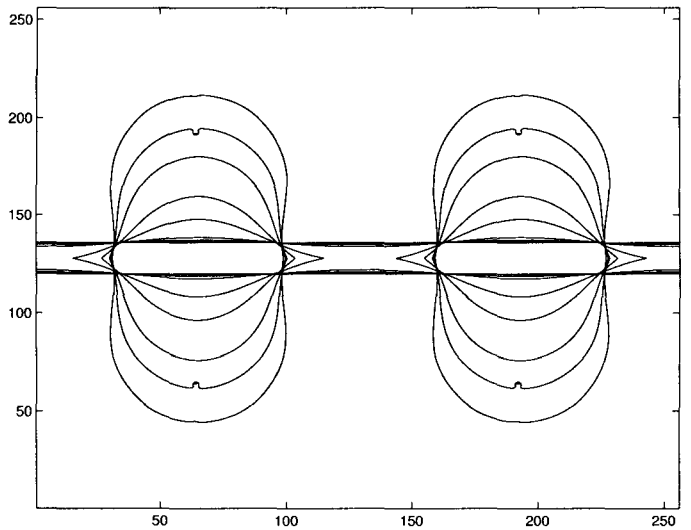

Figure 4.7: Evolution of phase boundaries with mismatched normal (part I)

until it touches the bubbles from the neighboring cells and the region occupied by phase 2 becomes a strip again. Ultimately, the boundaries of this strip flatten and tend to the lines $x_1 = 0$ and $x_1 = 0.5$, which define an equilibrium position - equal volume fraction with phase boundaries having matched normal $n = e_1$.

Returning to the case when the initial interfaces are straight and not perturbed, an interesting simulation shows how the presence of the precipitate inclusions can lead to instability and force the phase boundary to evolve to an equilibrium position. Again, the two interfaces are initially placed at the coordinates $j = 120$ and $j = 136$ respectively and the initial level set function is chosen to be the signed distance function. We place four spherical inclusions with centers at the points $(\frac{1}{4}, \frac{1}{4})$, $(\frac{1}{4}, \frac{3}{4})$, $(\frac{3}{4}, \frac{1}{4})$ and $(\frac{3}{4}, \frac{3}{4})$ respectively.

Figures 4.6, 4.7 and 4.8 picture a sequence of evolving configurations of the phase boundaries. The inclusions act as attractors to the interface and force the interfaces to leave their unstable equilibrium position. The portions of phase 2 strip aligned with the obstacles starts growing as its other part starts shrinking and it breaks into two bubbles, as can be noticed in Figure 4.6, which shows plots the interfaces at the instances $t = 0.005, 0.01, 0.012, 0.013, 0.015, 0.016, 0.017, 0.0175, 0.018$. As the two bubbles grow, they loop around the inclusions and leave circular traces around them.

As the bubbles grow, they eventually reach the boundary of the unit square and they touch the bubble from the neighboring cell, giving birth to a new topological change. The region of phase 2 becomes a collection of strips again, this time with the correct normal orientation. Figure 4.7 shows the interfaces at the instances $t = 0.018, 0.0185, 0.019, 0.0195, 0.02, 0.0205, 0.021, 0.0215, 0.022, 0.0225$. Finally, the two strips flatten as the region of phase 2 tends to a stable equilibrium (with volume fraction $\frac{1}{2}$ and boundaries of normal e_1), see Figure 4.8, which pictures the interfaces at the instances

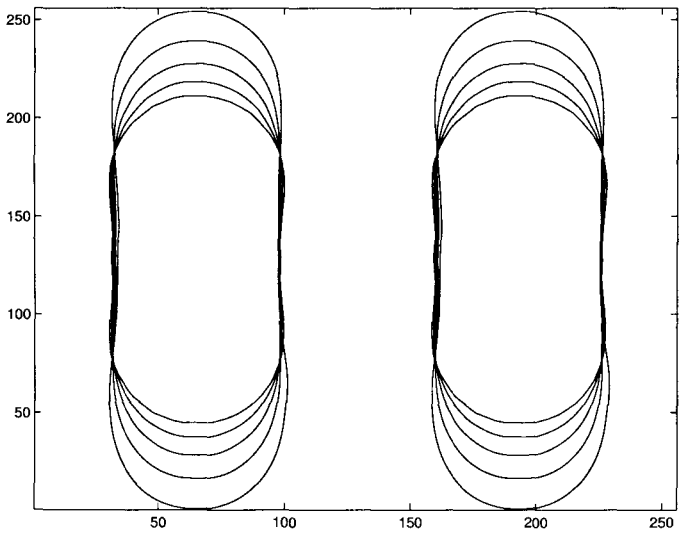

Figure 4.8: Evolution of phase boundaries with mismatched normal (part II)

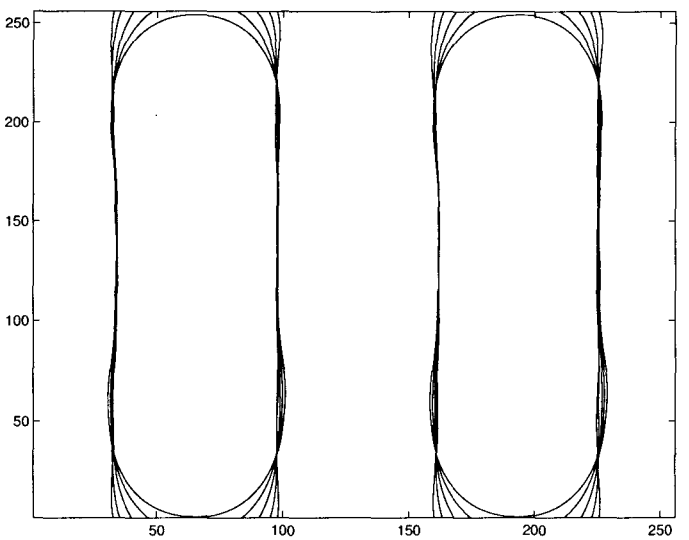

Figure 4.9: Evolution of phase boundaries with mismatched normal (part III)

$t = 0.0225, 0.023, 0.0235, 0.024, 0.0245, 0.025, 0.0255, 0.026, 0.0265, 0.027.$

4.6 Delay scaling

We consider the evolution in $\mathbb{R}^2$ of a phase boundary Γ with no interfacial energy in an infinite medium with a single inclusion $B(0,R)$. Assume that the inclusion is circular and we choose the coordinate axes such that the origin coincides with its center. If R denotes the radius of the inclusion, we set the initial phase boundary to be the horizontal line $x_2 = -2R$. In the absence of applied stress, the strain field induced by this geometry is given by (4.7):

$$(\nabla u^R)_\alpha(x) = \frac{\xi_{2\beta} - \xi_{1\beta}}{2\pi} \int_{\Gamma^R} \frac{z_\beta - x_\beta}{|x-z|^2} n_\alpha(z) ds_z + \frac{\xi_{s(0)\beta} - \xi_{0\beta}}{2\pi} \int_{\partial B(0,R)} \frac{z_\beta - x_\beta}{|x-z|^2} n_\alpha(z) ds_z.$$

If we perform the change of variable $z = Ry$ inside the integrals, we get

$$\begin{aligned}(\nabla u^R)_\alpha(x) &= \frac{\xi_{2\beta} - \xi_{1\beta}}{2\pi} \int_{\Gamma^1} \frac{Ry_\beta - x_\beta}{|x-Ry|^2} n_\alpha(y) R ds_y + \frac{\xi_{s(0)\beta} - \xi_{0\beta}}{2\pi} \int_{\partial B(0,1)} \frac{Ry_\beta - x_\beta}{|x-Ry|^2} n_\alpha(y) R ds_y \\ &= (\nabla u^1)_\alpha(\frac{x}{R}).\end{aligned}$$

This, together with (1.7), implies that the normal velocity for such a geometry is subject to the scaling law

$$v_n^R(x) = v_n^1(\frac{x}{R}).$$

By scaling both the x and t variables in (4.11) with R, we conclude that the geometric nature of the motion of the interface in such a geometry is independent of R (i.e., is determined up to the scaling factor). In particular, this implies that the delay introduced by the inclusion in the average velocity of the front is proportional to the radius R:

$$\Delta t = CR.$$

The results of the simulation presented in the previous section indicate that the proportionality constant C is small.

Chapter 5

Conclusions

We have investigated the propagation of interfaces in heterogeneous materials and, in particular, the effect of precipitates on the motion of a phase boundary in a solid capable of martensitic phase transitions. We are interested in finding the effective motion of the interface or phase boundary when the heterogeneities are small compared to the macroscopic length scales. This is motivated by the shape-memory alloy NiTi. Typical commercial specimens contain small non-transforming precipitates of Ni_3Ti_4. These precipitates pin dislocations, but do not seem to affect the evolution of martensitic microstructure significantly.

We propose a simple model based on linear, homogeneous elasticity and linear kinetics to describe the evolution of phase boundary in a heterogeneous martensitic medium. We show that in this model the normal velocity of the phase boundary may be written as a sum of several terms: first a homogeneous (but non-local) term that one would obtain for the propagation of the boundary in a homogeneous medium, second a heterogeneous term describing the effects of the inclusions but completely independent of the phase or twin boundary and third an interfacial energy term proportional to the mean curvature of the boundary.

We then study certain simplified examples that are also of independent interest. The simplest case is the geometric motion, when the normal velocity is predefined everywhere as a function of position only. We employ the level set formulation to describe the geometric motion of a phase boundary, and this gives rise to an Hamilton-Jacobi equation. A homogenization theorem was known in the literature under the assumption that the normal velocity is continuous and positive everywhere. Unfortunately, this theorem does not provide an efficient tool for calculating the homogenized Hamiltonian or effective velocity. This thesis provides four new variational formulas (Theorems 2, 4, 5, 6) that characterize the effective velocity. The usefulness of these formulas are demonstrated through examples. Though homogenization theory requires the positivity and continuity of the normal velocity, we show through examples that it is possible to define an effective front in many examples where this fails. We show that our formulas indeed describe the evolution of these effective fronts.

We then turn to the curvature flow, where the normal velocity is the sum of a position-dependent function with a term that is proportional to the mean curvature of the interface. We prove a homogenization theorem and also some qualitative features of the homogenized front. In particular, we show that the effective motion is described by a geometric law independent of curvature and may be anisotropic. We study in detail the laminated microstructures and we prove an explicit formula for the effective velocity for the case when the curvature penalization coefficient is large. Some of the quantitative results we obtain are verified numerically.

Finally, we address the problem in full generality, for the case of an anti-plane shear deformation. We consider a medium that contains a periodic lattice of inclusions, all of which are circular and have a small radius. Motivated by Ni_3Ti_4 precipitates in NiTi, we assume that inclusions have a self-strain that is symmetric with respect to both phases. We estimate algebraically the contribution to the normal velocity due to the presence of the inclusions and we show that their effect is localized. Next, we employ the level set formulation for a numerical study of the propagation of the interface. Our simulations show that these precipitates have a very local effect on the propagation of twin boundaries. Further, we show they can provide the perturbation to push twin boundaries out of metastable states, as for example when the interfaces are not correctly aligned. In particular, our results explain why Ni_3Ti_4 precipitates don't affect the shape memory effect in NiTi.

Bibliography

[1] Abeyaratne R., Chu C., James R. D., *Kinetics of materials with wiggly energies: theory and application to the evolution of twinning microstructures in a Cu-Al-Ni shape memory alloy*, Philosophical Magazine A **73** (1996), 457-497.

[2] Abeyaratne R., Knowles J. K., *On the driving traction acting on a surface of strain discontinuity in a continuum*, J. Mech. Phys. Solids **38** (1990), 345-360.

[3] Acerbi S., Buttazzo G., *On the limits of periodic Riemannian metrics*, J. Analyse Math. **43** (1984), 183-201.

[4] Barles G., Soner H. M., Souganidis P. E., *Front propagation and phase field theory*, SIAM J. Cont. Opt. **31** (1993), 439-469.

[5] Bensoussan A., Lions J.L., Papanicolaou G., *Asymptotic Analysis for Periodic Structures*, North-Holland (1978).

[6] Bhattacharya K., *Phase boundary propagation in a heterogeneous body*, P. Roy. Soc. Lond. A Mat. **455** (1982), 757 - 766.

[7] Chang Y. C., Hou T. Y., Merriman B., Osher S. J., *A level set formulation of Eulerian interface capturing methods for incompressible fluid flows*, J. Comp. Phys. **124** (1996), 449-464.

[8] Chen Y.-G., Giga Y., Goto S., *Uniqueness and existence of viscosity solutions of generalized mean curvature flow equations*, J. Diff. Geometry **33** (1991), 749-786.

[9] Chen Y.-G., Giga Y., Goto S., *Remarks on viscosity solutions for evolution equations*, Proc. Japan Acad. Ser. A **67** (1991), 323-328.

[10] Concordel M., *Periodic homogenization of Hamilton-Jacobi equations: additive eigenvalues and variational formula*, Ind. Univ. Math. J. **45** (1996), 1095-1117.

[11] Concordel M., *Periodic homogenization of Hamilton-Jacobi equations: 2. Eikonal equations*, Proc. Roy. Soc. Edinburgh **127A** (1997), 665-689.

[12] E W., *A Class of homogenization problems in the calculus of variations*, Comm. Pure Appl. Math. **XLIV** (1991), 733 - 759.

[13] Evans L.C., *Periodic homogenization of certain nonlinear partial differential equations*, Proc. Roy. Soc. Edinburgh **120A** (1992), 245-265.

[14] Giga Y., Goto S., Ishii H., Sato M.-H., *Comparison principle and convexity preserving properties for singular degenerate parabolic equations on unbounded domains*, Indiana Univ. Math. J. **40** (1991), 443-470.

[15] Gurtin M. E., *Configurational forces as basic concepts of continuum physics*, Springer (2000).

[16] Hou T. Y., Rosakis P., LeFloch P., *A level-set approach of the computation of twinning and phase-transition dynamics*, J. Comp. Phys. **150** (1999), 302-331.

[17] Jiang G.-S., Peng D., *Weighted ENO schemes for Hamilton Jacobi equations*, SIAM J. Sci. Comput. **21** (2000), 2126-2143.

[18] Kellogg, O. D., *Foundations of Potential Theory*, Springer (1929).

[19] Lions P. L., *Generalized solutions of Hamilton Jacobi equation*, Research Notes in Mathematics **69**, Pitman (1982).

[20] Lions P. L., Papanicolaou G., Varadhan S. R. S., *Homogenization of Hamilton Jacobi equation*, preprint (1987).

[21] Osher S., Sethian J. A., *Fronts propagating with curvature-dependent speed: algorithms based on Hamilton-Jacobi formulation*, J. Comp. Phys. **79** (1988), 12-49.

[22] Phillips R., *Crystals, defects and microstructures: Modeling across scales*, Cambridge University Press (2001).

[23] Rosakis P., *Compact zones of shear transformation in an anisotropic solid*, J. Mech. Phys. Solids **40** (1992), 1163-1195.

[24] Shu C.-W., *Total variation diminishing time discretizations*, SIAM J. Sci. Stat. Comput. **9** (1988), 1073-1084.

[25] Soravia P., *Generalized motion of a front propagating along its normal direction: a differential games approach*, Nonlinear Analysis TMA **22** (1994), 1247-1262.

[26] Sussman M., Smereka P., Osher S., *A level set approach for computing solutions to incompressible two-phase flow*, J. Comput. Phys. **114** (1994), 146-159.